UNIVERSITY OF KWAZULU-NATAL

END-PUMPED SOLID-STATE LASERS

by

Wayne S. Koen

Submitted in fulfillment of the academic requirements for the degree of Master of Science in the School of Physics, University of KwaZulu-Natal, Durban.

Supervisors:

Prof. Andrew Forbes

Dr. Christoph Bollig

August 2010

To Ernst

Abstract

This dissertation consists of four sections, with the focus on near- and mid-infrared lasers using Yttrium Lithium Fluoride (YLF) crystals doped with various rare-earth ions as a gain medium.

As introduction a general overview of the concepts pertaining to end-pumped solid-state lasers are presented. The basic principles, components and operation of lasers are discussed. Stimulated emission, laser gain media, pump sources and pump geometries are elaborated upon. Three-, four-, quasi-three- and quasi-four-level laser schemes are described. Finally, the advantages and disadvantages of end-pumping as opposed to side-pumping schemes for solid-state lasers are discussed.

Thereafter, the design and results of a high-powered diode-end-pumped Nd:YLF laser is presented. In conjunction with previously demonstrated methods, the thermal fracture issues of Nd:YLF were addressed by utilizing the natural doping gradient along the boule of the crystal. This, in addition to a novel crystal mounting technique, resulted in the highest reported output power from a diode-end-pumped Nd:YLF laser as well as record pumping powers.

In the third section, a compact Ho:YLF oscillator-amplifier system is reported. The novel setup utilised the unpolarised pump power from a fibre-laser efficiently by using the pump light transmitted by the oscillator crystal to pump the amplifier crystal, which produced $21.3\,\mathrm{mJ}$ at $1\,\mathrm{kHz}$, with an M^2 better than 1.1.

Lastly, the conclusion is drawn that YLF as a host material can be used in a highly successful manner for high-power applications. Additionally, the novel pumping scheme implemented in the Ho:YLF oscillator-amplifier has been shown to be scalable by a subsequent system which delivered record performance.

Acknowledgements

I am indebted to many people that supported and encouraged me throughout my studies. In particular I want to express my endless gratitude towards:

My supervisors, Dr. Christoph Bollig and Prof. Andrew Forbes. Christoph, your passion for lasers are the sole reason I got hooked on this wonderful field of study. You already inspired me in my early undergraduate days to pursue my postgraduate studies in laser physics. Thank you for teaching me the bulk of what I know today about solid-state lasers. It's been a wonderful experience. Andrew, you are a great supervisor and mentor. Thank you for your support and encouragement when needed. Your invaluable feedback and advice has always been taken to heart and is greatly valued.

Daniel Esser. You were always available to answer any questions - even the silly ones - over a cup of espresso or two. Thank you for the hours spent helping me in the lab and for reading my dissertation. Your comments have enabled me to improve it to the standard it now is - a standard to be truly proud of.

Dieter Preussler. Thank you for sharing your vast experience and many tricks in the lab. My acquired skills in the lab would have surely been poorer without it.

All my other colleagues at the National Laser Centre, thank you for being the great bunch of people you are. Its been great working amongst such a group of wonderful people.

The National Laser Centre for the financial support that made my MSc possible. A special thanks for enabling me to present my work at the Europhoton conference in Paris.

My parents and family, for all their encouragement, advice and love. Thank you for the great example that you have set me. Ernst. You are the greatest blessing in my life. Thank you for your never-ending support and love.

Declaration 1

The experimental work described in this dissertation was carried out at the CSIR National Laser Centre (Pretoria) while I was enrolled at the School of Physics, University of KwaZulu-Natal (Durban), from February 2007 to March 2009, under the supervision of Dr. Christoph Bollig and Prof. Andrew Forbes.

These studies represent original work by the author and have not otherwise been submitted in any form for any degree or diploma to any tertiary institution. Where use has been made of the work of others it is duly acknowledged in the text.

Signed: _____

On this _____ day of _____ 2010

As the candidate's supervisor I have approved this dissertation for submission.

_____

Prof. Andrew Forbes

On this _____ day of _____ 2010

Declaration 2 - Plagiarism

I, _____ declare that

1. The research reported in this thesis, except where otherwise indicated, is my original research.

2. This thesis has not been submitted for any degree or examination at any other university.

3. This thesis does not contain other persons data, pictures, graphs or other information, unless specifically acknowledged as being sourced from other persons.

4. This thesis does not contain other persons' writing, unless specifically acknowledged as being sourced from other researchers. Where other written sources have been quoted, then:

   a. Their words have been re-written but the general information attributed to them has been referenced.

   b. Where their exact words have been used, then their writing has been placed in italics and inside quotation marks, and referenced.

5. This thesis does not contain text, graphics or tables copied and pasted from the Internet, unless specifically acknowledged, and the source being detailed in the thesis and in the References sections.

Signed: _____

Declaration 3 - Publications

Peer-Reviewed Journal Papers

1. **W. Koen**, C. Bollig, H. Strauss, M. Schellhorn, C. Jacobs, and M.J.D. Esser, "Compact Fibre-Laser-Pumped Ho:YLF Oscillator-Amplifier System," *Journal of Applied Physics B*, 21 November, 2009,

   URL: *http://www.springerlink.com/content/m823265551470079*

   DOI: *10.1007/s00340-009-3819-y*

International Conference Papers

1. C. Bollig, H.J. Strauss, M.J.D. Esser, **W. Koen**, M. Schellhorn, D. Preussler, K. Nyangaza, C. Jacobs, E.H. Bernhardi and L.R. Botha, "Compact Fibre-Laser-Pumped Ho:YLF Oscillator-Amplifier System," CLEO Europe, Munich, Germany, 14-19 June, 2009.

2. C. Bollig, M. J. D. Esser, C. Jacobs, **W. Koen**, D. Preussler, K. Nyangaza and M. Schellhorn, "70 mJ Single-Frequency Q-Switched Ho:YLF Ring Laser - Amplifier System Pumped by a Single 82 W Tm Fibre Laser," Middle-Infrared Coherent Sources, Trouville, France, 8-12 June, 2009 **(invited)**.

3. M. J. Daniel Esser, H. Strauss, **W. S. Koen**, D. Preussler, K. Nyangaza and C. Bollig, "Q-switched Ho:YLF Laser Pumped by a Tm:GdVO4 Laser," Middle-Infrared Coherent Sources, Trouville, France, 8-12 June, 2009.

4. H. J. Strauss, **W. Koen**, C. Bollig, M. J. D. Esser, D. Preussler, K. Nyangaza and C. Jacobs, "Efficient Fiber-Laser-Pumped Ho:YLF Oscillator and Amplifier Utilizing the Transmitted Pump Power of the Oscillator," CLEO, Baltimore, USA, 31 May - 5 June, 2009.

5. C. Bollig, **W. Koen**, H. Strauss, E.H. Bernhardi, R. Botha, M.J.D. Esser and D. Preussler, "Exploiting the natural doping gradient of Nd:YLF crystals for high-power end-pumped lasers," In Proceedings of the *3rd EPS-QEOD Europhoton Conference*, Paris, France, 31 August - 5 September, 2008.

6. M.J.D. Esser, C. Bollig, D. Preussler, C. Jacobs, **W. Koen** and E.H. Bernhardi, "High power diode end pumped Tm:GdVO$_4$ laser operating at 1818 nm and 1915 nm," In Proceedings of the *Marie Curie Chair Conference Recent advances in laser spectroscopy and laser technology*, Lodz, Poland, 29-31 May, 2007.

National Conference Papers

1. C. Bollig, M. J. D. Esser, C. Jacobs, **W. Koen**, D. Preussler and K. Nyangaza, "High-energy single-frequency Q-switched 2-μm Ho:YLF oscillator - amplifier system pumped by a thulium fibre laser" in South African Institute of Physics 54th annual conference, University of KwaZulu-Natal, KwaZulu-Natal, July, 2009.

2. C. Jacobs, C. Bollig, M. J. D. Esser and **W. Koen**, "Electronic feedback control to stabilise a high-energy Ho:YLF ring laser" in South African Institute of Physics 54th annual conference, University of KwaZulu-Natal, KwaZulu-Natal, July, 2009.

3. M. J. D. Esser, C. Jacobs, S. Ngcobo, **W. Koen**, H. Strauss, D. Preussler, L.R. Botha and C. Bollig, "Development of high-energy 2 m solid-state lasers" in South African Institute of Physics 54th annual conference, University of KwaZulu-Natal, KwaZulu-Natal, July, 2009.

4. M.J.D. Esser, C. Bollig, D. Preussler, **W.S. Koen**, E. H. Bernhardi, H.J. Strauss, and M. Schellhorn "Tm:GdVO4 Laser as Pump Source For a Ho:YLF Laser Oscillator" in South African Institute of Physics 53srd annual conference, University of Limpopo, Polokwane, July, 2008.

5. **W. Koen**, C. Bollig, H. Strauss, R. Botha, E. Bernhardi, and M. J. D. Esser, "Power Scaling of a High-Power End-Pumped Nd:YLF Laser" in South African Institute of Physics 53srd annual conference, University of Limpopo, Polokwane, July, 2008.

6. H. J. Strauss, C. Bollig, M. J. D. Esser, M. Schellhorn, D. Preussler, C. Jacobs, K. Nyangaza and **W. Koen**, "High energy fibre laser pumped Ho:YLF $2\,\mu$m laser" in South African Institute of Physics 53srd annual conference, University of Limpopo, Polokwane, July, 2008.

7. C. Bollig, D. Preussler, M. J. D. Esser, S. Ngcobo, C. Jacobs, R. C. Botha, **W. S. Koen**, E. H. Bernhardi, A. R. Sarmani and L. R. Botha, "Solid-state laser source research at the CSIR - National Laser Centre" in South African Institute of Physics 52nd annual conference, University of the Witwatersrand, Johannesburg, July, 2007.

8. M.J.D. Esser, C. Bollig, D. Preussler, C. Jacobs, **W. Koen** and E.H. Bernhardi, "Diode-end-pumped Tm:GdVO$_4$ laser at selected wavelengths" in Proceedings of the *52nd South African Institute of Physics Conference*, University of the Witwatersrand, Johannesburg, South Africa, July, 2007

9. **W. S. Koen**, C. Bollig, A. Forbes, A. R. Sarmani, R. C. Botha and M. J. D. Esser, "Ultra short-pulse (USP) laser development" in South African Institute of Physics 52nd annual conference, University of the Witwatersrand, Johannesburg, July, 2007.

10. R. C. Botha, C. Bollig, **W. S. Koen**, A. R. Sarmani, L. R. Botha and C. Jacobs, "Energy scaling techniques in ultra-short pulse lasers" in South African Institute of Physics 52nd annual conference, University of the Witwatersrand, Johannesburg, July, 2007.

11. R. C. Botha, C. Bollig, **W. S. Koen** and N. V. Kuleshov, "High-Power Continuous-Wave and Passively Q-switched 1314 nm Nd:YLF laser" in South African Institute of Physics 50th annual conference, Pretoria, 2005.

Signed: _____

Contents

List of Figures

List of Symbols and Abbreviations

λ	Wavelength
h	Planck's constant
ν	Frequency
σ_e	Effective stimulated emission cross-section
f	Thermal Boltzmann factor
g_0	Small signal gain coefficient
M^2	Beam Quality Factor
AOM	Acousto Optic Modulator
CW	Continuous Wave
ESA	Excited State Absorption
ETU	Energy Transfer Upconversion
CCD	Charge Coupled Device
FWHM	Full Width Half Maximum
LASER	Light Amplification through Stimulated Emission of Radiation
NA	Numerical Aperture
PBS	Polarising Beam Splitter
PEM	Photoelectromagnetic detector
PRF	Pulse Repetition Frequency
TEC	Thermo-Electric Cooler
YAG	Yttrium Aluminium Garnate
YLF	Yttrium Lithium Fluoride

Chapter 1

Introduction to End-Pumped Solid-State Lasers

1.1 Introduction

Since the first laser was demonstrated nearly half a century ago in 1960 (Maiman, 1960), lasers have become an important part of modern life having contributed to nearly every aspect of living.

Lasers are used today for research in the fields of physics, medical science, chemistry, biology and earth science. In industry they are used to manufacture cars, CPUs and even cellphone components; they are even used to entertain us. There are hundreds of millions of diode lasers around the world tirelessly working in CD, DVD and Blue-Ray players for our entertainment. Even laser televisions are now becoming a reality (Coherent, 2009). Lasers are used for purposes varying from the seemingly frivolous (laser hair removal), to the very serious (cancer treatment, defence, safety and security).

It is therefore no surprise that so many different kinds of lasers have been developed to address these many divergent applications and needs. There are gas lasers and bulk solid-state lasers, such as Nd:YAG lasers, and fibre lasers, that are the work horses of industry. There are semiconductor lasers which are small, robust and efficient and are thus used veritably everywhere. In addition there are waveguide lasers, dye lasers, Raman lasers, Free-electron lasers, and chemically- and nuclear-pumped lasers (Pachotta, 2008).

A discussion on the complete assortment of lasers however, is beyond the scope of this dissertation. Instead, this work focuses on end-pumped solid-state lasers, in particular a Nd:YLF laser system, and a compact Ho:YLF oscillator-amplifier system which are both state of the art.

The architecture of these two laser systems are of interest due to the advantages that they possess over many other systems. They are more efficient than lamp-pumped lasers and have high average powers. Their design is simpler than lamp-pumped or any other side-pumped lasers for that matter. The resultant simpler cooling geometry is easier to implement. Solid-state lasers like these have higher brightness and sharper emission spectra than conventional diode lasers. Finally, both the systems that are presented exhibit good beam quality with nearly diffraction-limited output beams.

Additionally, the active laser materials used in these two systems have some excellent properties that were exploited. The long upper-state lifetimes of Nd and Ho in YLF can both deliver pulses with high peak powers. The host crystal (YLF) has a natural birefringence, eliminating depolarisation losses in high-powered lasers, unlike YAG which is isotropic. YLF also has a far weaker thermal lens than other host materials, which is advantageous for the construction of lasers with diffraction limited beam quality.

In this chapter the basic principles and processes relating to laser operation are presented, after which the basic components of solid-state lasers are discussed. Since the focus of this work is end-pumped bulk solid-state lasers, specific attention is given to pumping schemes. The basic layout of side-pumping and end-pumping is explained, and the advantages and disadvantages of each scheme are weighed up against each other.
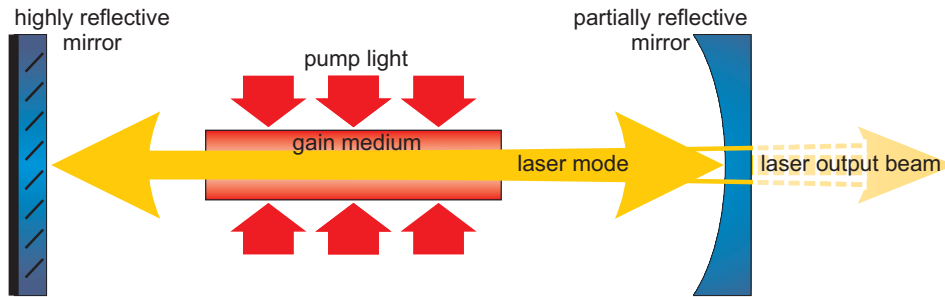
Figure 1.1: A schematic diagram of a bulk solid-state laser.

1.2 The Basic Principles and Components of Solid-State Lasers

In its most basic form, a laser consists of two mirrors, a gain medium and an energy source, as depicted in Figure 1.1. The two mirrors are placed opposite each other to form a cavity. Either one or both of the mirrors may be curved so that light travelling from the one side of the cavity to the other side will be repeatedly reflected between the two mirrors. If the mirrors are properly aligned, the light will remain in the cavity, travelling along the optical axis of the resonator. However, without replenishing or amplifying the light in the cavity, less and less light will remain as some of the light is lost with each round trip. Thus, a gain medium is needed to amplify the light with each round trip by converting energy supplied by the energy (pump) source into light travelling along the optical axis.

If the the gain is less than the resonator losses, the light in the cavity will diminish with time, until there is none left. When the gain is equal to the losses the amount of light, or optical power, stays the same. If the gain exceeds the losses, the optical power in the cavity increases with each round trip. This increase in optical power can not continue indefinitely as the intra-cavity intensity will eventually saturate the gain. After some time a steady state will be reached where the gain will exactly match the losses. This steady state is also called continuous wave (cw) laser operation (Siegman, 1986; Pachotta, 2009).

To extract a laser beam from the cavity one can make one of the mirrors slightly
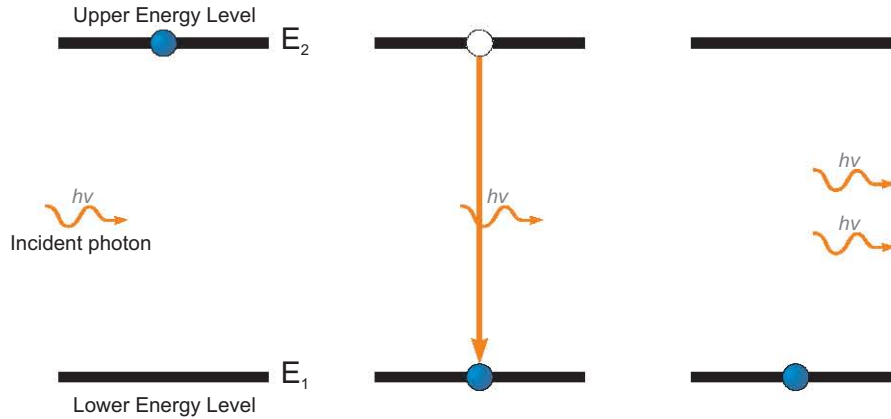
Figure 1.2: A schematic diagram illustrating stimulated emission of a photon from an atom in an excited state; before (left), during (centre) and after (right) stimulated emission.

transmissive. This output coupler then transmits a certain fraction of the intra-cavity power. The output coupler's chosen transmission depends on the gain and the overall resonator losses of the laser.

As the acronym **LASER**, or rather **L**ight **A**mplification through **S**timulated **E**mission of **R**adiation, states; the amplification of light is achieved through the process of stimulated emission within the gain medium. This is further elaborated upon in the next few sections.

1.2.1 Stimulated Emission

An excited atom or ion may, after some time, decay into some lower energy level, releasing the energy in the form of a photon which is emitted in a random direction. This is called spontaneous emission. Spontaneous emission plays an integral part in many of today's most common pieces of technology such as fluorescent lights, television screens (cathode ray tubes) and plasma displays, not to mention the common light bulb. It's also the process that provides the first photons for lasing to begin in a resonator. Classically, a single photon of the correct energy, resulting from spontaneous emission, travelling in the correct direction in a laser cavity, is the first photon that

starts stimulated emission of more photons in the gain medium, resulting in gain, and subsequent lasing (resonator losses permitting).

Stimulated emission provides the gain in the resonator. This process was first predicted by Albert Einstein in 1917 (Einstein, 1917). It can be explained by referring to Figure 1.2. Assume we have an atom which is in an excited state E_2 (Figure 1.2, left). If a photon which passes nearby the excited atom has an energy similar to the energy difference between the excited state E_2 and a lower state E_1 of the atom ($h\nu = E_2 - E_1$), stimulated emission may occur. This happens when the atom decays, releasing a photon with the same energy and direction as the original incoming photon. The incoming photon or radiation is therefore amplified. This process is the basis on which light amplification in lasers and amplifiers operate.

1.2.2 Three- and Four-Level Lasers

In the energy level scheme studied in the previous section, there are only two energy states an atom may find itself in (Figure 1.2). Consider a group of such atoms. Atoms in an excited state can amplify light by decaying and thus emitting photons. Atoms in the ground state can absorb photons to excite them back to the upper energy level. In an optically pumped two-level scheme, the number of photons emitted can not exceed the number of photons absorbed in the long term. There is therefore no net amplification.

Positive amplification is only possible when more than half of the atoms are in the excited state, in other words, when there is a population inversion. Population inversion through optical pumping becomes feasible when we have a three-level system. The diagram on the left in Figure 1.3 shows such a scheme. Pump photons can be absorbed by atoms, exciting them from the ground state to the highest state (Pump level). From the pump level, the atoms can quickly de-excite, through nonradiative decay, to the upper laser level, which has a relatively long lifetime. The atom can then decay back to the ground state through the laser transition, by stimulated emission. However, in this scenario pump light can no longer induce stimulated emission from the upper laser level to the ground state since the energy difference between the upper laser level and the ground state differs too much from the pump photon energy. Therefore a population inversion for the laser transition is now possible if there is sufficient pump light to
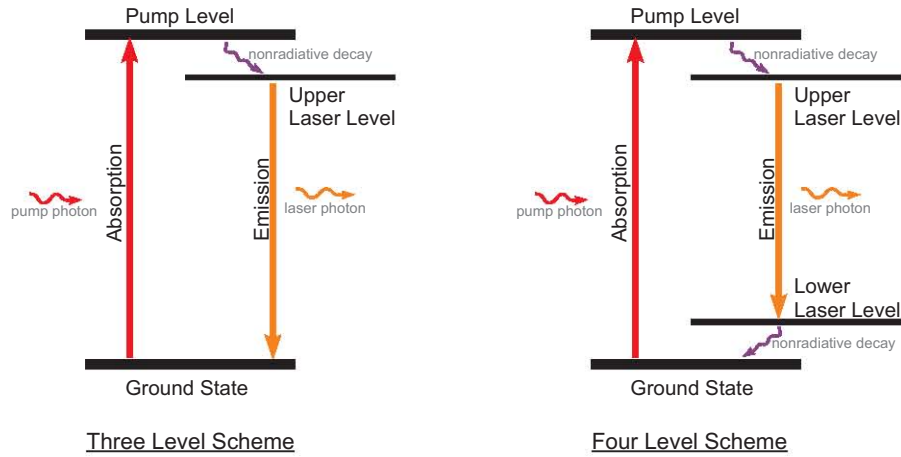
Figure 1.3: A diagram of a three-level (left) and four-level (right) laser energy scheme.

excite the atoms at a rate faster or equal to the rate at which the atoms de-excite from the upper laser level to the ground state (Walsh, 2009).

Population inversion and gain can be more easily achieved if there is some mechanism by which the number of atoms in the lower energy level is kept low by quickly removing them from that state after each emission process. This can happen when they quickly decay into an even lower state, and this is the case for the four-level system (Figure 1.3, right). The lower laser level is above the ground state so that fast decay to the ground state keeps the lower laser level population small. It means that fewer atoms are required in the upper laser level for a population inversion to occur. Therefore only moderate pumping is required for laser amplification.

1.2.3   Quasi-Three- and Quasi-Four-Level Lasers

Pure three- and four-level lasers are not the only lasers in existence. Many systems exist which do not fall into these two categories, but do exhibit similar properties of either. These are called quasi-three- and quasi-four-level lasers. The following manner, recently proposed by Walsh, by which to classify these lasers according to the ratio of the thermal Boltzmann factors of the laser energy levels, help explain the quasi-three- and quasi-four-level behaviour (Walsh, 2009):

The concept of quasi-three- and quasi-four-level lasers is easily understood by looking at the laser gain. The small signal gain coefficient is given by (Barnes *et al.*, 1996)

$$g_0 = \sigma_e[\gamma N_2 - (\gamma - 1)C_A N_s] \tag{1.1}$$

where σ_e is the effective stimulated emission cross-section, and N_2 is the population in the upper laser manifold, C_A is the concentration of active ions, N_s the number density of the sites where the active ions can reside, and $\gamma = 1 + f_l/f_u$ where f_l and f_u are the thermal Boltzmann factors in the lower and upper laser levels respectively.

When $\gamma = 1$ we have a true four-level laser and when $\gamma = 2$ we have a true three-level laser. We can therefore see that when γ is closer to 1 than to 2, we have a quasi-four-level laser, and when γ is closer to 2, we have a quasi-three-level laser.

To explain why this is the case, we refer back to Figure 1.3. In a three-level laser, the lower laser level is the ground state and therefore has a thermal population. In a four-level laser, the lower laser level is an excited state with a negligible thermal population. It follows from $\gamma = 1 + f_l/f_u$ that γ must be 2 for a three-level laser when $f_l = f_u$, and γ must be 1 for a four-level laser when $f_l = 0$.

If one considers a quasi-four-level laser's structure, it resembles that of a three-level laser. However, its f_l is small but not negligible, and accordingly behaves more like a four-level laser; hence being labelled as quasi-four. Formally lasers with $\gamma < 1.5$ are called quasi-four-level lasers, and lasers with $\gamma > 1.5$ are called quasi-three-level.

Examples of quasi-four-level lasers, according to this definition, are Ho:$^5I_7 \rightarrow {}^5I_8$ (wavelength $\sim 2.0\,\mu$m) and Tm:$^3F_4 \rightarrow {}^3H_6$ ($\sim 1.9\,\mu$m) (Walsh, 2009).

Historically though, the energy level structure of an active ion in a given host material was used to classify a laser as quasi-three- or quasi-four-level, and not the actual behaviour of the material for a given operating environment (Eichorn, 2008). Only time will tell whether the more recent and possibly more appropriate definition proposed by Walsh will come into wide spread use.

1.2.4 Gain Media for Solid-State Lasers

As previously mentioned, a laser gain medium (also called an active laser medium) can amplify light. It can either be used to compensate for resonator losses in a laser, or in an optical amplifier (Pachotta, 2009).
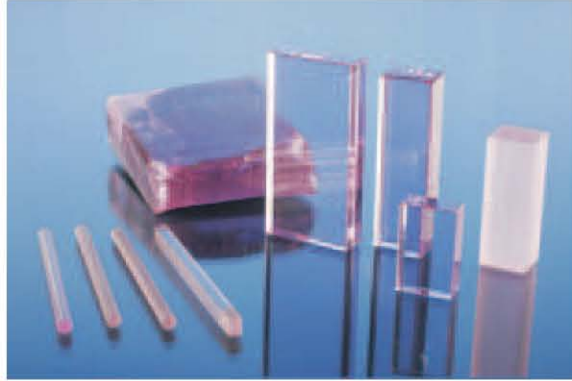
Figure 1.4: YAG crystals doped with Neodymium (Bagdasarov Crystals Group, 2009). The pink tint of the crystals is caused by the Neodymium.

Many physical properties of the gain medium are important when considering which gain material is most suited for a laser system (Koechner, 1999; Pachotta, 2008; Pachotta, 2009):

- The gain material must have a laser transition at the required wavelength. It is desirable that the maximum gain occurs in this wavelength region.

- The gain medium must be highly transparent for this wavelength region, to minimise loss.

- Pump sources should be available for the wavelength at which the gain material needs to be pumped at. Pump absorption should be efficient.

- The upper-state lifetime of the upper laser level should be suitable for the application. Long upper-state lifetimes are required for Q-switched operation, while it should be short enough if fast modulation of the optical power is required.

- High quantum efficiency is desired. The gain medium's energy output should not be far less than the energy input.

- The gain medium should be robust, with a long lifetime. It should be chemically stable.

- To obtain high gain and a low threshold pump power, the emission cross-section and upper-state lifetime product should be large.

- Strong pump absorption is desirable when using pump sources with low beam quality.

- A large gain bandwidth is required for wavelength tuning.

- A high optical damage threshold and not too high saturation fluence is required of the gain medium for high-energy pulse lasers and amplifiers.

The following criteria have specific bearing on bulk solid-state gain media:

- The host medium should be of good optical quality and be available in the required size.

- The host material should have lattice sites that can accept the dopant ions. The local crystal field must induce the required spectroscopic properties in the ions. For some applications it must allow for high doping with laser-active ions without clustering.

- It must be chemically stable. For example, it should not be hygroscopic.

- It must have a good thermal conductivity to facilitate cooling.

- Low thermo-optic coefficients are required for weak thermal lensing during high-power operation.

- High resistance to mechanical stress is needed to avoid fracture.

- Optical isotropy can be desirable. However, in other cases birefringence is desired to reduce thermal depolarisation losses.

- Polarisation-dependent gain may be preferable for polarised laser emission.

As can be seen, there are some conflicting criteria. For example, a large bandwidth generally entails having a small cross-section, and low quantum efficiency. Also, a high quantum efficiency is not compatible with strong four-level behaviour. A high pump absorption may be advantageous for pump sources with low beam quality, but the accompanying short absorption length increases thermal issues.

It is apparent from this that different circumstances put widely varying requirements on the gain medium. It is therefore imperative that the right gain medium is chosen for the circumstances to ensure optimal system performance.

Host Materials for Solid-State Lasers

There are three main types of host materials used in solid-state lasers. The most common materials are crystals and glasses, followed by ceramics. Specifically, the most highly used crystal in use today is yttrium aluminium garnet, more commonly known as YAG (VLOC YAG Brochure, 2008). The work presented in this dissertation, however, uses yttrium lithium fluouride (YLF) crystals. More detail will be given on this material in the subsequent chapters.

Active Ions for Solid-State Lasers

Rare-earth ions are excellent dopants for use in solid-state laser materials. They have numerous emission lines throughout most of the visible and infrared part of the spectrum (Weber, 2001). The spectral properties of the ions are not seriously affected by the crystal field of various host materials (Stark effect) because the energy levels of interest for laser transitions are shielded from the near crystal field by a filled outer shell of electrons (Koechner, 1999).

The most common rare earth ion for use in lasers today is Neodymium (Nd^{3+}). It is mostly used as dopant in YAG crystals (Figure 1.4). One of the two lasers presented in this work uses Neodymium as the active ion. The second system uses Holmium (Ho^{3+}).

Since the gain medium adds energy to the amplified light, it requires energy from an external source. This process, called pumping, is typically done through electrical currents (electrical pumping of diode lasers) or incident light (optical pumping). In this work, optical pumping is implemented through the use of laser diodes (for the Nd:YLF laser) and a fibre laser (for the Ho:YLF oscillator-amplifier). Optical pump sources for solid-state lasers are discussed further in the next section.

1.2.5   Pump Sources for Solid-State Lasers

As pump source for optically-pumped systems, one may use lamps, diode lasers, fibre lasers, or any other laser for that matter. Each of these sources has their own advantages and disadvantages which need to be considered when designing a laser system.

The first laser demonstrated was pumped by a flash lamp (Maiman, 1960). Today

flash lamps are still widely used despite laser diodes increasingly becoming a more desirable alternative. Flash lamps are particularly attractive for pulsed laser systems, delivering high pulse energies and peak powers, since they are for the moment still cheaper than laser diodes for this application. They are therefore a common pump source for pulsed solid-state lasers with low repetition rates and high peak power (Pachotta, 2009). However, flash lamps have several drawbacks. They tend to be inefficient as they emit broadband radiation while most solid-state gain media have far narrower absorption spectral regions. They require gain media with broadband pump light absorption in spectral regions accessible with flash lamps. For lamp-pumped systems, most of the electrical energy inserted into the system is converted to heat, which needs to be removed to avoid damage to the system and degraded performance caused by thermal effects. Flash lamps can only be used in side-pumped configurations, making cooling of the laser crystal rods more difficult. Flash lamps require high-voltage power supplies, an added safety hazard, and are a strong source of electromagnetic interference which is undesirable in many laser applications. Although flash lamps are relatively robust, their usable lifetime is fairly limited when compared to diode lasers.

Diode lasers have become the dominant laser as well as the dominant pump source for solid-state lasers as their costs have decreased, while their output powers and available wavelengths have increased. The emission spectra of laser diodes are narrow, which allows for strong and efficient absorption of the pump light in the laser crystal. The subsequent decrease in the heat load in the laser crystal also alleviates detrimental thermal effects. The increasingly wider range of wavelengths at which diode lasers operate, allows for a wide range of laser gain media (Weber, 2001). Diode laser light is strongly directional, allowing either end-pumping or side-pumping of laser crystals. Their electrical to optical efficiencies can be very high. This, in addition to efficient pump absorption, can result in laser systems with high wall-plug efficiencies. Diode-pumped lasers can be very compact when compared to similar lamp-pumped systems.

Laser diodes as a pump source do have a few drawbacks. They are very sensitive to static discharges. Excessive currents and overheating, even for short durations of time, can lead to damage. However, when operated within their specifications, they have operating lifetimes in excess of tens of thousands of hours; far longer than that of flash lamps. They are ideally suited for cw (continuous wave) and high repetition rate systems (Pachotta, 2009).

Solid-state lasers can also be pumped by other solid-state lasers such as fibre lasers or slab lasers. The added complexity of having another solid-state laser in the system generally complicates the design, and lowers the overall efficiency of the system. However, this is often a feasible and efficient approach when certain characteristics are required from a laser system. It may be that a specific laser material's pump wavelength is inaccessible by any other existing approach such as flash lamps or laser diodes. It could be that the required pulse energy or pulse duration is easiest to obtain by a laser-pumped laser system. These, as well as other arguments have led to many demonstrated and commercial laser systems of this type (Weber, 2001). In Chapter 3 a Ho:YLF laser system is presented which uses a Tm:fibre laser as pump source. The fibre laser, in turn, is pumped by diode lasers.

1.2.6   Pumping Configurations

There are two dominant configurations to optically pump bulk solid-state lasers, namely side-pumping and end-pumping (Koechner, 1999). Figure 1.5 depicts the two pumping schemes. The top of Figure 1.5 shows the side (left) and front (right) view of a side-pumped circular laser rod, while the end-pumped scheme is shown at the bottom. The pump light is indicated by the red arrows, the excited area of the crystal is shaded red, and the laser mode is depicted by the yellow lines (side view, left) and yellow circles (front view, right).

In the side-pumped scheme, the gain medium is pumped approximately perpendicular to the laser resonator mode (top, Figure 1.5). In this scheme most of the crystal is filled with pump light and therefore the whole crystal volume is excited, with most pump light being absorbed, and therefore most excited ions being near the outer edge of the crystal. However, energy is extracted only from the excited ions which spatially overlap with the laser resonator mode in the centre. The energy deposited outside this region is wasted and increases the heat load, contributing to the thermal stresses in the crystal. The fact that most of the energy delivered by the pump is deposited in the outer region of the crystal, where it's not being extracted again as laser light, makes this scheme less efficient. The higher absorption at the edge of the crystal results in the gain being higher in the outer region than in the centre, where the laser mode is. This can cause higher order modes to lase. The additional lasing of the higher
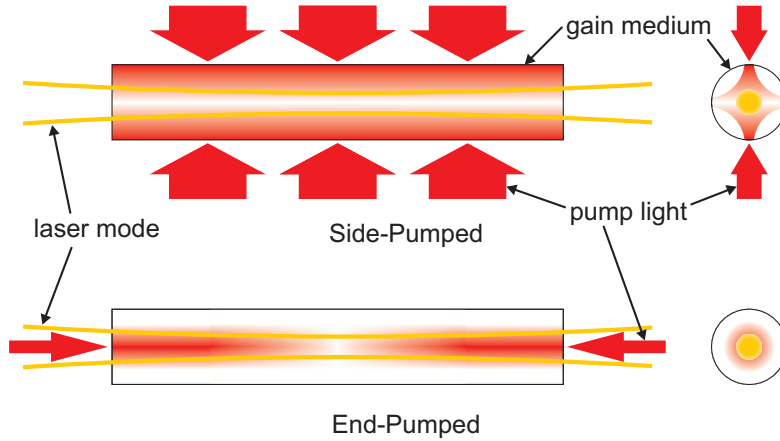
Figure 1.5: A schematic diagram of side-pumped (Top) and End-Pumped (Bottom) schemes. The pump light is indicated by the red arrows, the excited area in the crystal is shaded red, and the resonator mode is indicated by the yellow lines.

order modes then degrades the beam quality of the laser. Special care thus needs to be taken to prevent these higher order modes from lasing by designing the resonator to force the laser to operate only on the fundamental TEM_{00} mode. This can be done by inserting an aperture into the resonator cavity which only transmits the fundamental mode, or increasing the losses for the higher order modes in some other fashion. The side-pumped scheme is often used for diode-pumped, multi-kilowatt lasers.

In the end-pumped scheme, also known as longitudinal pumping, the gain medium is pumped co-linearly with the resonator mode (bottom, Figure 1.5). End-pumping tends to be more efficient than side-pumping since the pumped (and therefore excited) volume is mostly restricted to the region where the laser mode is. This leads to higher gain, allowing the generation of shorter Q-switched pulses (Pachotta, 2009). The good spatial overlap of the resonator mode and pumped volume in the gain medium also lowers the heat load. Since the sides of the crystal need not be accessible for pumping, the crystal surface can be in direct contact with a cooled mount, simplifying cooling significantly. The drawback is that end-pumping requires a pump source with sufficient beam quality in order that the pump beam is sufficiently collimated over the length

of the crystal, or at least the absorption length thereof. Another drawback is that most of the pump light is absorbed at the end of the crystal, where there is no contact with a cooling surface. The heat deposited subsequently leads to thermal stresses and thermal lensing. This is discussed in greater detail in Sections 2.3.3 to 2.3.6. Despite this, end-pumped lasers often achieve better beam quality than similar side-pumped lasers.

In the work reported, only end-pumped configurations are considered.

Chapter 2

High-Power Diode-End-Pumped Nd:YLF Laser

2.1 Introduction

A relatively short time after the first laser was demonstrated in 1960 (Maiman, 1960), the first reported Neodymium laser (Nd:CaWO$_4$) was demonstrated at Bell Laboratories by L.F. Johnson and K. Nassau (Johnson & Nassau, 1961). Three years later J.E. Geusic, H.M. Marcos and L.G. van Uitert demonstrated what was to be the most widely used solid-state laser, namely the Neodymium-doped Yttrium Aluminium garnet (Nd:YAG) laser (Geusic *et al.*, 1964). Since then Nd lasers using many different host materials have been demonstrated (Weber, 2001).

The first Neodymium-doped Yttrium Lithium Fluoride (Nd:YLF) laser was demonstrated in 1982 by T.M. Pollak et al. (Pollak *et al.*, 1982). This could have been a particularly attractive material for use in high-power end-pumped solid-state lasers if not for its low thermal fracture limit.

The YLF crystal's weak thermal lens on the σ-polarisation enables the construction of lasers with diffraction-limited beams, while the long upper laser level lifetime of $525\,\mu$s (Ryan & Beach, 1992) of Neodymium in YLF crystals support efficient pulsed operation. In addition, the natural birefringence of YLF eliminates thermally induced depolarisation in high-power applications.

However, the relatively low thermal conductivity of Nd:YLF, which can lead to
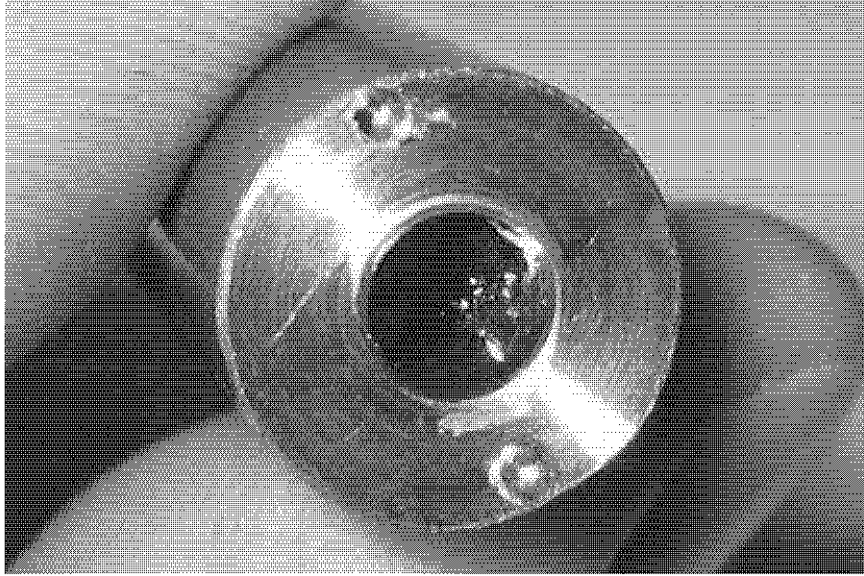
Figure 2.1: A mounted Nd:YLF rod, fractured from thermally induced stress (Bollig *et al.*, 2005).

thermal runaway effects, and its low thermal fracture limit has made power scaling difficult (Bernhardi, 2008). Furthermore, the astigmatic thermal lens of YLF also requires special consideration when designing a resonator that compensates for this (Hardman *et al.*, 1999).

In this chapter a state of the art high-power diode-end-pumped Nd:YLF laser is presented. The aim of this project was to demonstrate a Nd:YLF laser with high average output power delivered in a diffraction limited beam, while being highly efficient in both continuous and pulsed mode. The subsequent good results were achieved by addressing the issues mentioned above in several ways.

2.2   Previous Work

The highest previously reported diode-end-pumped Nd:YLF laser delivered 60.3 W cw (Bollig *et al.*, 2005). When Q-switched it delivered an average power above 52 W for

all repetition rates between 5 and 30 kHz while maintaining a good beam quality. This good performance was achieved by addressing the above-mentioned issue of thermal fracture in several ways. The average doping concentration of the Nd:YLF crystals was decreased to 0.5 at.% from the generally used 0.7 to 1.1 at.% doping (Clarkson, 1998; Esser, 2004). Off-peak or "wing" pumping was implemented by pumping the crystals at 805 nm instead of the conventional 792 nm where the absorption cross section peak is (Figure 2.2). This resulted in a longer absorption length and improved heat distribution in the crystals as well as equal absorption on the σ- and π-polarisation. This also had the added advantage that laser diode modules were more readily available at this wavelength.

The resonator was designed to support a relatively large mode radius of $w = 0.5$ mm inside the crystals. The astigmatic thermal lens, which was a detrimental effect in previously demonstrated lasers, was addressed by using two crystals and rotating the c-axis of the crystals by 90 degrees with respect to each other, with a $\lambda/2$-plate between them. This caused the two astigmatic thermal lenses from the two crystals to compensate for each other, resulting in a net non-astigmatic lens, while allowing the laser beam to be the same polarisation in both crystals with regard to their crystal lattices.

Though these measures resulted in significant improvement on previous results (Esser, 2004), one of the two crystals cracked when the laser repetition rate was reduced to 5 kHz (Figure 2.1).

It was initially proposed that the fracture problem might be addressed by increasing the pump and laser mode diameter in the crystals. The mode size was subsequently increased to $w = 1.3$ mm. However, even after the mode size was increased, another crystal was fractured.

It was then proposed that the doping concentration should be reduced even further (Bollig, 2006). However, this would have entailed having crystals specially manufactured as no crystals of such low doping were readily available. During the subsequent discussions with crystal manufacturer VLOC, a lesser known fact was discovered in that low-doped Nd:YLF crystals have an inherent doping gradient. It was thought that either this inherent doping gradient of low-doped Nd:YLF crystals or improper mounting may have been the reason why the one crystal fractured in the 60 W laser, while the other remained intact - despite being pumped at full power while not lasing.

Aside from being the possible reason for the crystal fractures, the inherent doping
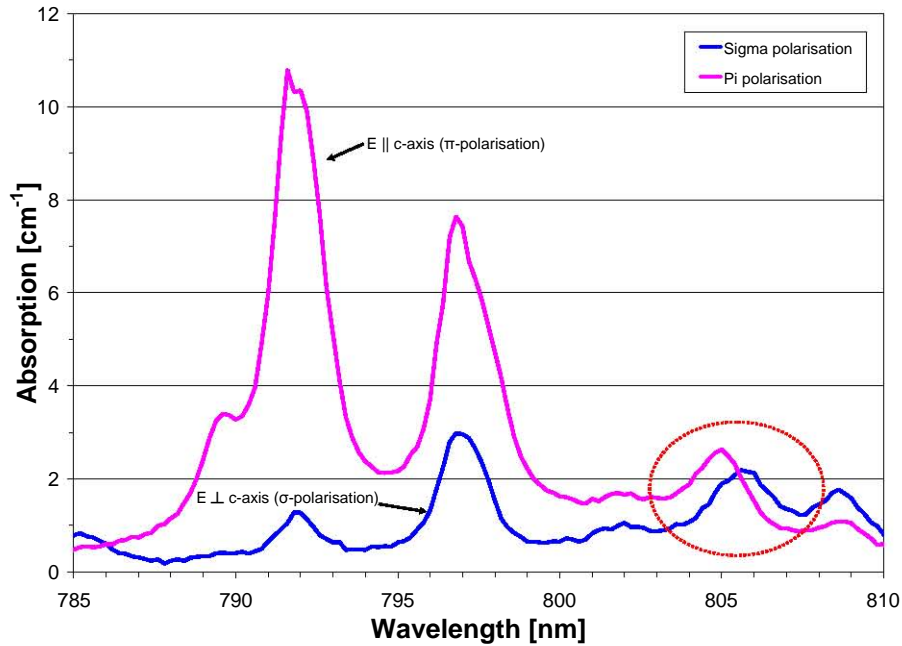
Figure 2.2: The absorption spectra of 1 % doped Nd:YLF for the σ - and π - polarisation (Cross, 2005).

gradient of low-doped Nd:YLF crystals could be exploited for the further power scaling of Nd:YLF lasers. This idea has been successfully demonstrated in the work presented in this chapter.

2.3   Properties of Nd:YLF

2.3.1   The Absorption and Emission Spectra of Nd:YLF

The absorption and emission spectra for Nd:YLF at the wavelengths relevant to this work are shown in Figure 2.2 and 2.3 respectively.

The absorption spectra are essential for deciding at which wavelength the gain medium should be pumped. Figure 2.2 shows the absorption spectra of Nd:YLF from 785 nm to 810 nm. This region is of interest for the laser-diode-pumping of Nd:YLF as there are several absorption peaks in this region and laser-diodes are readily available at these wavelengths.

Conventionally, Nd:YLF lasers which are pumped by laser-diodes are pumped at
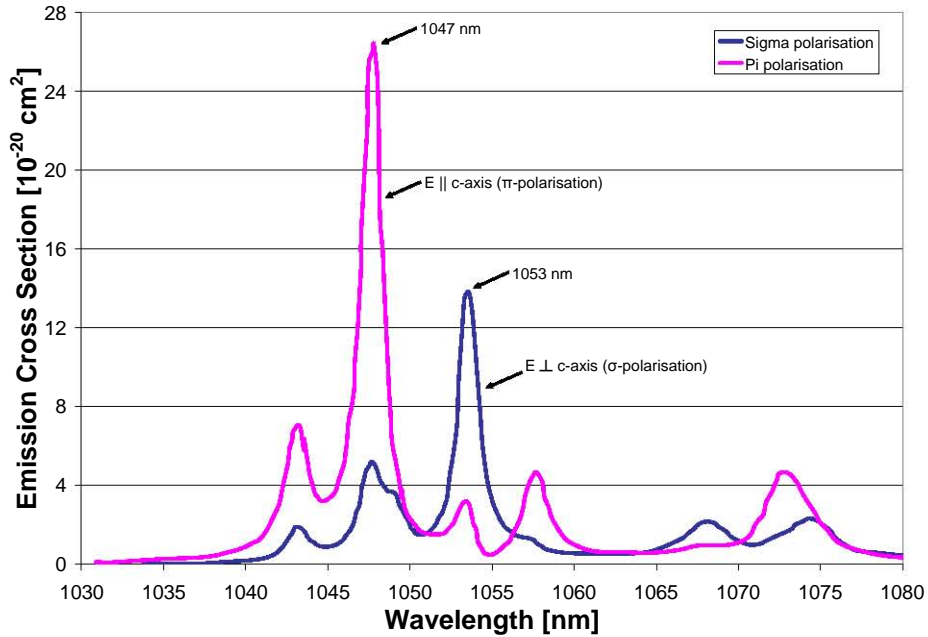
Figure 2.3: The emission spectra of Nd:YLF for the σ - and π - polarisation (Czeranowsky, 2002).

792 nm, where the highest of these absorption peaks for the π-polarisation occurs. One should note that at 792 nm the absorption of pump light is highly polarisation dependent, with the absorption of σ-polarised light being far weaker ($\sim$10 times) than for π-polarised light. The polarisation of the pump source is thus of utmost importance.

Alternatively one can pump at 805.5 nm where the absorption of σ- and π-polarised light is the same (Figure 2.2, red ellipse). The crystal can then be pumped by an unpolarised pump source such as a fibre-coupled laser-diode. However, the absorption at 805.5 nm is $\sim$5 times weaker than at the conventionally used 792 nm, resulting in a longer absorption length. This is actually an advantage, as mentioned in the previous section, and will be elaborated upon in the subsequent sections.

The emission cross-sections for the wavelength region in which the largest emission peaks of Neodymium in YLF occur, are shown in Figure 2.3. From this graph it can be seen that the emission cross-sections differ drastically for the σ- and π-polarisation. The highest emission cross-section ($\sim 25 \times 10^{-20} \text{cm}^2$) is at 1047 nm on the π-polarisation. Since the gain is highest at this wavelength, this is the most likely wavelength at which
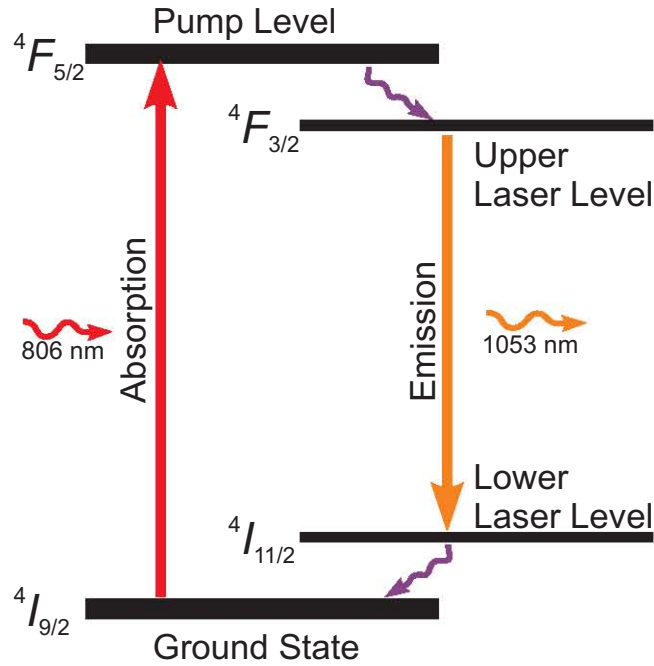
Figure 2.4: Schematic of the Nd:YLF four-level laser relevant to this work.

a Nd:YLF laser will operate. Another peak, which is roughly half that at 1047 nm, is to be found at 1053 nm on the σ-polarisation. A Nd:YLF laser can also be made to work at this wavelength, depending on the resonator design. Lasing on the σ-polarisation instead of on the π-polarisation is highly desirable due to the σ-polarisation's far weaker thermal lens. This is further discussed in Section 2.3.5.

2.3.2   The Four-Level Nd:YLF Laser

The four-level laser scheme of Neodymium in YLF relevant to this work is shown in Figure 2.4. Initially the ions are in the ground state $^4I_{9/2}$. When an ion absorbs a pump photon ($\sim$805 nm) it gets excited from the ground state to the pump level $^4F_{5/2}$ (red arrow). The pump photon energy is similar to the energy difference between these two states. From the $^4F_{5/2}$ pump level, the ion relaxes to the upper laser level ($^4F_{3/2}$) through fast non-radiative decay (purple arrow). This is a meta-stable state with a long lifetime. Given that pump light is absorbed at a sufficient rate, this allows a population inversion to occur between the upper and lower laser level ($^4F_{3/2}$ and

$^4I_{11/2}$). The excited ion can then de-excite through stimulated emission by emitting a photon of 1053 nm (orange arrow). From the lower laser level $^4I_{11/2}$ the ion relaxes fast though non-radiative decay to the ground state, ready to be excited by a pump photon once more.

2.3.3   Heat Generation in Nd:YLF

The energy difference between the pump photon and the laser photon, also called the quantum defect, introduces heat into the gain medium. This happens through the fast decay from the pump level to the upper laser level; as well as from the lower laser level to the ground state. Subsequently, 23.6 % of the absorbed pump light is converted into heat inside the crystal when the laser is operating at 1053 nm, while being pumped at 805 nm (QuantumEfficiency $= 1 - E_l/E_p = 1 - \lambda_p/\lambda_l$) (Hardman *et al.*, 1999). Neglecting other heat-generating processes, this alone warrants serious consideration in heat management for the laser crystal.

In addition to heat resulting from the quantum defect, the absorption of pump light to levels other than the pump level, fluorescence, spontaneous non-radiative transitions, and upconversion processes such as excited state absorption (ESA) and energy-transfer upconversion (ETU), contribute to the heat load (Hardman *et al.*, 1999).

Absorbed pump light may excite Nd^{3+} ions to levels other than just the pump level $^4F_{5/2}$, depending on the other energy levels of Nd^{3+} and the spectral bandwidth of the pump source. The relaxation processes that follow lead to extra heat in the crystal. However this results in less heat in diode-laser-pumped systems, when compared to arc-lamp pumped systems, due to the good spectral overlap of the laser diodes with the $^4I_{9/2}$ to $^4F_{5/2}$ transition.

A small amount of heat is deposited in the gain medium by fluorescence and non-radiative decay when an excited ion does not decay through stimulated emission. This becomes nearly insignificant when the laser operates far above threshold and when there is a good overlap between the volume of excited ions and the laser mode, which ensures that most of the excited ions relax via stimulated emission (Pollnau *et al.*, 1998). Fluorescence is especially low in diode-end-pumped lasers thanks to the good spatial overlap of the laser mode and pump light in this architecture.

Excited state absorption (ESA) can occur when the population of the upper laser
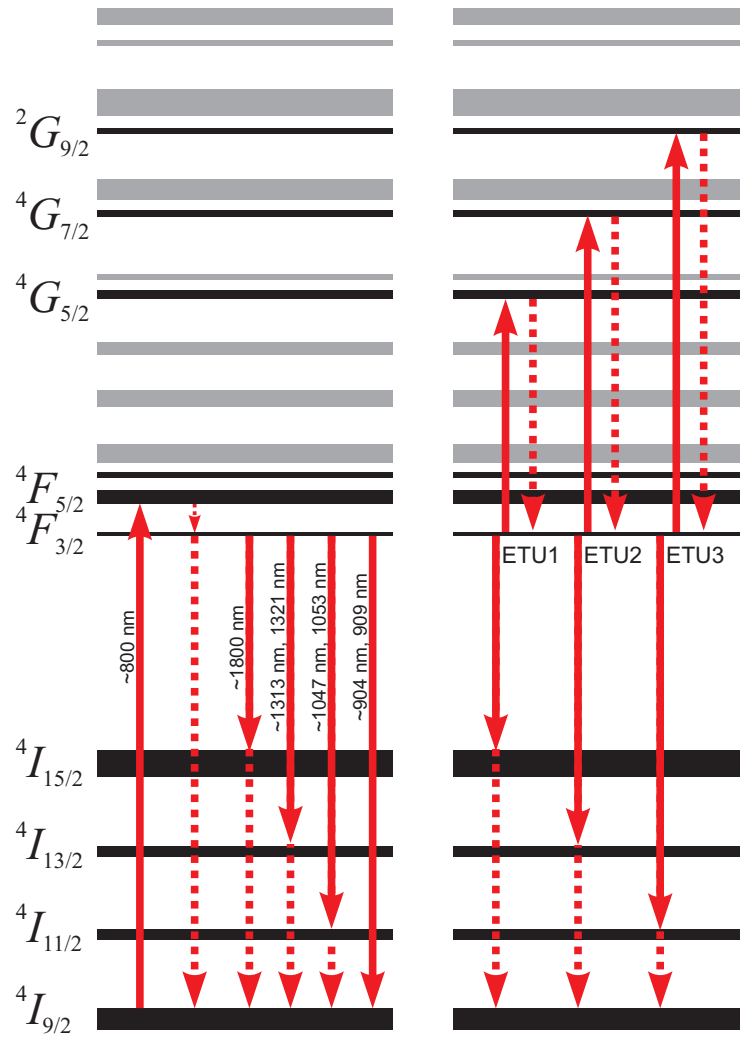
Figure 2.5: Energy level scheme of Nd:YLF without (left) and with (right) energy transfer upconversion (ETU) indicated. The dashed lines indicate heat generating transitions (Hardman *et al.*, 1999; Koechner, 1999; Weber, 2001).
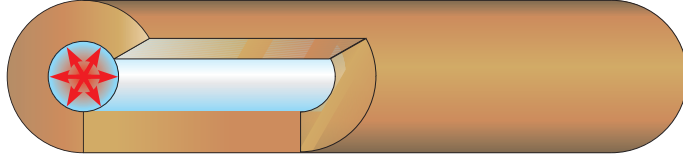
Figure 2.6: Radial heat flow (red arrows) from the centre of an end-pumped crystal rod, where heat is created, to the edge of the crystal which is in thermal contact with a cooled copper mount.

level $^4F_{3/2}$ leads not only to stimulated emission to the lower laser level $^4F_{3/2}$, but also to absorption processes for the pump or laser radiation where laser ions are excited to a higher energy level (Pachotta, 2009). Not only does this lead to heat being deposited in the crystal by the subsequent relaxation of the ion, but the additional loss can raise the threshold pump power of the laser while reducing the slope efficiency.

When an excited ion in the upper laser level $^4F_{3/2}$ relaxes to a lower level and transfers its energy to a nearby excited ion which was also in the upper laser level, it is called Energy-transfer upconversion (ETU). The possible ETU transitions in Nd:YLF is shown in Figure 2.5 (Hardman *et al.*, 1999). In addition to generating heat, this also reduces the upper laser level population, shortening the apparent upper laser level lifetime. ETU may be decreased by decreasing the crystal's doping concentration, but the resulting increase in the pump absorption length demands a pump source with sufficient beam quality. Also in this regard end-pumped lasers have the advantage as the architecture allows crystals of longer lengths.

2.3.4   Effects resulting from heat generation in Nd:YLF

The heat created by the various processes discussed in Section 2.3.3 results in a rise in temperature in the crystal. In the case of end-pumped lasers, the crystal is usually cooled along the edge of the rod, which results in a radially symmetric temperature distribution (Figure 2.6).

Figure 2.7 shows the calculated radial and longitudinal temperature distribution in an axial cross-section of an end-pump Nd:YAG rod. The highest temperature is found
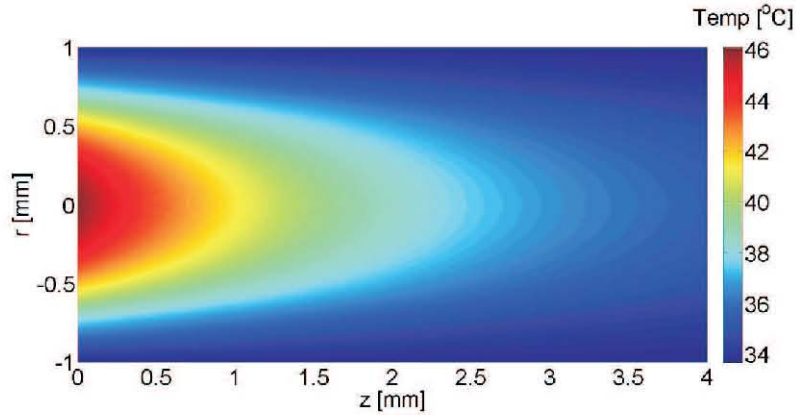
Figure 2.7: The analytical temperature distribution in a Nd:YAG laser rod which is pumped by a 8.5 W top-hat beam with a radius of 650 μm from (Bernhardi, 2008).

in the centre of the end-face of the crystal on the side where it is pumped. This is where the amount of pump light absorbed is highest.

As a result of the pump-induced temperature profile, several properties of Nd:YLF come into play:

- The crystal's refractive index changes. The refractive index of Nd:YLF has a negative dependence on temperature. Furthermore, the crystal is anisotropic in this regard with the change in refractive index with temperature (dn/dT) for the π-polarisation (E∥c) being -4.3x10^{-6} K^{-1} and -2.0x10^{-6} K^{-1} for the σ-polarisation (E⊥c) (Barnes & Gettemy, 1980; Pollak *et al.*, 1982; Pfistner *et al.*, 1994).

- The crystal expands. The Nd:YLF crystal also has different thermal expansion coefficients for the a- and c-axis. These coefficients are also temperature dependent (Hardman *et al.*, 1999). At 300 K the thermal expansion coefficients are 13x10^{-6} K^{-1} for the a-axis (⊥c) and 8x10^{-6} K^{-1} for the c-axis (∥c) (Koechner, 1999).

- Stress in the crystal arises from the non-uniform thermal expansion of the crystal, also contributing to a change in the refractive index (Weber *et al.*, 1999).

These effects give rise to thermal lensing and aberrations, and may result in thermal fracture caused by thermally induced stress.

2.3.5   Thermal lensing in Nd:YLF

Several effects contribute to the thermal lens in an end-pumped YLF crystal:

- The temperature gradient mentioned earlier causes a gradient in the refractive index of the crystal. The resulting difference in the optical path across this gradient effectively forms a lens (Pollnau *et al.*, 1998).

- End-face bulging caused by differential thermal expansion of the crystal. This is also complicated by the temperature dependence of the thermal expansion coefficients.

- Stress-induced changes in the refractive index caused by the photo-elastic effect (Weber *et al.*, 1999).

The thermally induced lens for the π-polarisation is negative due to the strong negative contribution from dn/dT which dominates the positive contribution from the end face bulging (Hardman *et al.*, 1999).

In the case of the σ-polarisation's thermal lens, the end face bulging dominates the contribution from the smaller negative dn/dT, resulting in a very weak positive lens (Hardman *et al.*, 1999).

The contribution to the thermal lens by stress-induced changes of the refractive index is negligible in comparison to the contribution from the temperature dependent change in the refractive index of Nd:YLF since the crystal has a strong natural bire-fringence (Pollnau *et al.*, 1998). The natural birefringence of the crystal also prevents depolarisation losses caused by stress-induced birefringence - a common problem in Nd:YAG lasers (Weber *et al.*, 1999; Clarkson, 2001).

Solely considering the thermal lensing behaviour for the two polarisations, one may conclude that it is desirable to operate the laser on the σ-polarisation, which has the weaker thermal lens. However, care must be taken to lase on the σ-polarisation since it has a lower cross-section than the π-polarisation.

Compared to YAG or YVO$_4$, YLF has a much weaker thermal lens, especially on the σ-polarisation, and should be a superb material for high power applications where the thermal lens normally plays a dominating role in laser performance.

2.3.6   Thermally induced fracture

Unfortunately the development of high powered Nd:YLF lasers is limited by the thermal fracture problem which is much worse for YLF than it is for YAG, YVO$_4$ and other crystals.

The temperature gradient inside the laser rod caused by the pump light induces stress in the crystal. When the induced stress in the laser rod exceeds the tensile strength of the material, the crystal will fracture.

This is of particular concern for Nd:YLF lasers as Nd:YLF has a tensile strength of only 33 MPa (Northrop Grumman Space Technology, 2009) to 40 MPa (Koechner, 1999). Compared to that of Nd:YAG, which has a tensile strength of 280 MPa (VLOC YAG Brochure, 2008), this is very low.

Nd:YLF is also susceptible to thermal runaway effects since its thermal conductivity decreases as the temperature increases. This can occur when the laser losses increase, while still being pumped with the same pump power. The increased heat deposited through increased upconversion will then lower the thermal conductivity of the crystal even further, decreasing heat extraction, and thus leading to even higher temperatures. This may continue to the point where the thermally-induced stresses fracture the crystal.

From the various effects caused by heat in the crystal, it is apparent that proper thermal management of the laser crystal is of the utmost importance for good system performance and reliability.

In conclusion to this section, it can be stated that Nd:YLF would be an excellent gain material, superior to Nd:YAG, for high-powered lasers if one were to solve the thermal fracture problem. The aim of the work presented here was to address this problem. Subsequently, record pumping of Nd:YLF crystals without crystal fracture was obtained.

2.4   Scaling Strategy

Pachotta defines power scaling as "a procedure for substantially increasing the output power of lasers." He however qualifies it as more than mere power increases with: "The actual meaning of this term should include: a well-defined systematic scaling

procedure which makes it possible to increase substantially and repeatedly the output power **without making the main problems more severe**" (Pachotta, 2009).

With this in mind, to enable successful power scaling of Nd:YLF, the following requirements have to be met to manage the detrimental effects discussed earlier:

- Upconversion has to be reduced.

- The heat load has to be spread more uniformly.

- The cooling efficiency has to be increased.

These requirements were met by taking the following actions:

- Crystals of even lower doping was used.

- The intrinsic doping gradient in low-doped YLF crystals were exploited by pumping the crystals from their lower doped side.

- "Wing" pumping or "Off Peak" pumping was implemented in conjunction with a large pump beam size.

- Crystals were mounted using a novel mounting technique.

- Four crystals were used, each pumped by their own laser diode module.

The actions mentioned above had several consequences. By using crystals of lower doping, the crystals needed to be longer to allow for the increase in the absorption length. This resulted in a larger cooling surface. Since the heat was also distributed in a larger volume, the crystal temperature was also lower, decreasing thermal effects. The increased crystal length required a pump beam of higher quality in order for the pump light to be collimated over the whole length of the longer crystal.

The intrinsic doping gradient in low-doped YLF crystals was exploited by pumping the crystals from their lower doped side. This also improved the heat distribution through the length of the crystal, decreasing the end-face temperature - critical to the management of thermal stress, and the thermal lens. This is discussed further in Section 2.6.

The "Wing" pumping in conjunction with a large pump beam size led to a longer absorption length and pumped volume. This method can be explained by referring

to the absorption spectra of Nd:YLF shown in Figure 2.2 (Cross, 2005). The typical wavelengths at which to pump Nd:YLF are 792 nm or 797 nm; on the absorption peaks of the gain medium. For this experiment the crystals were pumped in the region of 805 nm, where the absorption coefficient is much lower. This increases the absorption length and pumped volume. This also had the practical advantage that diode-laser modules at this wavelength were easily obtainable and that the absorption of the pump light is far less polarisation dependent, as later shown in Section 2.6.1.

The novel mounting technique improved the cooling of the crystals, as discussed in Section 2.6. The better thermal contact lowered the thermal stress by improving both heat removal and uniform cooling.

In the following three sections the implementation of the aforementioned solutions are discussed in greater detail for the pump source, the gain medium and the resonator design.

2.5 The Pump Source

Four Jenoptik fibre-coupled laser diode modules were used in continuous wave mode to pump the Neodymium laser (JOLD-75-CPXF-2P). Each module delivered a maximum of 75 W optical output power through a 0.4 mm diameter, 0.22 numerical aperture (NA) fibre.

The four modules were labelled LD1 (Serial number: 06-160), LD2 (Serial number: 06-161), LD3 (Serial number: 06-158), and LD4 (Serial number: 06-159). The diode modules included thermo-electric coolers (TEC) to actively control and set the temperature with external temperature controllers (Ostech). The modules were mounted on water cooled copper heat sinks in order to remove the heat from the hot sides of the internal TECs (Figure 2.8). The water circulating in the copper heat sinks was cooled by Thermo Haake (TC200) and Thermo Neslab (M33) chillers. The laser diodes were powered by two Delta Elektronika power supplies (SM 15-100), each power supply connected to two laser diodes in series. The current on both supplies was limited to 58 A in order to prevent exceeding the absolute maximum rating of the laser diodes. At 25 °C and full output power (I=56 A), the laser diodes' respective wavelengths were specified by the manufacturer as 804.5 nm for LD1, 804.5 nm for LD2, 804.3 nm for LD3, and 804.3 nm for LD4. The FWHM (Full Width Half Maximum) spectral width

Figure 2.8: Jenoptik 75 W laser diode modules mounted on a water-cooled copper heat sink.

was specified as 2.6 nm for LD1, LD2, and LD3, and 2.4 nm for LD4. This is ideal for wing pumping of Nd:YLF. By having 4 of these laser diode modules, we had a laser diode module for each of the four crystals and twice the available pump power than the previous Nd:YLF laser discussed in Section 2.2.

2.5.1   Characterization of the Laser Diodes

The optical output power of the laser diodes at 25 °C was measured using a HTD-LM200 power head with a Coherent Fieldmaster GS power meter. As shown in Figure 2.9, it is clear that the power output was linearly dependent on the input current, making the linear fit $P_{out} = 1.6 \times I_{in} - 15.5$ a very good approximation. The manufacturer specified slope of 1.6 W/A was therefore confirmed.

The dependency of the laser diodes' wavelength on temperature and input current was measured using an Ocean Optics HR4000 High Resolution Spectrometer (Figure 2.10). It was found that the average increase in wavelength with regard to increase in temperature is 0.29 nm/°C with the total variance in wavelength over the operating temperature range of 20-30 °C and input current range of 10-55 A being 5 nm. These results were essential to easily measure the wavelength dependence of the Nd:YLF crystals' absorption of pump light at a later stage.
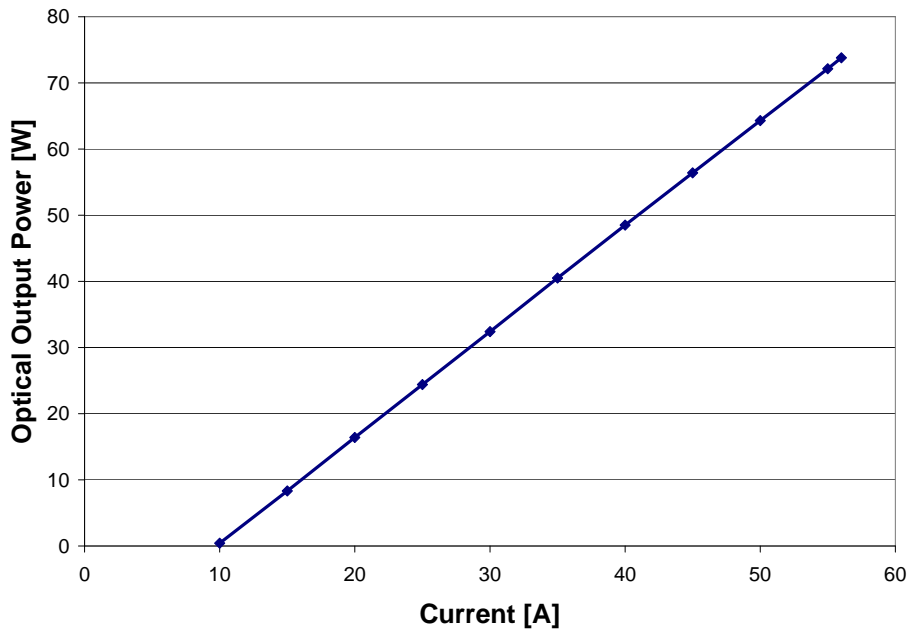
Figure 2.9: Average measured efficiency slope of Jenoptik laser diode modules at 25 °C. The individual laser diode modules's properties matched each other nearly exactly.
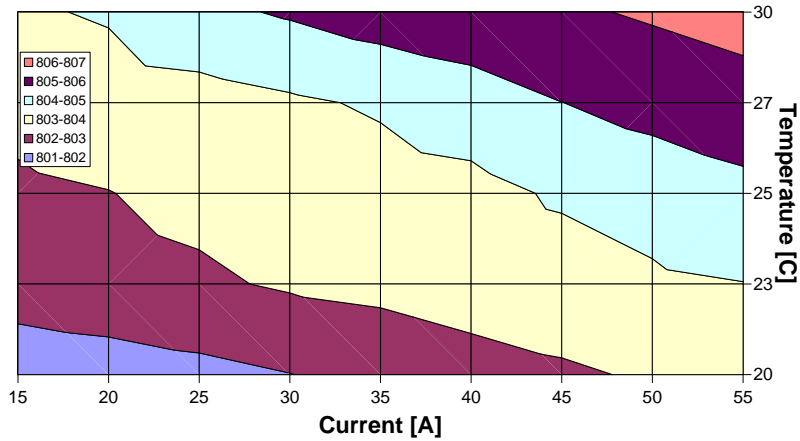
Figure 2.10: The measured dependence of output wavelength on temperature and current for one of the Jenoptik laser diode modules. The other modules exhibited the same behaviour, with very similar values.
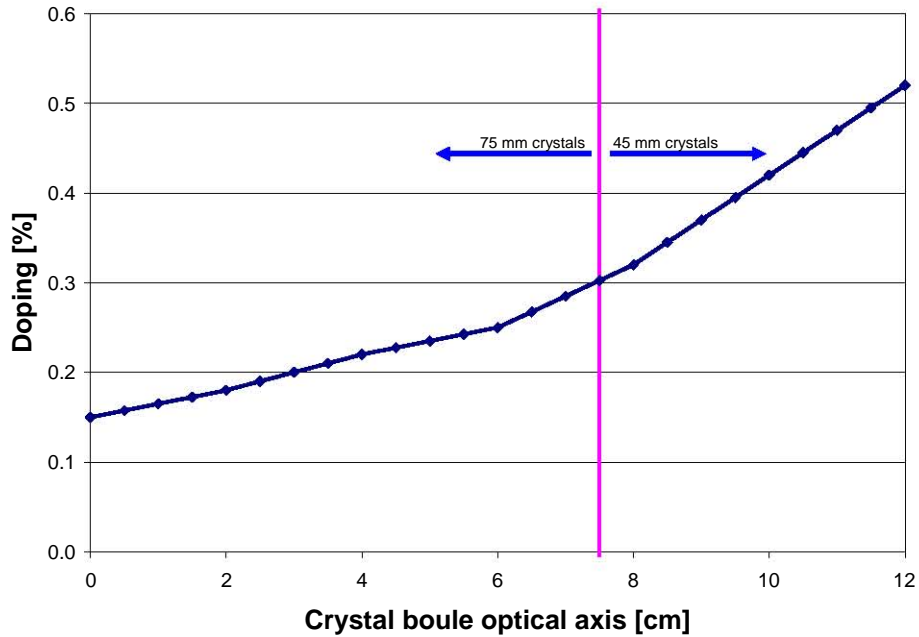
Figure 2.11: Nd:YLF crystal boule doping concentration along the optical axis as estimated by VLOC.

2.6 The Gain Medium

A Nd:YLF crystal boule (single-crystal ingot produced by synthetic means) was specially manufactured by VLOC. This boule had a much lower doping concentration than those generally used. Subsequently, it exhibited the desired doping gradient along the chosen optical axis, which is not as significant in higher doped crystals. The lower doping concentration results in a longer absorption length of the pump light in the crystals, and by pumping the lower concentration side of the crystals, the pump light is absorbed more uniformly along the length of the crystals. The combination of these two properties results in a more uniform heat load, and lower temperature at the pump face of the crystal, and thus decreases the stresses experienced by the crystal under high-power pumping.

The crystal orientation information was maintained during the manufacturing process of the individual crystals. The estimated Neodymium doping gradient along the optical axis ($\perp$ to crystal c-axis) was provided by VLOC (Figure 2.11). Four 45 mm and four 75 mm long rods were cut from the boule, each with a diameter of 6 mm
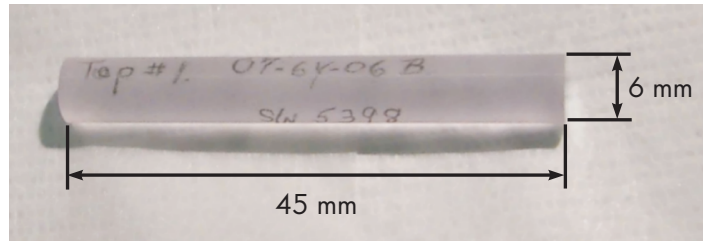
Figure 2.12: A 45 mm Nd:YLF crystal rod. The lower doped side is indicated by "Top" by the manufacturer.

(Figure 2.12). The 75 mm crystal rods were extracted from the material on the left side of the pink line in Figure 2.11, while the 45 mm rods came from the right side of the line. As a result the integrated doping over the entire length of the crystals was approximately the same for the 75 mm and 45 mm crystals. Therefore the average absorption would be the same as well.

For the reported work, only the 45 mm rods were used and are subsequently discussed as the longer 75 mm crystals posed greater difficulties for the mounting technique implemented. The four rods were labelled 1 (serial number: 5398), 2 (serial number: 5397), 3 (serial number: 5400) and 4 (serial number: 5399). The 45 mm crystal rods' estimated doping gradient is shown in Figure 2.13. The low-doped or pump side (indicated by arrow in Figure 2.13) had a relative doping concentration of 0.30 % with a nearly linear increase along the optical axis resulting in a concentration of 0.52 % on the other end, with an average doping of 0.41 %.

A finite element analysis of the temperature in these crystals was done by E. Bernhardi using programs he developed during his studies for his Master's Degree in Science (Bernhardi, 2008). For this analysis the same parameters as those of the laser presented in this chapter were used, but a flat-top beam profile was assumed for the pump to make the calculations easier. The resultant graphs are shown in Figure 2.14. The results showed that the temperature of a crystal pumped from the high-doped end would be significantly higher than the temperature of the same crystal when pumped from the low-doped end with the same power. It was further found that to reach the thermal fracture limit of the crystal when pumped from its low-doped end, it can be pumped 58 % harder than when the crystal is pumped from its high-doped end. This further supported the view that this would be a successful scaling approach.
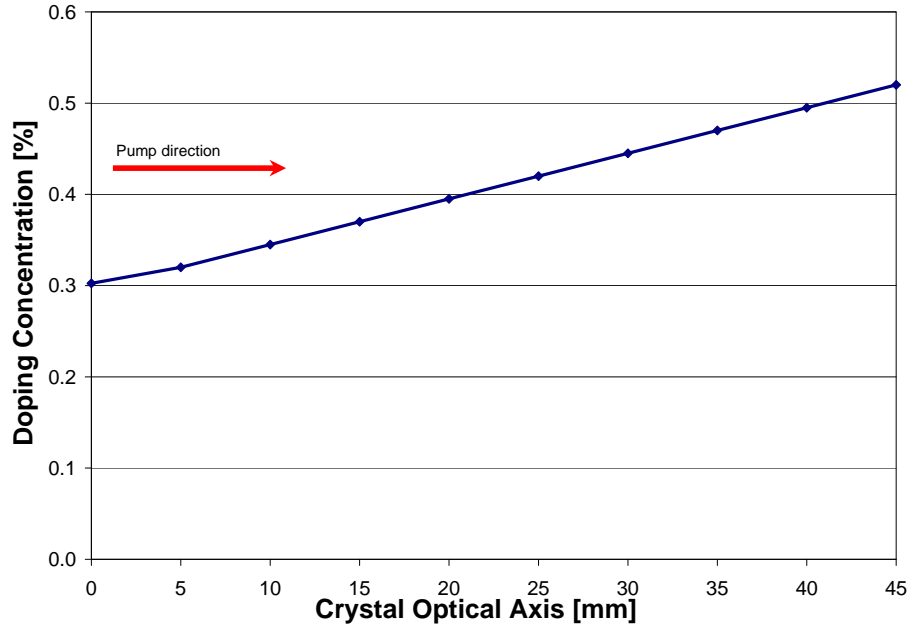
Figure 2.13: Estimated doping concentration of the four 45 mm Nd:YLF crystals along the optical axis.
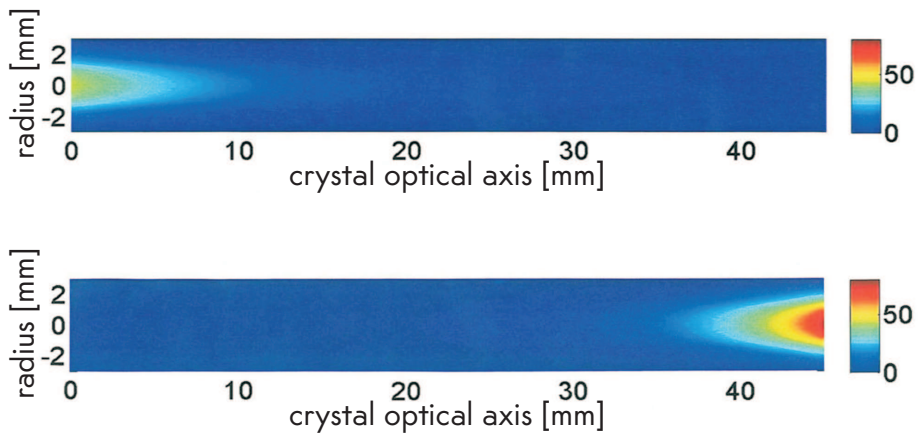
Figure 2.14: The simulated temperature in the 45 mm Nd:YLF crystals when pumped with 75 W from the low-doped end (top) and the high-doped end (bottom) (Bernhardi, 2008).
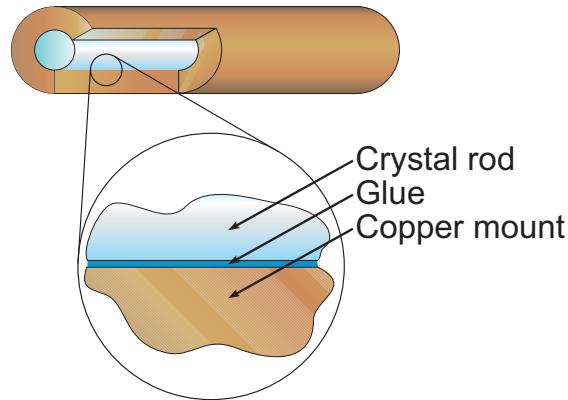
Figure 2.15: Design of mounted Nd:YLF crystal.

For proper cooling the crystal rods were glued into copper sleeves with Norland Optical Adhesive No. 61 (Figure 2.15). To ensure maximum accuracy in the diameter and straightness of the holes in the sleeves, the holes were canon drilled and reamed. The holes' diameters were between 20 and 30 μm larger than the crystals, thus the resultant gap between the copper and crystal surfaces would be between 10 and 15 μm. Decreasing this gap to less than 10 μm resulted in great difficulty during the gluing process. By gluing the rods in this fashion, uniform conductive cooling was obtained throughout the length of the crystals.

With these round rods, the crystal axis needed to be rotated while lasing in order to orientate them correctly in the resonator to obtain lasing on the σ-polarisation.

The copper-sleeved crystals were then clamped into copper mounts which were cooled with water supplied from the same chillers that cooled the laser diodes. The water temperature was kept in the region of 18 °C. The four mounted crystals are shown in Figure 2.16.

2.6.1   Absorption of laser diode light

To find the optimum wavelength at which to pump the crystals for maximum pump light absorption, the wavelength dependence of the crystals' absorption of pump light was measured for both σ- and π-polarised pump light. Once the optimum wavelength was found from the results, the laser diode modules' temperature could then be adjusted accordingly for the chosen wavelength by referring to the wavelength variance graph
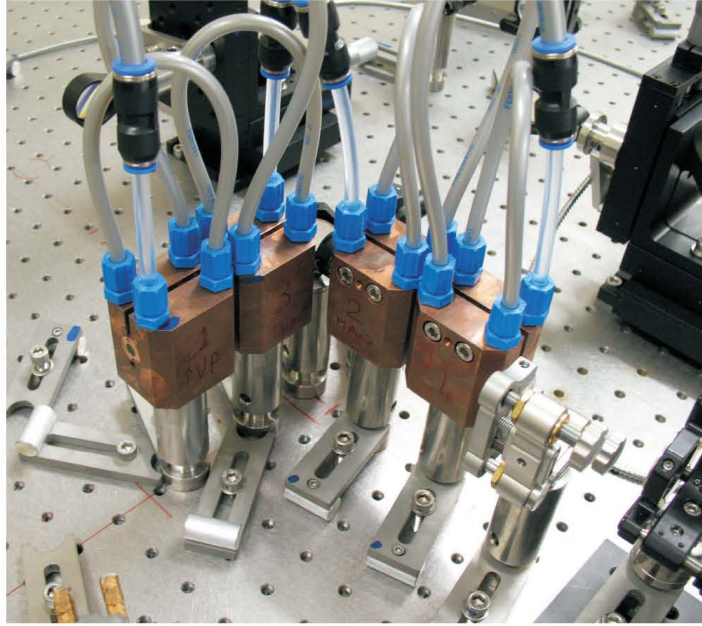
Figure 2.16: Four mounted Nd:YLF crystals in resonator.

shown in Figure 2.10. The experimental set-up is illustrated in Figure 2.17. The laser light emitted from the fibre was collimated using a spherical lens with a focal length of 25 mm and was then passed through a polarising beam splitter cube. The transmitted light was thus linearly polarised. The polarisation could then be arbitrarily rotated by changing the $\lambda/2$-plate's orientation. It was therefore possible to measure both the σ- and π-absorption values with ease. An aperture was put in front of the crystal so that only the crystal and not the mount was illuminated. The total and the transmitted pump light was measured with a HTD-LM45 Coherent power meter by inserting and removing the crystal in a reproducible manner. The pump light's wavelength was adjusted by changing the laser diode's temperature and was measured using the same Ocean Optics spectrometer which was used to obtain the results shown in Figure 2.10. The laser diode's operating current was in the region of 40 A. After any adjustment of the laser diode, measurements were only made well after the output power and wavelength of the laser had stabilised. The crystals were kept at a temperature of $\sim$18 °C.

The resultant absorption spectrum for crystal 1 is shown in Figure 2.18. The other three crystals displayed similar characteristics. The averaged absorption peak in the
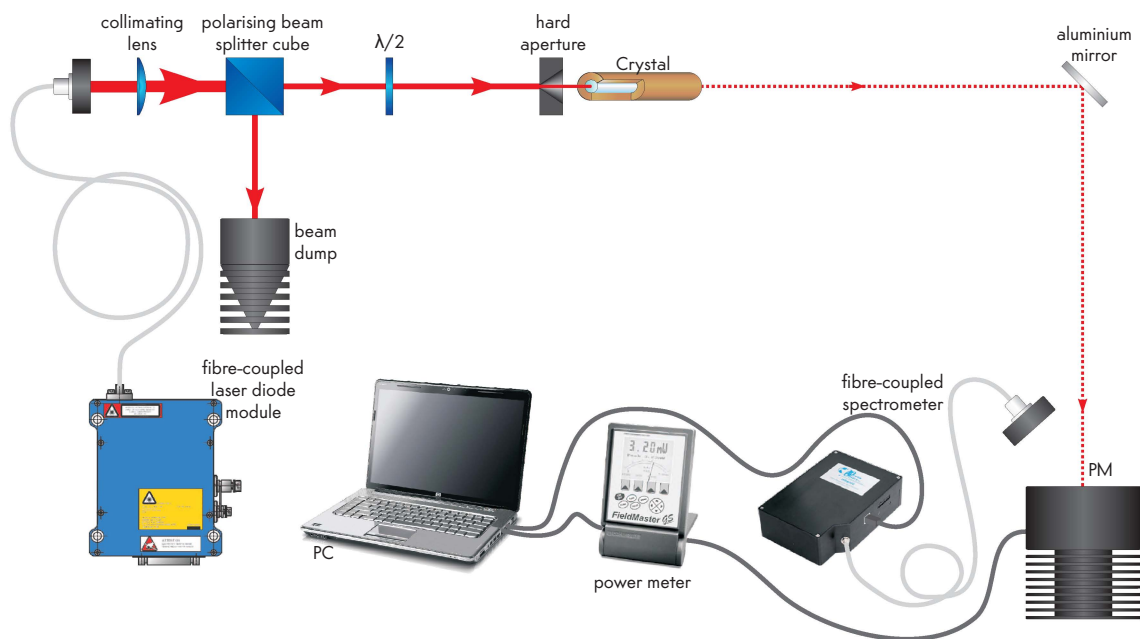
Figure 2.17: Nd:YLF crystal pump light absorption setup. The pump light is split into its two polarisations by a polarising beam splitter cube. The subsequently polarised transmitted light's polarisation could then be changed by rotating the $\lambda/2$-plate to have either σ- or π-polarised light for the absorption measurements.
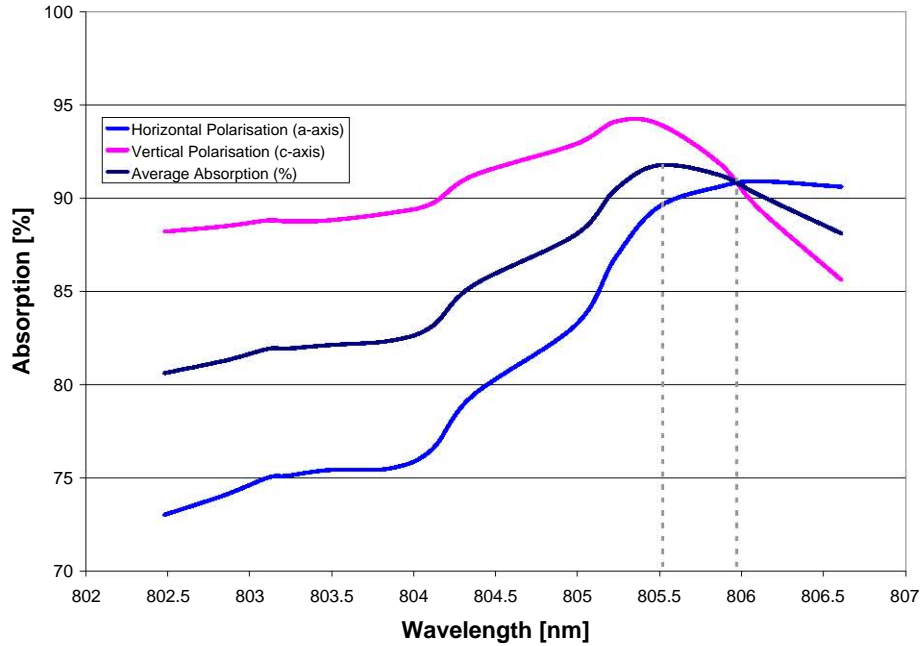
Figure 2.18: Nd:YLF crystal 1 absorption of pump light. The other crystals exhibited similar behaviour.

measured region was at 805.5 nm with the σ and π absorption being 94 % and 89 % respectively. 806 nm was also a feasible pump wavelength as the σ- and π-absorption values are the same in that region, resulting in more uniform absorption. It was concluded from Figure 2.18 and 2.10 that at full power ($\sim$55 A), the laser diode temperatures should be set to 27 °C which resulted in a pump wavelength of 805.5 nm for maximum pump absorption efficiency.

Normally the remaining 10 % of pump light that is transmitted through each crystal in the resonator would be wasted. By placing the crystals back to back, as shown in Figure 2.16, each crystal also absorbed the pump light transmitted by the crystal standing right next to it, leading to optimal pump light absorption.
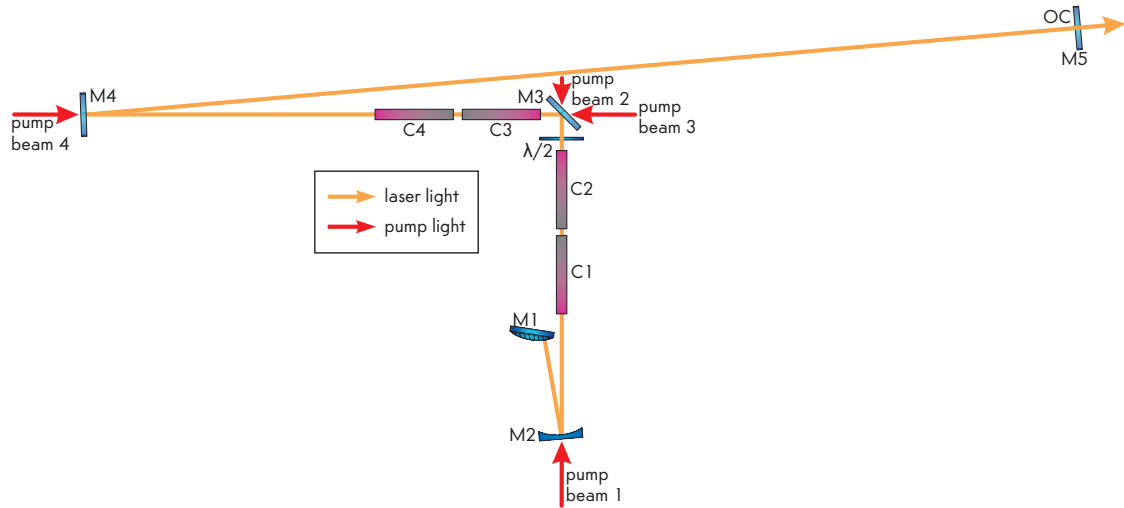
Figure 2.19: Nd:YLF laser resonator layout.

2.7   The Resonator

The desired attributes mentioned in Section 2.1 in conjunction with the properties of the materials and equipment used, impose the following criteria on the resonator design:

- The resonator should be adjustable to compensate for the varying thermal lens strengths of the crystal rods under different pump powers.

- The astigmatic thermal lens of the Nd:YLF crystals should be compensated for by the resonator design.

- Lasing should be ensured on the 1053 nm (σ-polarisation) laser transition to exploit the weak thermal lens, despite this polarisation having a lower emission cross-section than the π-polarisation (1047 nm). This can be accomplished by designing the resonator to be unstable for stronger negative thermal lensing which induces high losses for the π-polarisation and thus forces the laser to operate on the σ-polarisation.

- The resonator should be relatively long to increase the cavity round trip time of

the laser light and subsequently increase the pulse build-up time when the laser is operated in Q-switched mode. The resulting longer pulses reduces the chance of damage, and the long build-up time facilitates AOM switching.

- Too high gain should be avoided as this may surpass the losses introduced by the AOM, thereby causing the system to lase even when the AOM is active. This would prevent pulsed operation.

- The resonator mode on the mirrors should be large in order to avoid optical damage due to too high energy densities on their dielectric surfaces.

- The low doping end of all four crystals should be accessible for end-pumping by the fibre-coupled laser diodes. There should be a good spatial overlap of the pump beam and the resonator mode to ensure efficient use of the excited area in the gain medium (Clarkson, 1998).

- The resonator mode in the crystals should be large. This results in having as large an active volume as possible to maximise energy storage for optimal pulsed operation.

As just mentioned, for maximum energy storage the resonator mode in the crystals should be large in order to have as large an active volume as possible. However, this increases the lasing threshold, as can be seen from the lasing threshold pump power equation (Fan & Byer, 1988):

$$P_{TH} = \frac{h\nu_P}{4\eta_P \sigma_L^{em} \tau} (A_P + A_L)(T + L) \tag{2.1}$$

where $h\nu_P$ is the pump photon energy, η_P the pump efficiency, σ_L^{em} the effective emission cross-section and τ the upper laser level lifetime. A_P and A_L are the cross-sectional areas of the pump and laser beams respectively. T is the output coupler transmission at the laser wavelength and L includes the other resonator losses.

The slope efficiency of the laser is given by (Fan & Byer, 1988)

$$\eta_{slope} = \eta_P \frac{h\nu_L}{h\nu_P} \left(\frac{T}{T + L} \right) \tag{2.2}$$

where $h\nu_L$ is the laser photon energy.
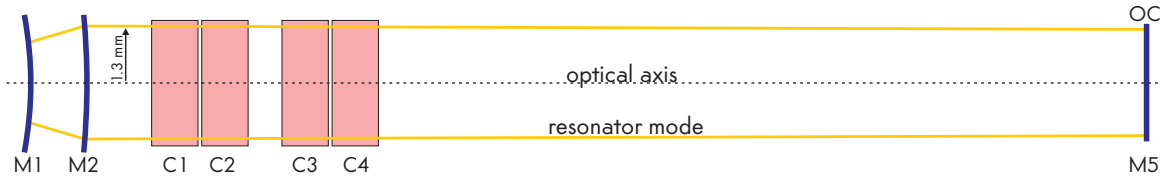
Figure 2.20: A beam diagram of the resonator mode as calculated by Paraxia software.

From these equations, one can see that while increasing the output coupler transmission increases the laser threshold, it also increases the slope efficiency, and is therefore beneficial for laser performance. However, while increasing A_P and A_L would increase the laser Q-switching performance, it also increases the laser threshold while the slope efficiency remains unchanged, therefore decreasing cw performance. Thus it is required that both pulsed performance and cw performance are taken into consideration when designing a laser that need do both.

To comply with these criteria a folded resonator cavity was implemented. The physical layout of the resonator is shown in Figure 2.19. This resonator is conceptually a three mirror cavity consisting of a short arm, from mirror M1 to mirror M2, and a long arm, from M2 to M5, similar to the Nd:YLF laser discussed by D. Esser (Esser, 2004). By making M1 a convex mirror (as done by Esser) instead of a concave mirror (as done by Clarkson (Clarkson, 1998)), the short arm length becomes shorter and the spot size on mirror M1 increases. This is beneficial both from a space perspective and from an optical damage point of view. The mode in the long arm is relatively large and collimated in such a configuration, with the mode size being variable by changing the short arm length (Clarkson, 1998). The resonator mode for this configuration, as calculated by Paraxia software (SCIOPT, 2010), is shown in Figure 2.20. The long arm is folded further by flat mirrors M3 and M4 to enable end-pumping of crystals C2, C3 and C4.

Another feature of this resonator is that with a small adjustment of the short-arm, the mode size can be changed to compensate for the thermal lens. One can therefore compensate for the thermal lens introduced by the crystal rods by simply changing the distance between M1 and M2.

2.8   Experimental Setup

The overall layout of the experimental setup is shown in Figure 2.21. The light from the four laser diode modules was coupled through optical fibres 0.4 mm in diameter with a numerical aperture (NA) of 0.22. The light exiting the fibres were collimated using plano-convex lenses with a focal length of 25 mm and diameter of 25.4 mm placed approximately 25 mm from the end-tip of the fibre (Figure 2.22). After propagating 870 mm, the collimated light was focused into the crystals using a plano-convex lens, 25.4 mm in diameter, with a focal length of 175 mm. The beam waist was approximately 1.2 mm, occurring 226 mm from the focusing lens. This resulted in a pump beam with a waist well matched to the resonator mode's and a Raleigh length ($\sim$56 mm) longer than the crystal length (45 mm).

The intensity profile of light emitted from a highly multi-mode fibre is bell-shaped in the far field (Bollig *et al.*, 2005). This could be advantageous for end-pumping of the crystals as the pump intensity profile would then match the intensity profile of the laser light in the crystals, resulting in improved energy extraction from the gain medium (Strauss, 2009). The pump lens setup was done with this in mind, resulting in longer propagation distances between the collimation lens and focusing lens than one would think necessary.

Each of the four 45 mm long Nd:YLF crystals were placed so that the focus of a pump beam would be in the centre of the crystal. The low-doped end of each crystal faced the incoming pump light. The crystals were placed in pairs (C1, C2 and C3, C4) in order that any pump light transmitted by the one crystal (approximately 10 %) will be absorbed by the other. In order to pump each crystal from its low-doped end, the two crystal pairs were placed 90 ° with respect to each other.

The strong astigmatism of the thermal lens of the crystals was compensated for by using two crystals with the c-axis vertical and two with the c-axis horizontal with a $\lambda/2$-plate in-between the two pairs. The $\lambda/2$-plate ensured that the polarised laser light in the resonator would experience the same crystal orientation in both crystal pairs.

The laser cavity consisted of mirrors M1 through M5. M1 was a convex mirror with a 150 mm radius, with a highly reflective dielectric coating for 1053 nm light. M2 was a concave mirror with a radius of 400 mm, highly reflective for the 1053 nm laser
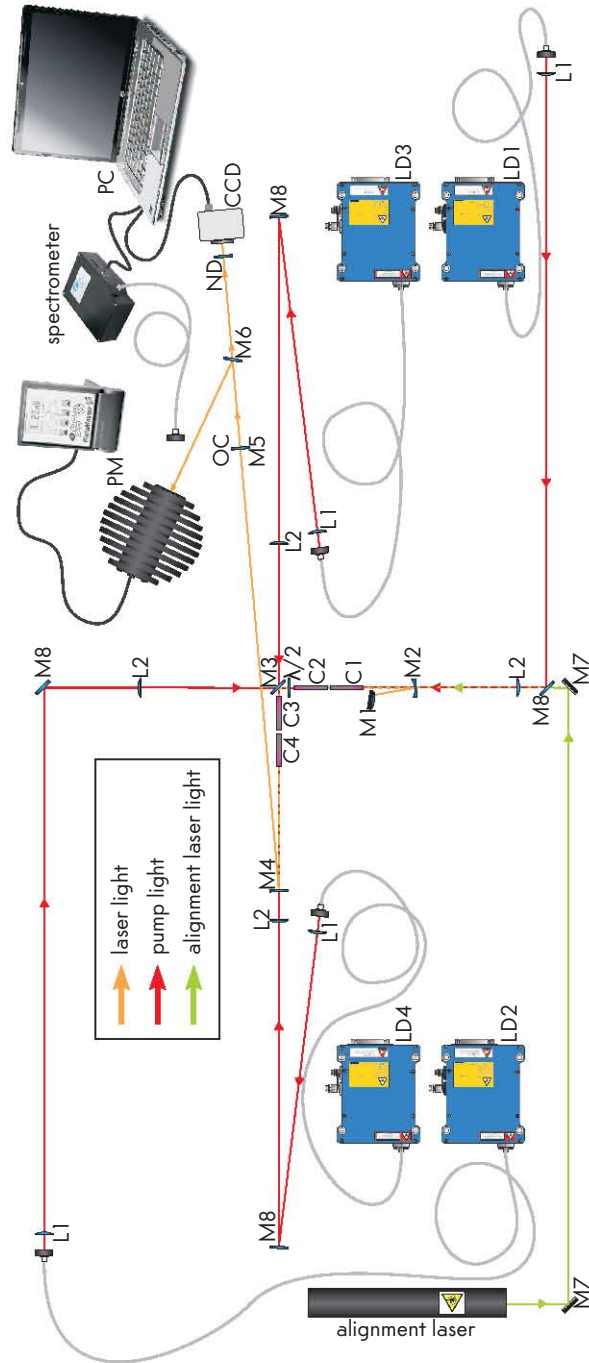
Figure 2.21: The experimental setup, including pump sources, laser resonator and diagnostics.
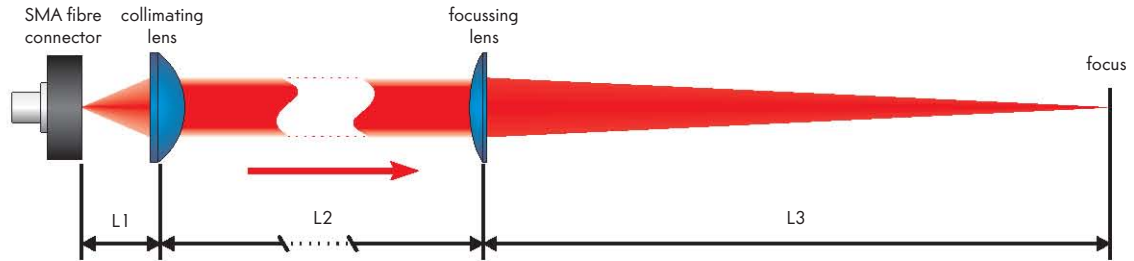
Figure 2.22: Pump optics setup. The light exiting the fibre is collimated with a f=25 mm lens and focused with a f=175 mm lens. Distances. L1, L2, and L3 are 25 mm, 870 mm, and 226 mm respectively.

light and highly transmissive for the 805 nm pump light. M3 and M4 were flat mirrors highly reflective at 1053 nm and highly transmissive for 805 nm. The output coupler mirror (M5) could be interchanged in order to use mirrors with reflectivity R=50, 70, and 80 % at 1053 nm.

The short-arm of the resonator was between mirrors M1 and M2. The distance between M1 and M2 was approximately 55 mm and could be varied by a few millimeters to compensate for the thermal lensing effects of the crystals. The long-arm was between M2 and M5. The distance between M2 and M3 was 185 mm, between M3 and M4 275 mm, while the distance from M4 to M5 was 600 mm, giving a total long-arm length of 1060 mm.

The diagnostic equipment consisted of a power meter, a spectrometer, and a CCD laser beam profiler connected to a computer. A 200 W Coherent LM-200 power meter head was used in conjunction with a Fieldmaster Power meter to measure the laser output power. An Ocean Optics HR4000 fibre-coupled spectrometer was used to measure the laser wavelength. To record the laser beam profile, a Spiricon CCD camera was used. Both the spectrometer and the CCD camera interfaced with the computer.
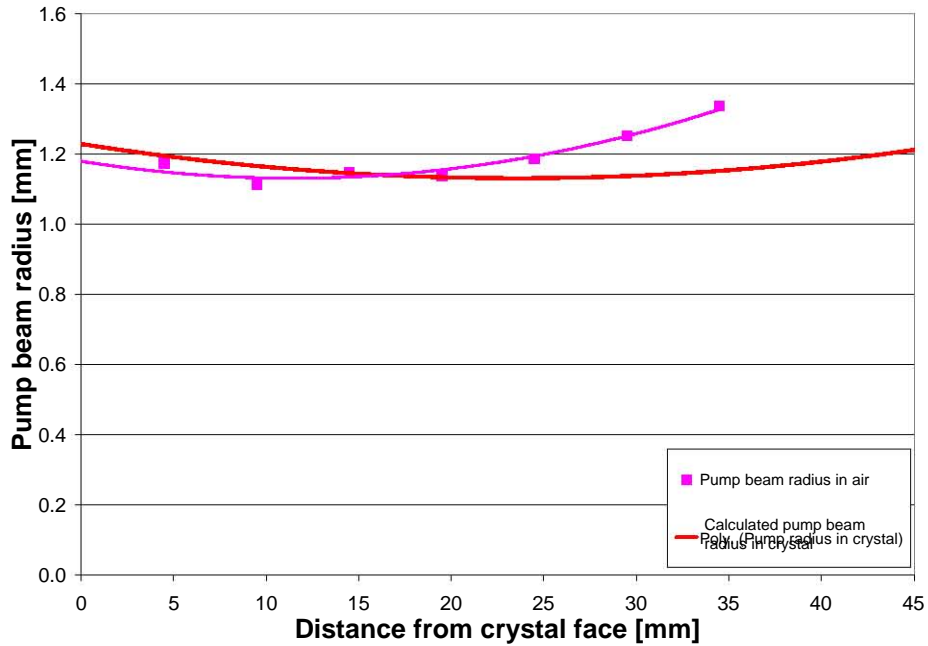
Figure 2.23: The pump beam radius at the crystal position for crystal C4. The measured pump beam radius in air is shown by the magenta squares. The calculated beam radius in the crystal is depicted by the thick solid red line. The crystal pump face is at 0 mm with the opposite end-face at 45 mm. The beam quality factor (M^2) can not be accurately calculated since there are no data points which are sufficiently far away from the focus.

2.9   Results

2.9.1   The Pump Light

The beam radii of the diode laser modules were measured using a Spiricon CCD camera to confirm that the pump light in the crystal matched well with the calculated resonator mode. These measurements were done with the laser diodes operating just above their lasing threshold where their beam sizes are roughly the same size as at full power.

The measured beam radius in air of laser diode LD4 where crystal C4 was situated is shown in Figure 2.23. However due to the higher refractive index of YLF (n=1.45), the focus of the pump light was farther along the optical axis in the crystal. Figure 2.23 therefore also shows the calculated pump beam radius in the crystal along its optical axis. From this we see that throughout the length of the crystal the pump beam radius
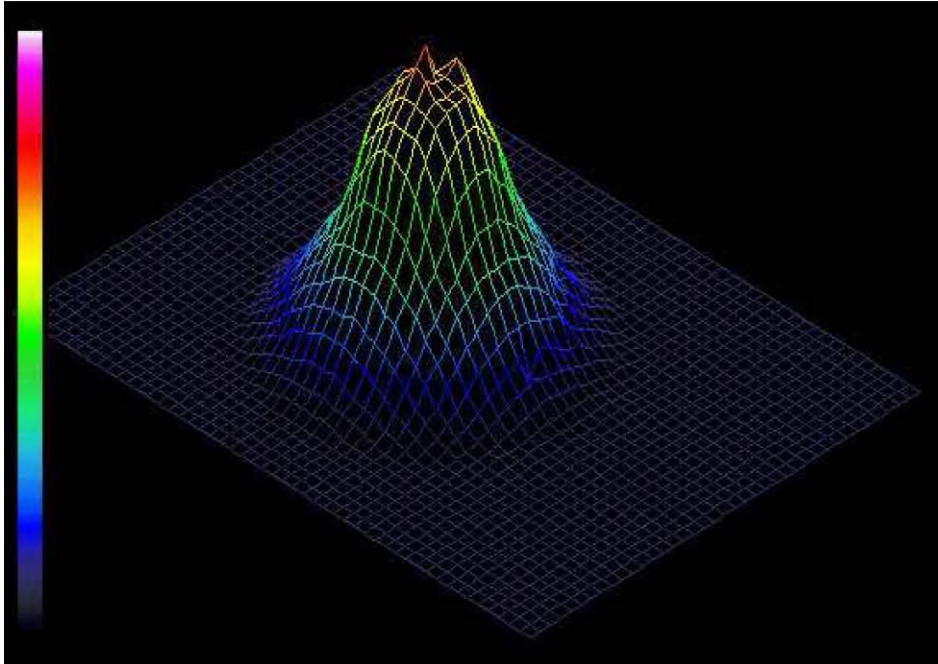
Figure 2.24: The pump beam intensity profile at the focus in the far field, as indicated in Figure 2.22.

varied between 1.1 and 1.2 mm with the focus being in the middle of the crystal. This was well matched with the calculated resonator mode size where the crystals were placed.

From the pump beam intensity profile shown in Figure 2.24 it was confirmed that it was bell-shaped. The other crystals were set up in a similar fashion.

2.9.2   Laser Performance

The efficiency slopes of the laser for various output couplers are shown in Figure 2.25. Output couplers with a reflectivity of 80, 70, and 50 % were used. The laser threshold with respect to pump power was 18 W, 26 W, and 44 W for the the output couplers respectively. The highest efficiency was obtained with the 50 % output coupler resulting in a maximum output of 87 W cw with a slope efficiency of 36.5 % with respect to diode power. This is the highest power from a diode-end-pumped Nd:YLF laser ever reported. Good beam quality was observed across the power range of the laser, with the beam diameter decreasing slightly with increased output power (Figure 2.26). Fluctuations
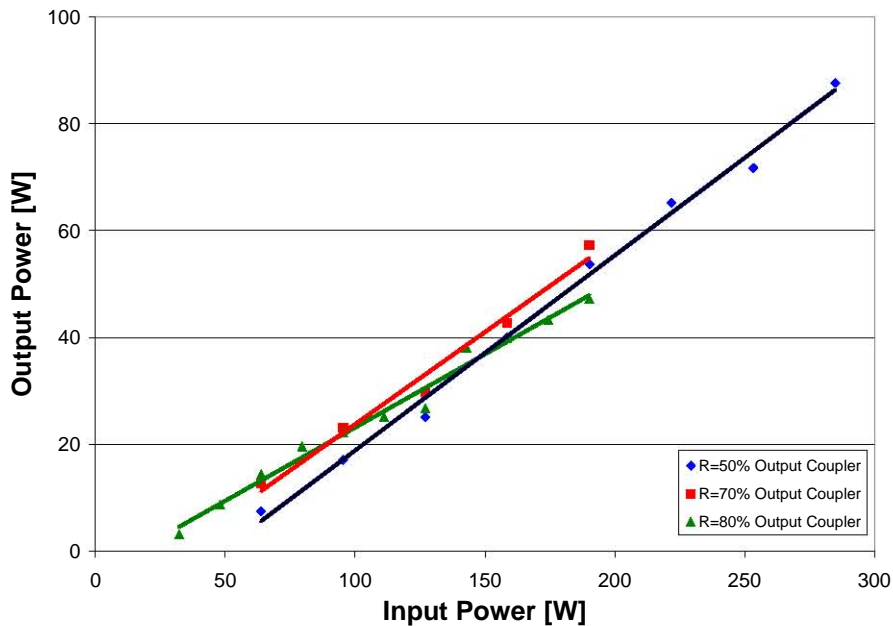
Figure 2.25: Nd:YLF laser output power vs. input power for various output couplers.

in the output power and beam pointing were observed with the output power dropping by up to 10 percent.

2.10 Discussion

No crystal fracture occurred during the experiments, even when all four diode laser modules were pumping the crystals at full power under non-lasing conditions - the case where thermal stresses are highest. When compared to other reported work where crystal fracture was mentioned, it may be deduced that the improved mounting of the crystals in addition to exploiting the doping gradient of low-doped crystals, resulted in a decrease of thermally induced stresses. This view is supported by the simulation work done by Bernhardi which indicated that the crystals can be pumped 58 % harder when pumping from the low-doped side before reaching the thermal fracture limit, when compared to the high-doped side (See Section 2.6) (Bernhardi, 2008).

The performance of the laser however, proved to be lower than expected when compared to the laser reported by Bollig et al. which delivered 60 W cw when pumped
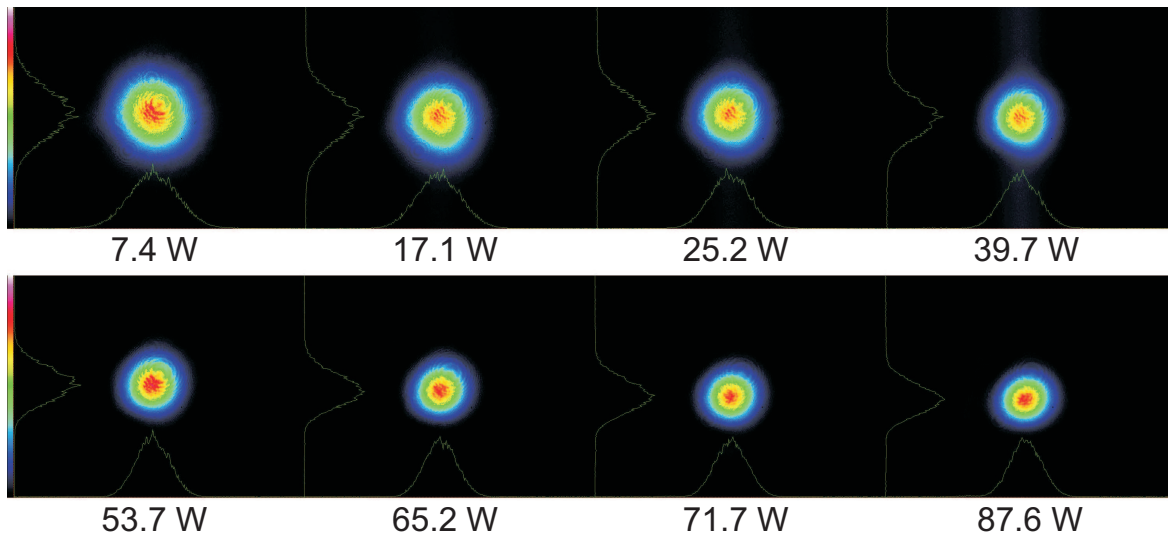
Figure 2.26: Beam profile of the Nd:YLF laser at various output powers for a R=50 % output coupler. The minor distortions seen were caused by various optics between the output coupler and the CCD.

by 158 W (Bollig *et al.*, 2005). In addition, the fluctuations in output power and beam pointing showed the laser to be rather unstable in the second timescale.

2.10.1 Findlay-Clay and Caird Loss Analysis

Subsequently, both the resonator design and experimental setup were scrutinised. Using the laser threshold and efficiency slopes for the various output couplers, the resonator loss was estimated using Findlay-Clay and Caird analysis and was found to be between 10 % and 15 % (Findlay & Clay, 1966; Koechner, 1970). This was far higher than one would expect. The laser and its separate components were therefore studied to ascertain what the cause of these high losses might be.

2.10.2 Laser Light Scatter Losses in Crystals

To determine whether the crystal rods were responsible for the high resonator losses, the transmission of laser light through the crystal rods was measured using the experimental set-up shown in Figure 2.27. From this one may deduce the total losses introduced into the resonator cavity by the crystals. A Coherent diode-pumped solid-
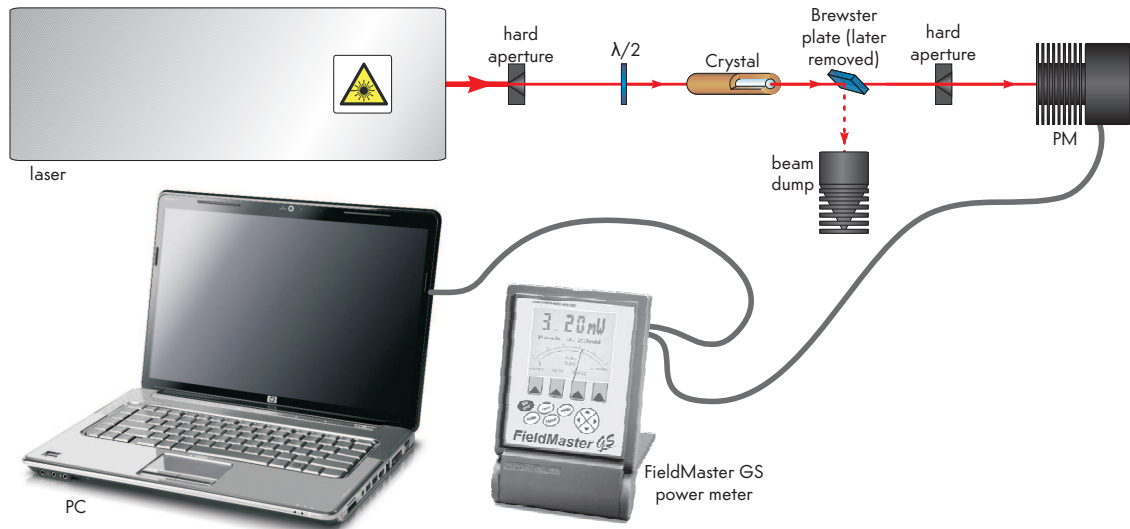
Figure 2.27: Nd:YLF crystal scatter loss setup. The Brewster plate was only for initial calibration of the polarisation and was later removed.

state laser emitting 10 W of linearly polarised, stable cw light at 1064 nm was used as the probe beam. Using a 2.0 mm hard iris, the laser beam size was reduced to fit into the crystal before passing through a rotatable $\lambda/2$-plate which enabled easy rotation of the plane of polarisation of the light before entering the crystal rod. Initially the $\lambda/2$-plate was used to see if the laser light transmission of the crystals was dependent on the polarisation. The transmitted light from the crystal was then passed through a second aperture shielding the HTD-LM45 power meter from as much scattered light as possible by placing the aperture close to the power meter, and the power meter as far from the crystal as possible. Thus even light scattered through a small angle would not reach the power meter's surface.

Even though the probe laser was very stable, care was taken to obtain accurate readings of the very small losses by using dedicated data logging software and averaging over long periods of time (in the order of tens of seconds). Many readings were taken for each crystal by repeatedly inserting and removing the crystal while the logging software was recording the optical power. Through this technique, the resulting uncertainty in the measurements was less than 0.1 %.

The Brewster plate was initially used to calibrate the orientation of the $\lambda/2$-plate and confirm the degree of polarisation of the probe laser, after which is was removed.

The results showed that all of the 45 mm crystal rods transmitted more than 99.7±0.1 % of the incident light. Therefore, inserting the four crystal rods into a resonator cavity, a maximum of 2.4 % is added to the resonator round trip loss.

It was concluded from these measurements that all the crystals were of good optical quality and therefore not the cause of the laser's behaviour.

2.10.3 Resonator Alignment Sensitivity

In order to evaluate the resonator design, the stability diagram of the laser is shown in Figure 2.28 for lasing at 1053 nm. The following analysis has been derived from work presented in (Magni, 1986). From Figure 2.28 we can see that the laser, depending on the short arm length, can operate in one of two zones (thanks is given to Hencharl Strauss for providing the helpful spreadsheet which generated this graph). With the short arm between 200 and 246 mm long the resonator would operate in zone I, whereas it would operate in zone II when the short arm is between 50 and 96 mm. The relative alignment sensitivity of the resonator is depicted by the blue X's. From this we can see that the resonator, when operating in zone I, is quite insensitive to changes in alignment and other interferences. However, one also observes that the resonator mode size on the convex (M1) mirror is very small, about 80 μm. This is far too small for high energy laser resonators as it will result in optical damage of the mirror. The alternative is to operate in zone II, which was the case for this experiment.

Operation in zone II entails working with a laser that is far more sensitive to alignment and environmental changes (vibration, air, etc.). However, it does have the advantage that the resonator mode on the mirrors is considerably larger, with the smallest spot on mirror M1 being 550 μm when the short arm length is 76 mm. In zone II there is a good spatial overlap of the pump light with the resonator mode in the crystals which should have boded well for optical-to-optical efficiency.

Due to restrictions discussed in Section 2.8, the long arm of the resonator was 1060 mm long. From the misalignment sensitivity shown in Figure 2.28 it is deduced that the issues the laser exhibited at this long arm length could be because the laser operated in the more sensitive area of zone II (indicated by arrow), which made the laser very sensitive to misalignment and to small fluctuations in the pump overlap and variations in diffraction in the air. The lower than expected output power may also be
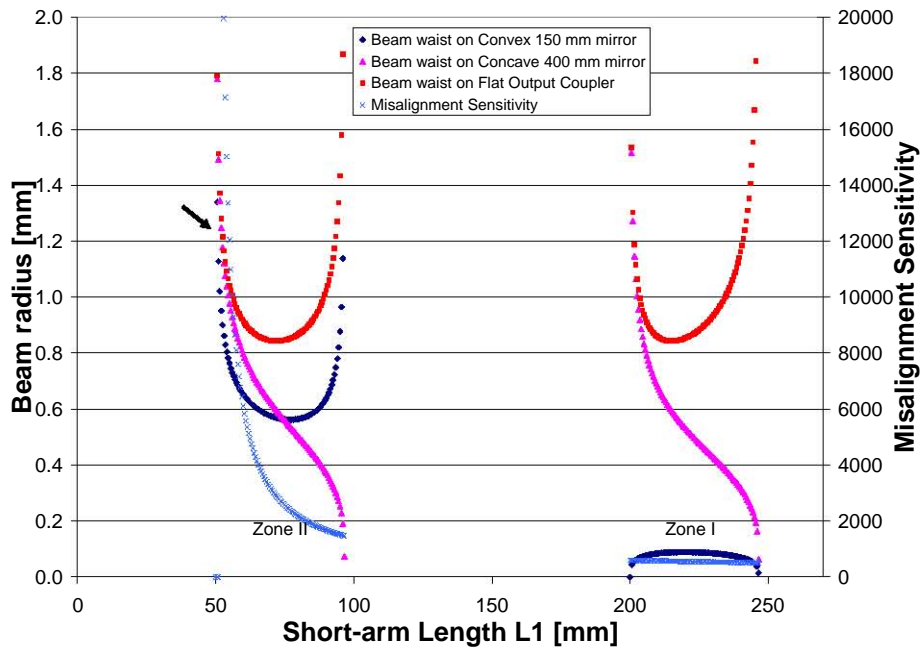
Figure 2.28: Mode size on resonator mirrors and misalignment sensitivity on short arm length of a resonator with a long arm length of 1060 mm. The area of operation is indicated by the arrow.
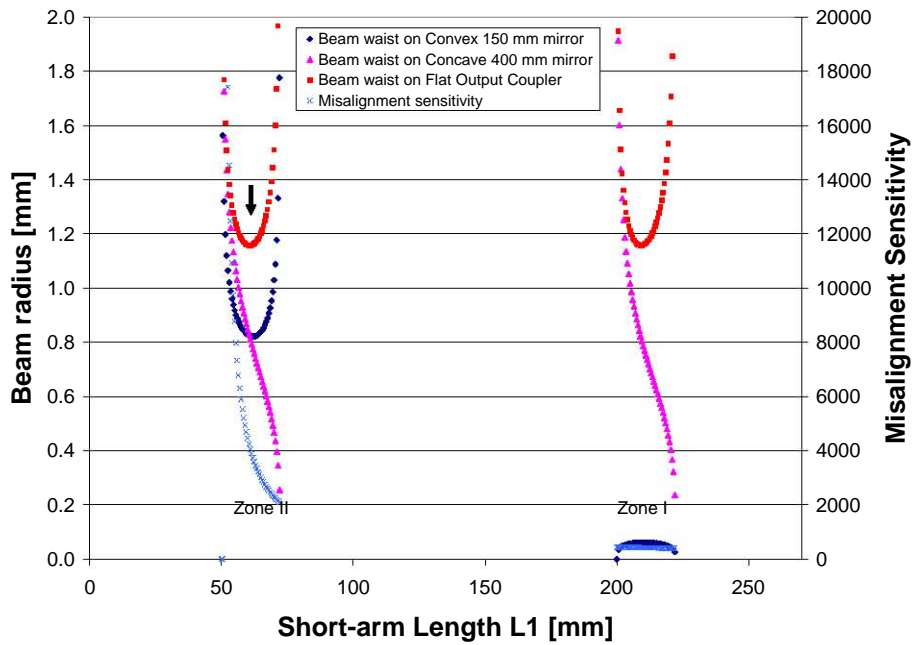
Figure 2.29: Mode size on resonator mirrors and misalignment sensitivity on short-arm length of a resonator with a long-arm length of 2000 mm. The intended area of operation is indicated by the arrow.

ascribed to this, rather than to fixed resonator losses.

For future work a better option would be to increase the long-arm length of the resonator to 2000 mm. The resulting graph is shown in Figure 2.29. One could then operate the laser more towards the centre region of zone II by changing the short-arm length to ∼60 mm. As one can see from the graph, the laser would then be far less sensitive to misalignment while still having a well-collimated mode of similar size in the crystals.

2.11   Conclusion

In this chapter the highest power diode-end-pumped Nd:YLF laser ever reported was presented (Bollig *et al.*, 2008). Our improved crystal mounting in conjunction with the exploitation of the doping gradient of low-doped Nd:YLF crystals has been shown to be effective in addressing the thermal fracture issues relating to Nd:YLF lasers. This approach allowed the pumping of Nd:YLF with record pumping powers, demonstrating further that this is a good approach for the power scaling of Nd:YLF lasers.

For future work, the laser should be redesigned to operate in the more stable area of zone II (Figure 2.29). Efficient and stable operation in excess of 100 W should then be achievable. Q-switched operation should also be investigated as it has the potential to yield high average powers, even at repetition rates below 5 kHz.

Chapter 3

Compact High Power Ho:YLF Oscillator and Amplifier

3.1 Introduction

Q-switched lasers operating in the eye-safe $2\,\mu$m wavelength region have applications in a number of areas, including remote sensing, defence, materials processing and medical applications. Some of these fields require reliable and efficient operation in a compact device.

Initial work on $2\,\mu$m Holmium lasers concentrated on Thulium-Holmium co-doped operation (Fan *et al.*, 1988). More recently, work has concentrated on Ho lasers resonantly pumped by Tm lasers, both pumped intra-cavity (Bollig *et al.*, 1998) and extra-cavity (Budni *et al.*, 2000). With the emergence of high-power Tm-doped fibre lasers, efficient and robust Ho:YAG lasers pumped by Tm-fibre-lasers were demonstrated (Lippert *et al.*, 2003; Shen *et al.*, 2004; Lippert *et al.*, 2006).

In order to achieve high-energy Q-switched operation, Ho:YLF is a more attractive laser material than Ho:YAG since it has a much longer upper laser level lifetime ($\sim$14 ms versus 7 ms in Ho:YAG) and higher emission cross-section ($1.5 \times 10^{-20}\,\text{cm}^2$ at 2050 nm versus $1.0 \times 10^{-20}\,\text{cm}^2$ at 2091 nm for Ho:YAG) (Payne *et al.*, 1992; Walsh *et al.*, 1998). In addition, the very weak thermal lens on the σ-polarisation helps to deliver diffraction limited beams even under intense end-pumping.

However, Ho:YLF has a somewhat stronger quasi-three-level nature than Ho:YAG

(see Section 3.2.1). To reach gain at the 2065 nm line, 22 % of the Ho ions need to
be pumped into the upper laser level (at room temperature), but it already reaches
transparency at the 1940 nm pump wavelength with only 56 % of the Ho ions in the
upper laser level (see Appendix). In addition, the pump absorption at 1940 nm is
relatively weak and strongly polarised (Figure 3.1). Subsequently, the laser design
requires a trade-off between efficient pump absorption and low laser threshold.

In this chapter a compact Ho:YLF oscillator-amplifier system in a novel setup which
utilised the unpolarised pump power from a fibre laser efficiently, and produced 21.3 mJ
at 1 kHz, with an M^2 better than 1.1 is presented. The amplified energies agreed
well with the predicted values from a two dimensional rotational symmetric amplifier
model developed by Dr Martin Shellhorn. His model considered upconversion losses
and ground-state depletion, as well as the spatial distribution of the pump beam (Koen
et al., 2009).

3.2   Properties of Ho:YLF

3.2.1   The Quasi-Three-Level Ho:YLF laser

The quasi-three-level laser scheme of Holmium in YLF relevant to this work is shown
in Figure 3.2.

Initially the ions are in the ground state $^5I_8$. When an ion absorbs a pump photon
($\sim$1940 nm) it gets excited from the ground state to the upper laser level $^5I_7$ (red
arrows). The pump photon energy is close to the energy difference between these two
states. This upper level is a meta-stable state with a long lifetime. The excited ion
can then de-excite back to the $^5I_8$ state through stimulated emission by emitting a
photon of either 2050 nm or 2064 nm (blue arrows). Through rapid thermalisation, the
Boltzmann distribution in the ground state population is restored on the picosecond
scale. Thereafter the ion is ready to be excited by a pump photon once more. Given
that there is enough pump light and absorption thereof, a sufficient population may
occur in the upper state ($^5I_7$) to create gain at either 2050 nm or 2064 nm for lasing to
occur.

It must be noted that according to Walsh's definition discussed in the introductory
chapter of this dissertation, this is a quasi-four-level laser (Section 1.2.3), and not a
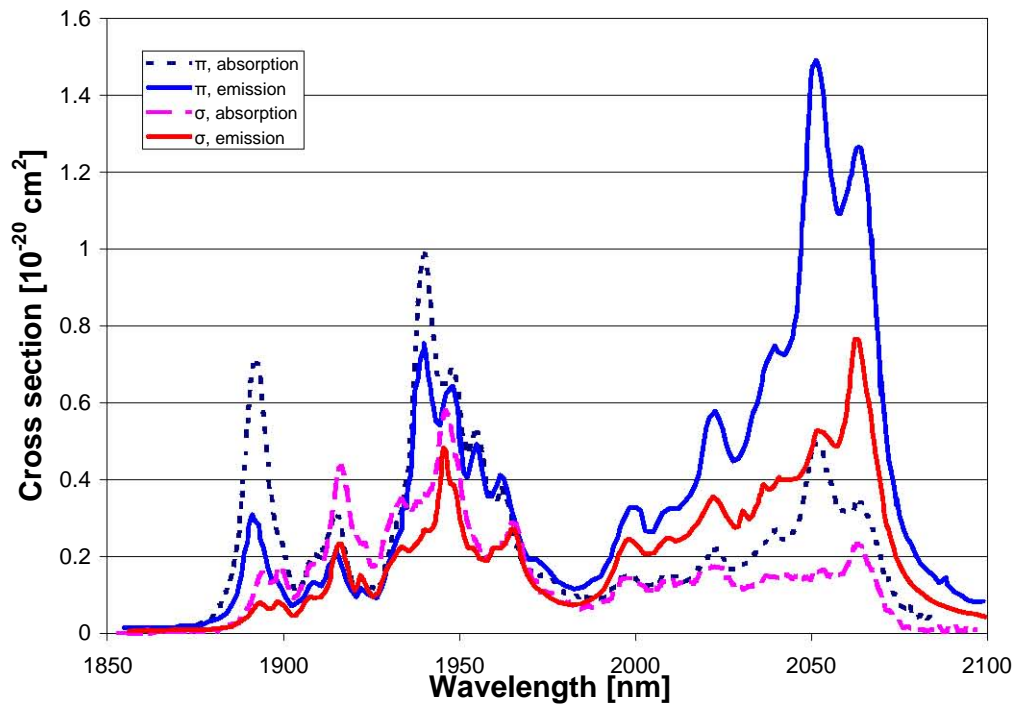
Figure 3.1: Ho:YLF absorption and emission cross-sections (Walsh *et al.*, 1998).
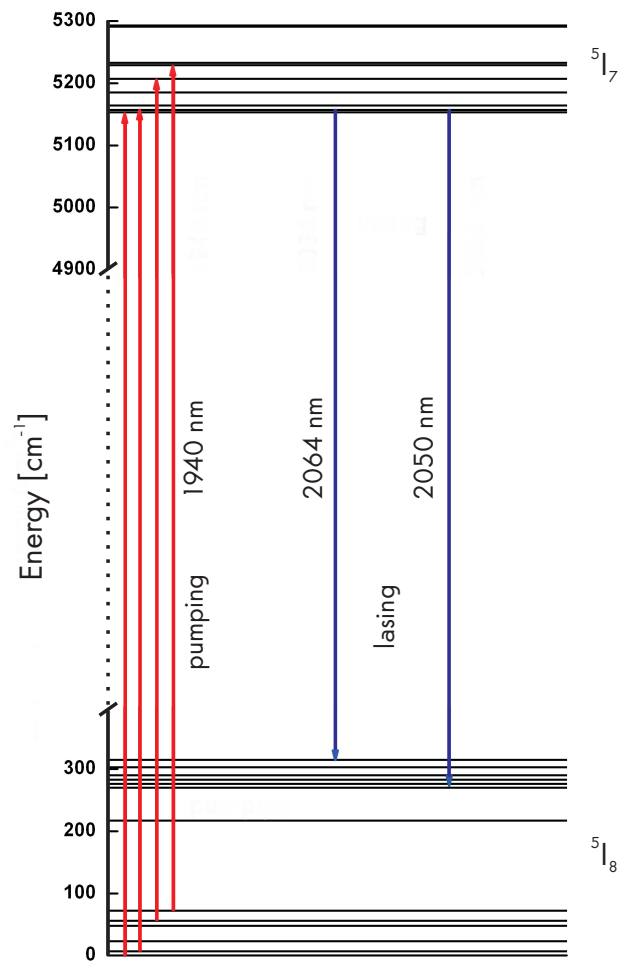
Figure 3.2: Schematic of the quasi-three-level Ho:YLF laser levels relevant to this work (Cross, 2005).
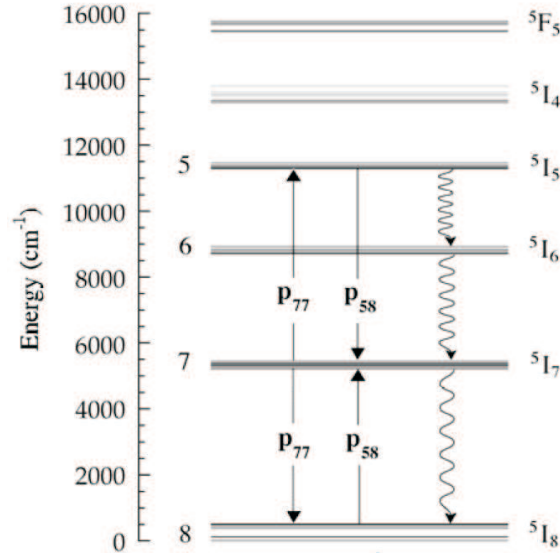
Figure 3.3: Schematic of the Ho-Ho energy transfer processes (Barnes *et al.*, 2003).

quasi-three-level, as described in the literature in the past decades. Walsh's definition however, is related to the gain of the laser and for these wavelengths and transitions the laser's gain does resemble a quasi-four-level laser more than a quasi-three-level.

However, if one studies the transitions in the energy-level diagram (Figure 3.2), it implies that this laser scheme is that of a quasi-three-level, despite behaving more like a quasi-four-level. Since the definition proposed by Walsh is fairly recent (Section 1.2.3 (Walsh, 2009)) and has yet to enjoy widespread use, historical convention is rather followed in this section, and therefore Ho:YLF lasers are referred to as quasi-three-level lasers in this chapter.

3.2.2   Ho-Ho Energy Transfer

Within the gain medium processes can occur where two Ho atoms interact so that one of the atoms is promoted from the $^5I_7$ manifold to the $^5I_5$ manifold, while the other atom is demoted from the $^5I_7$ manifold to the $^5I_8$ manifold. This upconversion process is indicated by the arrows in Figure 3.3 labelled as p_{77} (Barnes *et al.*, 2003). There is

also a self-quenching process where a Ho atom in the $^5I_5$ manifold and one in the $^5I_8$ manifold interact, resulting in two Ho atoms in the $^5I_7$ manifold. This is the reverse of the upconversion process p_{77}, and is denoted by p_{58}.

Although all energy transfer processes have a reverse process, their effectiveness depends on the specific energy level structure of the ion in the relevant host. With Ho:YLF the $^5I_5$ manifold decays quickly to the $^5I_6$ manifold and from there to the $^5I_5$ manifold through nonradiative transitions. The p_{77} process therefore has a low chance of being reversed. Subsequently this Ho:Ho upconversion has a net negative effect.

Since the upconversion process involves two Ho ions which are both in the $^5I_7$ manifold and spaced close together, this process is most likely to happen when the population density of the $^5I_7$ manifold is high. It is therefore most important when the energy storage in the gain medium is high, which is the case when a laser is Q-switched. Upconversion therefore limits energy storage in Ho lasers, lowering both pulse energy during Q-switching and laser efficiency. As upconversion is dependent on the doping of the crystal, it can be reduced and even eliminated through the use of low-doped crystals (Koen *et al.*, 2009).

3.3   Design Approach

Efficient fibre-laser-pumped Ho:YLF oscillators have previously been demonstrated (Bai *et al.*, 2007), but to scale the output energy further, an oscillator-amplifier system can be employed. The traditional approach when pumping an oscillator-amplifier system with one fibre-laser pump source is to split the unpolarised pump beam into two polarised beams in order to pump the oscillator and amplifier crystals separately, as shown in Figure 3.4 (Dergachev *et al.*, 2007).

In the novel approach presented here the full unpolarised beam from the fibre laser was used to pump the oscillator, after which the partially polarised transmitted pump light from the oscillator was used to pump the amplifier, with its crystal rotated by 90 ° with respect to the laser beam axis. This led to a small system footprint and kept the path length of the pump light short, reducing the adverse effects of water absorption (Rothman *et al.*, 2003).

Figure 3.1 shows the emission and absorption spectra of Ho:YLF. The emission is stronger on the π-polarisation than on the σ-polarisation. However, the σ-polarisation
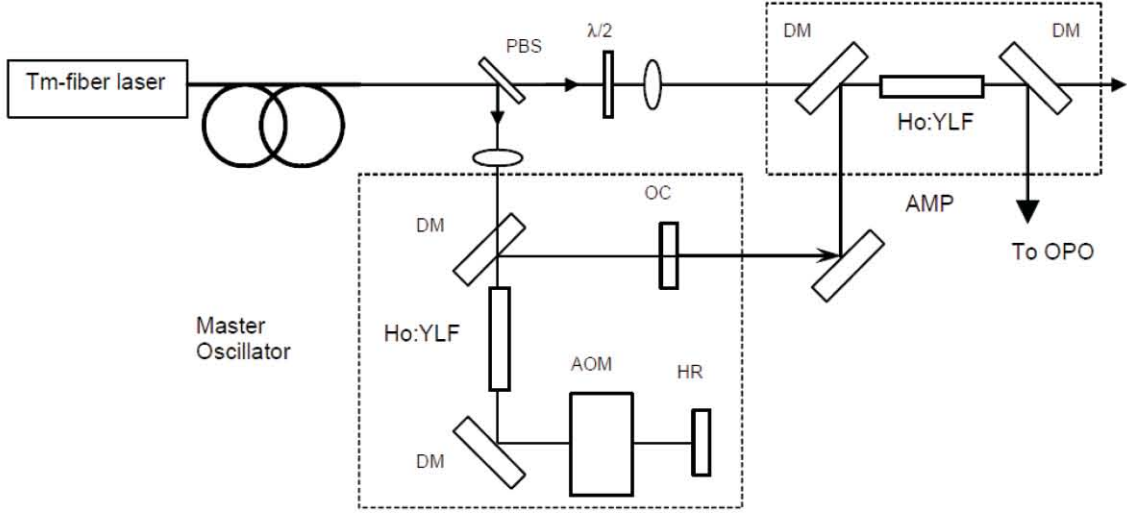
Figure 3.4: Schematic of a conventional layout for an end-pumped Ho:YLF Oscillator-Amplifier. The pump light is split into two polarised beams using a polarizing beam splitter (PBS). The one beam is then used to pump the oscillator while the second beam is used to pump the amplifier (Dergachev *et al.*, 2007).

has a much weaker thermal lens in YLF than the π-polarisation and is thus preferred for a high-power oscillator. In an amplifier, on the other hand, gain is the most important factor while the thermal lens is not as problematic as in an oscillator. Therefore, we chose to utilise the σ-polarisation for the laser oscillator and the π-polarisation for the amplifier.

3.4 Experimental Set-up

3.4.1 The Pump Source

A commercial Tm-fibre laser manufactured by IPG Photonics (Model TLR-80-1940) was used as pump source (Shown in Figure 3.5). The fibre laser required water cooling at a temperature setpoint of $20\,^{\circ}\mathrm{C}$ which was supplied by a $1\,\mathrm{kW}$ cooling capacity circulatory water chiller. The fibre laser delivered a maximum of $86.5\,\mathrm{W}$ in a near-diffraction-limited beam with a specified M^2 of 1.05. The fibre-laser's wavelength was specified to match the Ho:YLF absorption peak at $1940\,\mathrm{nm}$. It was subsequently

Figure 3.5: The IPG fibre laser used as pump source for the Ho:YLF oscillator-amplifier
system.

measured with a Jarrell Ash monochromator and found to be 1938.7 ± 2.5 nm at full
power. The output power of the fibre laser as a function of setpoint was measured
using a LM-100 Coherent power meter. The results are shown in Figure 3.6.

Since there are strong water absorption lines in the $1.9 \, \mu$m wavelength region, it
was necessary to investigate if water vapour in the atmosphere would pose a problem
with the Tm:fibre laser as pump source for the Ho:YLF oscillator-amplifier system. In
order to do so, the transmission spectrum of air in the region of 1940 nm was calculated
using HITRAN (Rothman *et al.*, 2003), and is shown in Figure 3.7. This calculation
was for a distance of 1 m in air with a relative humidity of 50 % at 300 K. The fibre
laser's emission spectrum was superimposed on the graph to determine if there are any
water absorption lines overlapping with the laser's output spectrum.

It was concluded that there are water absorption lines and that it should be inves-
tigated further. An experiment was devised where the fibre laser's beam profile was
measured with a Spiricon Pyrocam after propagating a certain distance. The resultant
beam profile is shown in Figure 3.8.

The absorption of the light led to heating of the air, resulting in turbulence which in
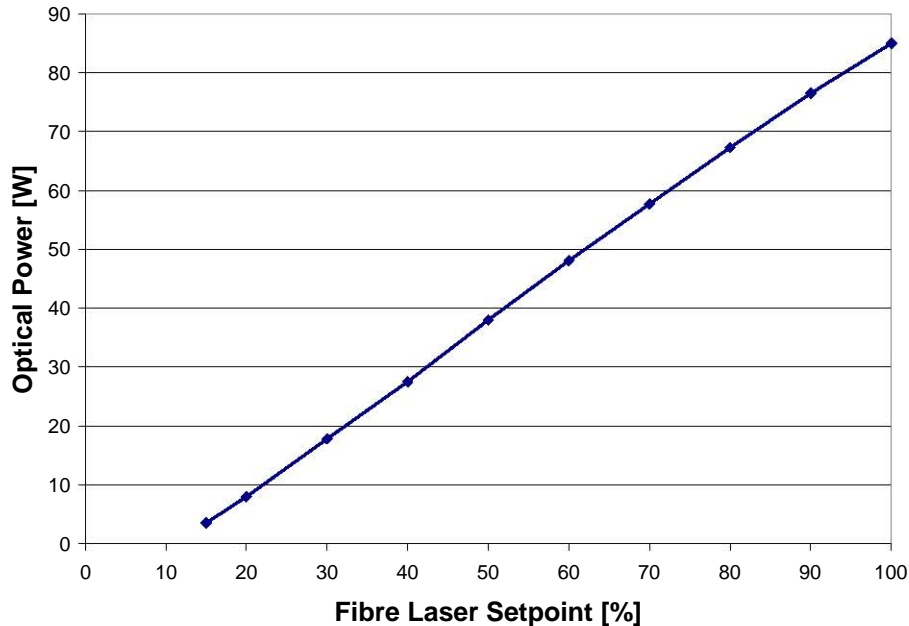
Figure 3.6: Power slope of the fibre laser with regard to the setpoint.

turn led to beam distortion and beam wandering. The beam profiles shown in Figure 3.8 illustrate how this affected the beam intensity profile. After propagating only 1.85 m, the collimated beam was distorted at lower powers and severe beam wandering was observed. This was despite the fact that only 4 % of the light was absorbed in the air with the fibre laser running at 50 %. At higher fiber laser powers, these detrimental effects decreased and the total amount of laser power absorbed was negligible. This is attributed to a shift in wavelength of the fibre-laser with an increase of its output power, possibly caused by the heating-up of the internal fibre Bragg grating of the fibre laser.

From these measurements it became apparent that water absorption of the fibre laser's light had to be taken into careful consideration when designing a system pumped by this laser, as pump beam distortion and beam wandering would affect an end-pumped system adversely.

There are several ways in which this problem is typically resolved:

- A fibre bragg grating can be used to shift the fibre-laser's wavelength to a region where there is no water absorption. There are limits to how far the laser's
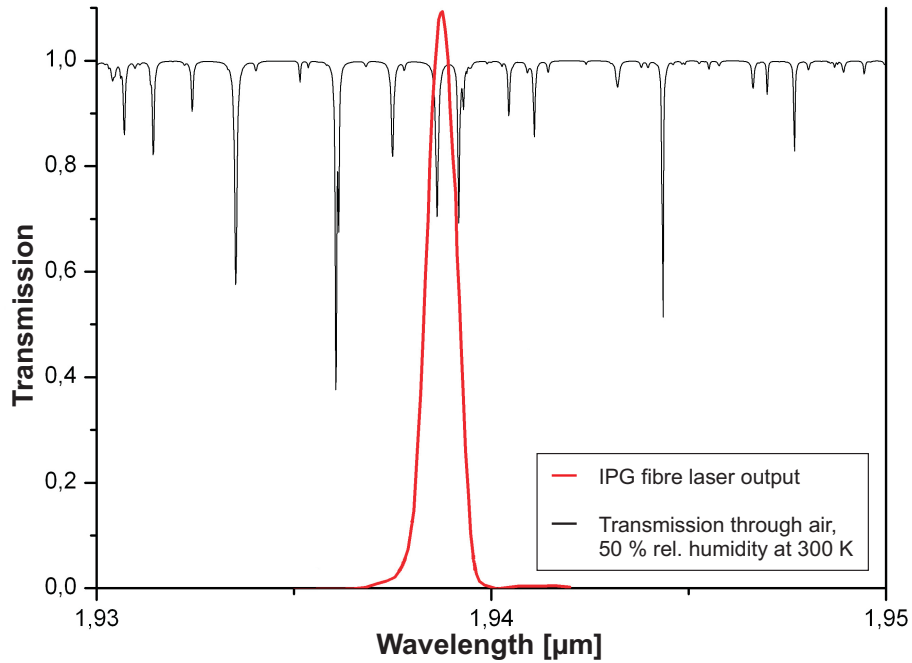
Figure 3.7: The transmission spectrum of air in the region of 1940 nm over a length
of 1 m with a relative humidity of 50 %, and temperature 300 K. The fibre laser's
wavelength at full power is also shown.
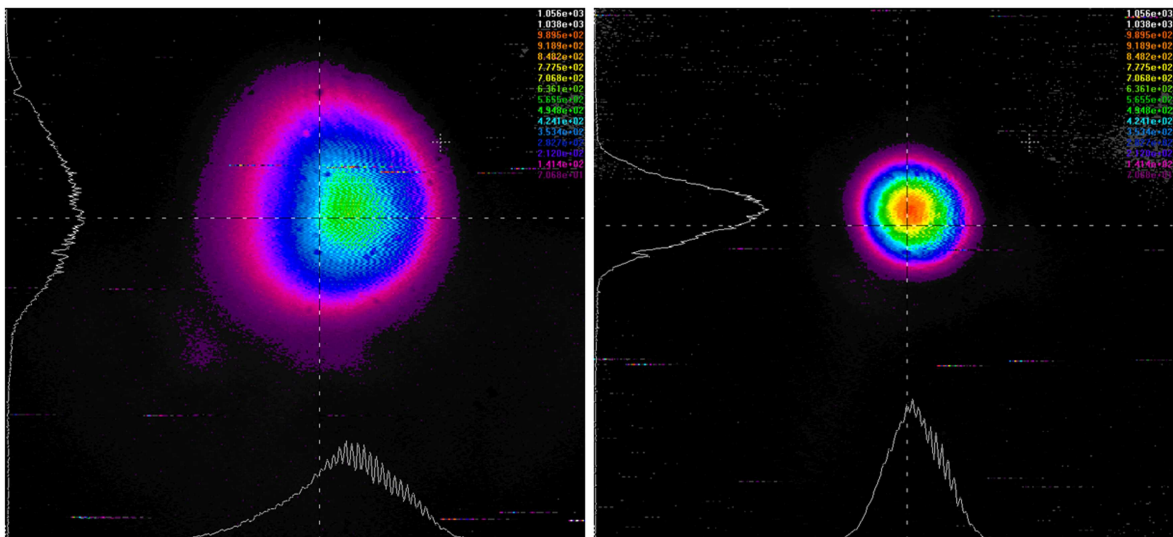
Figure 3.8: Beam profile measurements of the fibre-laser beam 1.85 m away from the
collimator at 50 % (left), and 100 % output power (right).

62
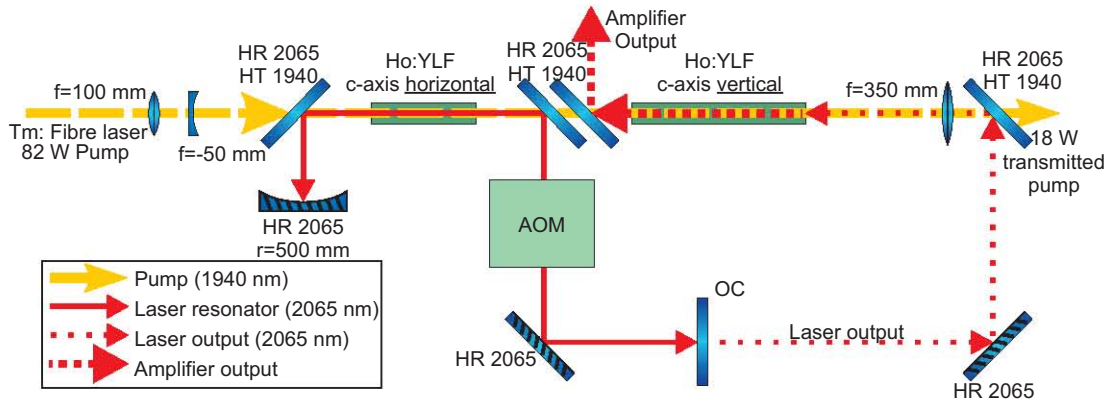
Figure 3.9: A schematic diagram of the fibre-laser-pumped Ho:YLF oscillator-amplifier system.

wavelength can be shifted though. This has already been implemented in the fibre-laser. The fibre laser could also be run at full power since the beam is least affected at full power. The beam must then be attenuated to obtain the desired pump power.

- The system could be encased in a box which is flushed with dry air. The subsequent decrease in humidity would lessen the water absorption of the laser light. This is the traditional solution to the problem.

- The distance the pump beam propagates in air before entering the laser crystal could be minimised. This imposes spatial restrictions on the setup.

From these options, it was decided to implement a scheme where the beam's propagation distance is minimised as it would be the most practical solution. This would entail having the oscillator crystal's pump-face as close to the fibre laser's end as possible, and the oscillator and the amplifier crystal close to each other. The spatial restrictions on the layout of the system imposed by this resulted in a compact laser.

3.4.2   The Resonator

As discussed, several criteria were imposed on the design of the resonator and amplifier, which resulted in the setup shown in Figure 3.9. The distance from the fibre laser's output to the Ho:YLF crystal in the resonator was kept to a minimum to minimise

63

beam distortion caused by the water vapour in the air. The pump light transmitted through the laser crystal was accessible by the amplifier crystal behind it with the distance between the two crystals as short as possible.

To ensure good efficiency and beam quality, the pump laser beam and resonator mode size inside the laser crystal had to match. To achieve this the pump laser beam was collimated and then sent through a convex lens with a focal length of $100\,\mathrm{mm}$ followed by a concave lens with a focal length of $50\,\mathrm{mm}$. After collimation the beam *diameter* was $\sim 4\,\mathrm{mm}$ and the pump spot *radius* after the two lenses was measured to be approximately $w_p = 600\,\mu\mathrm{m}$.

As with the Nd:YLF laser, the resonator had to be adjustable to compensate for the varying thermal lens of the crystal.

Ho:YLF crystal rods supplied by VLOC were used as the gain medium in the experiment. All crystals were a-cut and had a doping concentration of $0.5\,\mathrm{at.\%}$. They were $6\,\mathrm{mm}$ in diameter with respective lengths of $30\,\mathrm{mm}$ and $50\,\mathrm{mm}$. The crystals were mounted in water-cooled copper mounts in the same fashion as the Nd:YLF crystals used in the previous chapter. The water temperature was kept at $20\,^{\circ}\mathrm{C}$ with the same chiller used for the fibre laser. Either the $30\,\mathrm{mm}$ or the $50\,\mathrm{mm}$ crystals could be used in the resonator.

The subsequent resonator was $370\,\mathrm{mm}$ long with a $500\,\mathrm{mm}$ concave back-reflector and a flat output coupler which could be interchanged for various reflectivities. The setup is shown in Figure 3.10.

The resonator length could be easily changed to compensate for the weak thermal lens of the Ho:YLF crystal.

To keep the optical path of the pump light to the amplifier crystal to a minimum, the resonator was folded using $45\,^{\circ}$ dichroic mirrors with high transmission for the pump light (s- and p-polarisation), high reflection for s-polarised laser light, and $20\,\%$ transmission for p-polarised laser light, forcing the oscillator to operate on the vertical polarisation. Having the c-axis of the crystal horizontal, lasing was ensured on the σ-polarisation (E$\perp$c). Neglecting thermal lensing, the calculated TEM_{00} beam radius in the YLF crystal was $580\,\mu\mathrm{m}$, which was assumed to increase at higher pump powers due to the effect of the weak negative thermal lensing in Ho:YLF.

After the resonator's cw performance was tested, a water-cooled, plane cut, AR-coated crystalline quartz acousto-optic modulator manufactured by Gooch & Housego
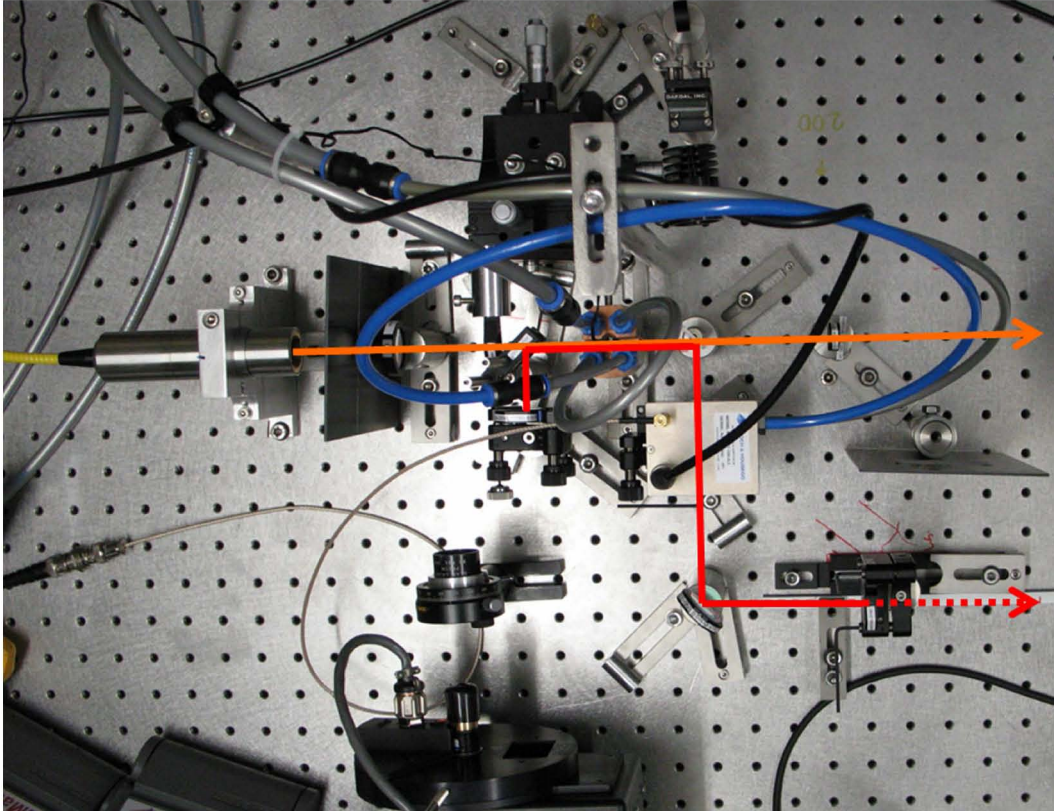
Figure 3.10: Top view of the Ho:YLF oscillator. The pump light is shown in orange,
the laser light in red.

(Model QS027-10M-NL5) was inserted for Q-switched operation. It delivered a loss
modulation of approximately $80\,\%$ at the maximum recommended RF power of $100\,\mathrm{W}$
at $27\,\mathrm{MHz}$. It was used with a gate time of $6\,\mu\mathrm{s}$ at $95\,\mathrm{W}$ of RF power.

3.4.3   The Amplifier

The transmitted pump power from the fibre laser was subsequently used to pump
the amplifier crystal. In this instance a $30\,\mathrm{mm}$ long crystal was used in the oscillator
while a $50\,\mathrm{mm}$ long amplifier crystal was placed as close to the oscillator as possible to
minimise atmospheric water absorption of the $1940\,\mathrm{nm}$ pump light which would lead
to heating of the air and subsequent thermal turbulence. This negated the need for
any enclosure or dry-air flushing typically used for such setups to prevent pump-beam
distortions caused by thermal turbulence in the air.
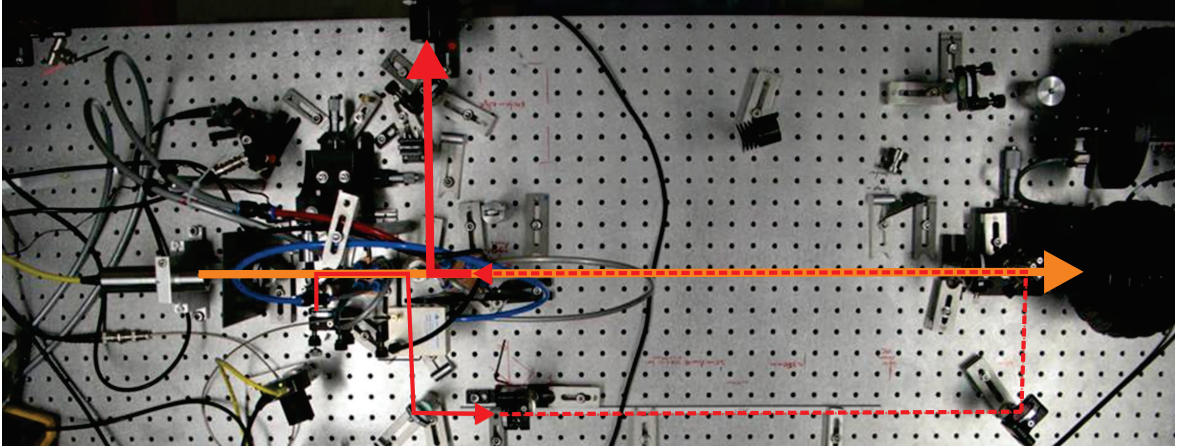
Figure 3.11: The Ho:YLF oscillator and amplifier. The pump light is shown in orange, the laser light and amplified light in red.

Since the absorption at 1940 nm in Ho:YLF is strongly polarisation dependent (Figure 3.1), there was a difference between the transmissions of the two polarisations. This made the transmitted light partially polarised. Therefore, in order to achieve maximum absorption in the amplifier crystal, it was orientated with its c-axis rotated by 90 ° with respect to the c-axis of the oscillator crystal. This effectively "swapped" the polarisations for the amplifier crystal. Thus, the π-polarisation, with the higher emission cross-section (Walsh *et al.*, 1998) but stronger thermal lens, was used for amplification while the σ-polarisation, with the weak thermal lens but lower cross-section, was used in the oscillator. The laser output was coupled into the amplifier crystal using a lens with a focal length of 350 mm. The complete oscillator-amplifier setup is shown in Figure 3.11.

3.5   Experimental results

3.5.1   Pump Light Transmittance

The oscillator-amplifier system was designed such that a large portion of the pump light was transmitted through the oscillator crystal in order to pump the amplifier crystal. In order to know the incident pump power on the amplifier crystal, the pump light transmitted through the laser crystal was measured. This was done for the different
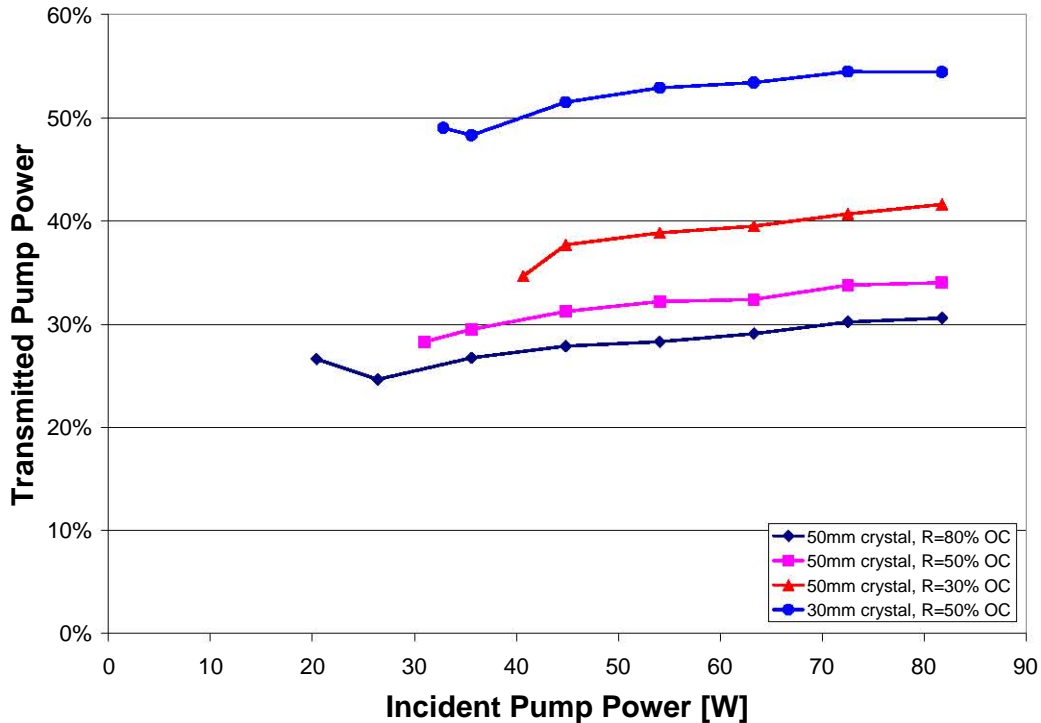
Figure 3.12: The percentage of pump power transmitted through the resonator versus
the incident pump power for various crystal lengths and output coupler reflectivities.

crystal lengths and output coupler reflectivities as it was expected that this would
influence the pump bleaching and therefore the amount of transmitted pump light.
The results are shown in Figure 3.12.

For all crystal and output coupler combinations, the percentage of transmitted
light increased slightly with an increase of pump light incident on the laser crystal.
The lowest percentage of pump light transmitted was when the 50 mm long crystal was
used in combination with a 20 % output coupler (R=80 %). For the same crystal length
of 50 mm, more pump light was transmitted for output couplers with lower reflectivities
due to a corresponding increase in pump bleaching within the crystal.

The highest percentage of pump light was transmitted when the 30 mm crystal was
used in combination with a 50 % output coupler. At full pump power this combination
transmitted 55 % of the incident pump light which could then be utilised to pump the
amplifier.
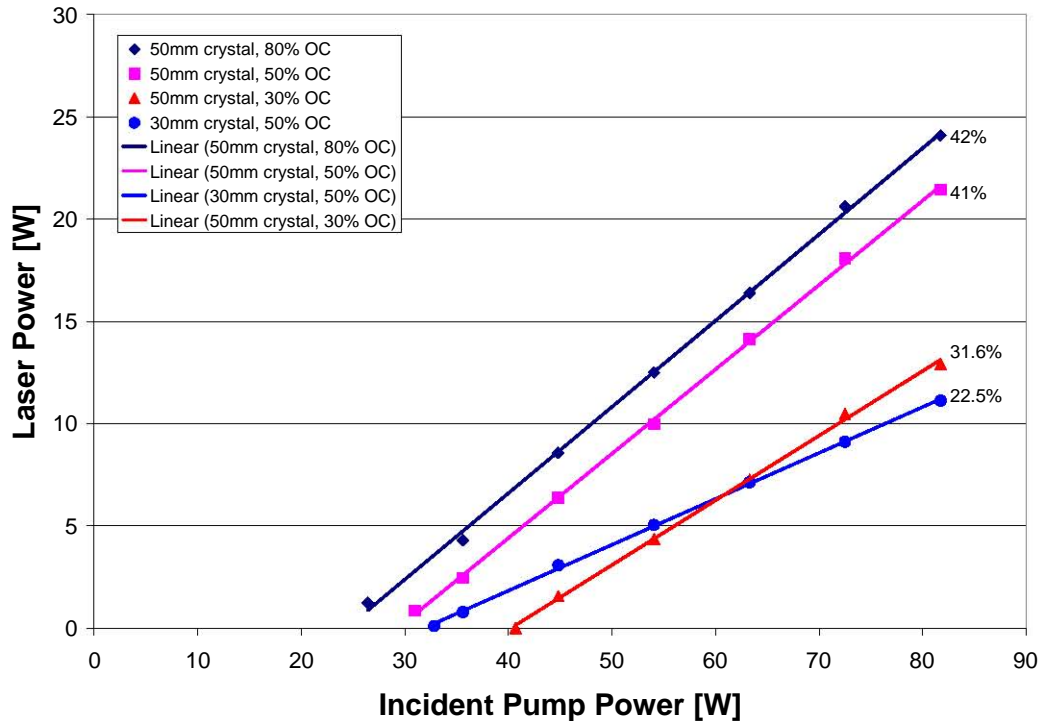
Figure 3.13: CW output power of the oscillator versus incident pump power for various
output couplers and crystal lengths.

3.5.2 CW Oscillator Performance

The performance of the laser under cw operation was measured for various output
coupler reflectivities and crystal length combinations.

Figure 3.13 shows the slope efficiencies for both the 30 mm and 50 mm crystals
in combination with R=30, 50, and 80 % reflective output couplers as a function of
incident pump power. All combinations exhibited a linear response to an increase in
incident pump power. The highest slope efficiency was obtained with the 50 mm long
crystal and R=80 % output coupler, with a slope efficiency of 42 %. The lowest lasing
threshold of 26.4 W was obtained with the 50 mm crystal and R=80 % output coupler.
The highest threshold of 40.7 W was obtained with the 50 mm crystal in combination
with the R=30 % output coupler. Threshold could not be reached with the available
pump power for the 30 mm crystal, R=30 % output coupler combination.

Figure 3.14 shows the slope efficiencies for both the 30 mm and 50 mm crystals
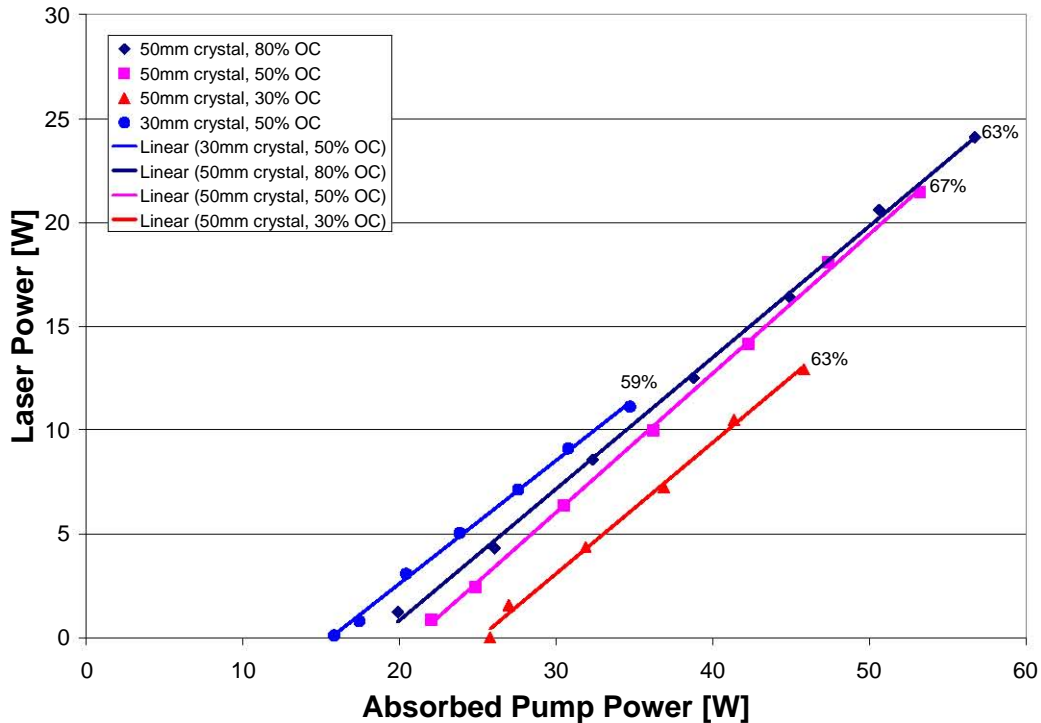
Figure 3.14: CW output power of the oscillator for various crystal lengths and output couplers as a function of absorbed pump power.

in combination with R=30, 50, and 80 % reflective output couplers as a function of *absorbed* pump power. All combinations exhibited a linear response to an increase in absorbed pump power. The highest slope efficiency was obtained with the 50 mm long crystal and R=50 % output coupler, with a slope efficiency of 67 %. The lowest lasing threshold of 15.8 W was obtained with the 30 mm crystal and R=50 % output coupler. The highest threshold of 25.8 W was obtained with the 50 mm crystal in combination with the R=30 % output coupler. When comparing Figures 3.13 and 3.14, one observes that the efficiency slopes differ drastically with regard to the incident pump power as opposed to the absorbed pump power. While the R=80 % output coupler and 50 mm crystal combination had the highest efficiency slope with regard to incident pump power, the R=50 %, 50 mm combination had the highest efficiency slope with regard to absorbed pump power. The latter combination would have been the obvious choice if the oscillator was to be the only part of the system.

However, since the amplifier used the transmitted pump light from the oscillator,

neither of these two combinations would have resulted in the most efficient oscillator-amplifier system, given the other choices, as they both absorbed the most pump light without having significantly higher efficiency slopes than the other combinations.

With the complete oscillator-amplifier system performance in mind, the R=50 % output coupler and 30 mm crystal combination was the best choice. Not only did it transmit far more pump light than the other combinations (see Figure 3.12), but it also had an efficiency slope not much worse than the rest with regard to absorbed pump light. In addition, this combination had the lowest absorbed pump threshold. Subsequently the R=50 % output coupler in combination with a 30 mm crystal was used in the oscillator for the final setup.

3.5.3   Pulsed Oscillator Performance

The laser was also operated in Q-switched mode. For initial performance measurements, a 50 mm long Ho:YLF crystal was used in the resonator, in conjunction with a R=30 % output coupler (Transmission of 70 %). The high output coupling was chosen for low intra-cavity energy in order to avoid possible optical damage. The laser was operated at pulse repetition frequencies (PRF) from 5 kHz down to 0.7 kHz. The results are shown in Figure 3.15.

The laser pulse length decreased with a decrease in the PRF, while the energy per pulse increased. The longest laser pulse and lowest pulse energy was obtained at a PRF of 5 kHz. At 5 kHz the laser delivered a 2.86 mJ pulse with a full width half maximum (FWHM) pulse of 250 ns. The highest pulse energy of 18.9 mJ (Total intra-cavity energy of 35 mJ) delivered in a 51 ns pulse was obtained at a PRF of 700 Hz. Lower repetition rates could not be attempted with this configuration since damage to the dielectric coating of the mirrors occurred when attempting to operate the laser at 600 Hz. Thereafter, configurations with lower intra-cavity peak intensities were examined in an attempt to avoid further damage to optical components in the laser.

The 50 mm long crystal in the resonator was swapped with a 30 mm one and the R = 30 % output coupler was changed to 50 % as threshold could not be reached with the R = 30 % output coupler. The results for pulsed operation is shown in Figure 3.16. This crystal/output-coupler combination resulted in an extra 10 % of pump light being
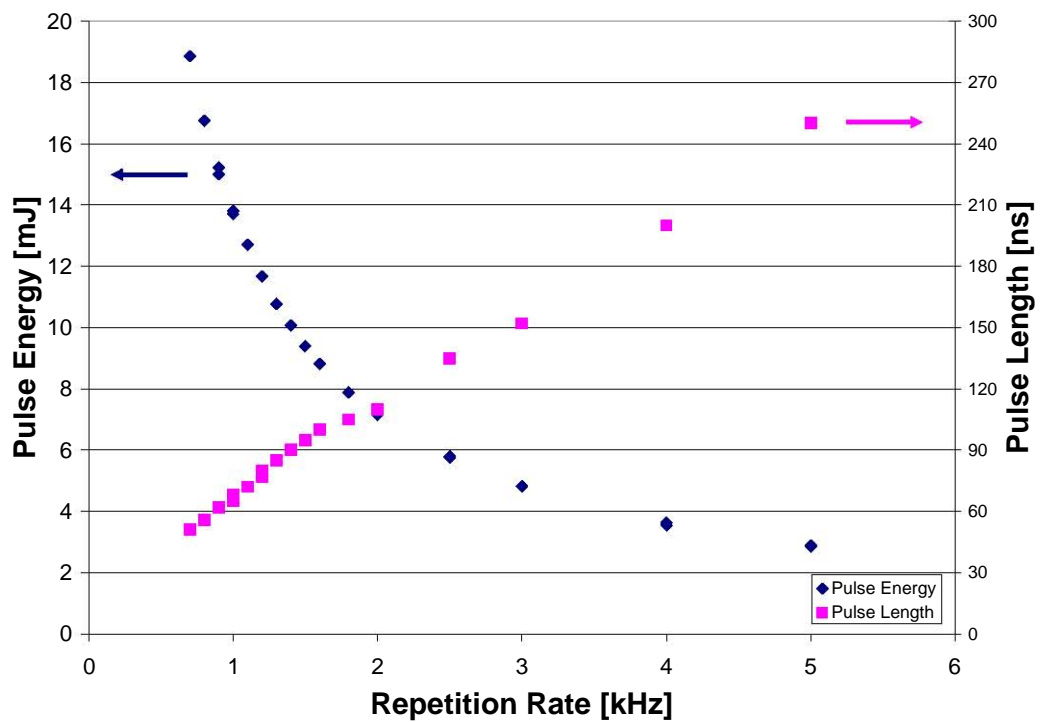
Figure 3.15: Oscillator pulse energy and FWHM pulse length as a function of the repetition rate at full pump power for the 50 mm long crystal and R=30 % output coupler.
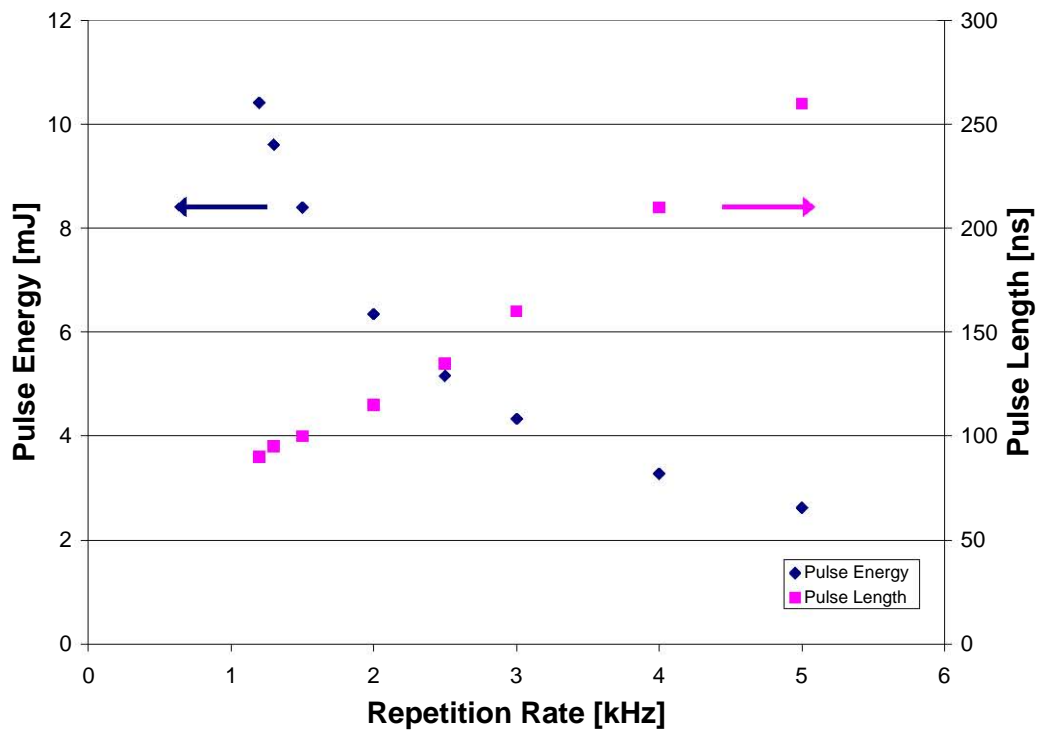
Figure 3.16: Oscillator pulse energy and FWHM pulse length as a function of the repetition rate at full pump power for the 30 mm long crystal and R = 50 % output coupler.

transmitted through the laser crystal, as discussed in Section 3.5.1 (Figure 3.12), which
could be efficiently utilised in the amplifier crystal. This configuration exhibited the
same behaviour as the preceding set-up, but with lower output power. The lowest PRF
attempted was 1 kHz at full pump power which delivered a pulse energy of 10.4 mJ
(Total intra-cavity energy of 31.3 mJ).

3.5.4   Amplifier Performance

After the oscillator's initial characterization was done, the amplifier setup was added.
The resonator configuration remained the same with a 30 mm crystal and 50 % output
coupler, while a 50 mm crystal was used for the amplifier. As shown in Figure 3.9, the
oscillator light was focused into the amplifier crystal using a convex lens with a 350 mm
focal length.

3.5.5   CW Amplifier Performance

The oscillator and amplifier output under cw operation is shown in Figure 3.17. The
navy data points indicate the laser output while the magenta points indicate the am-
plifier output power for various pump powers. The solid magenta line represents the
amplifier output power predicted by the theoretical model (See the Appendix, (Koen
et al., 2009)).

The oscillator had a threshold of 31 W (17 W absorbed) of pump power, with an
overall slope efficiency of 25 % (47 % vs. absorbed power). At 82 W of pump power
(incident), the oscillator power was 12.4 W and the amplified power was 23.7 W at
a centre wavelength of 2065 nm. This corresponds to a gain of the amplifier of 1.9.
The total pump power transmitted through the oscillator crystal was 47 W (55 % of
the pump power) at full power. The amplifier crystal absorbed 29 W (62 % of the
transmitted pump, 35 % of total pump), which left 18 W (22 %) of the total pump light
unused. The slope efficiency of the amplified beam versus total fibre pump power was
47 % with an overall optical-to-optical efficiency of 29 %. With respect to the total
absorbed power (35 + 29 W), the slope efficiency was 60 % and the overall efficiency
was 37 %. It is clear that the efficiency with respect to incident pump power could be
further increased by reflecting the 18 W transmitted pump light back into the amplifier
and oscillator crystals. This was not attempted as it was unclear at the time what
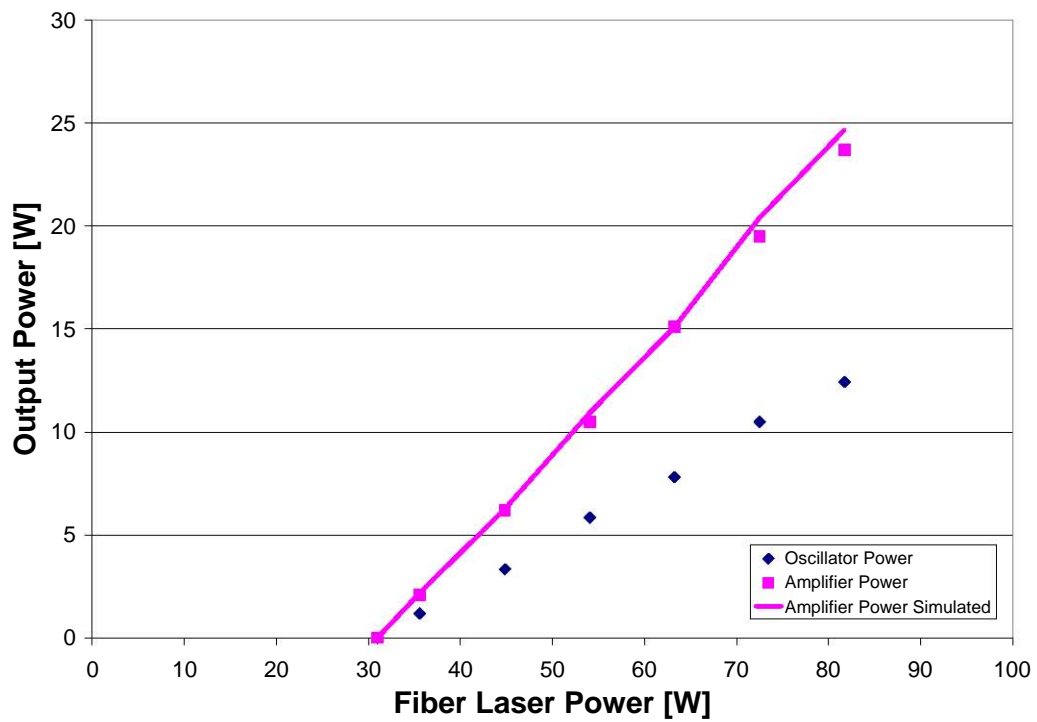
Figure 3.17: Oscillator and amplifier output power versus incident fibre pump power
under cw lasing conditions (dots) together with the results of a numerical simulation
(solid line) (Koen *et al.*, 2009).
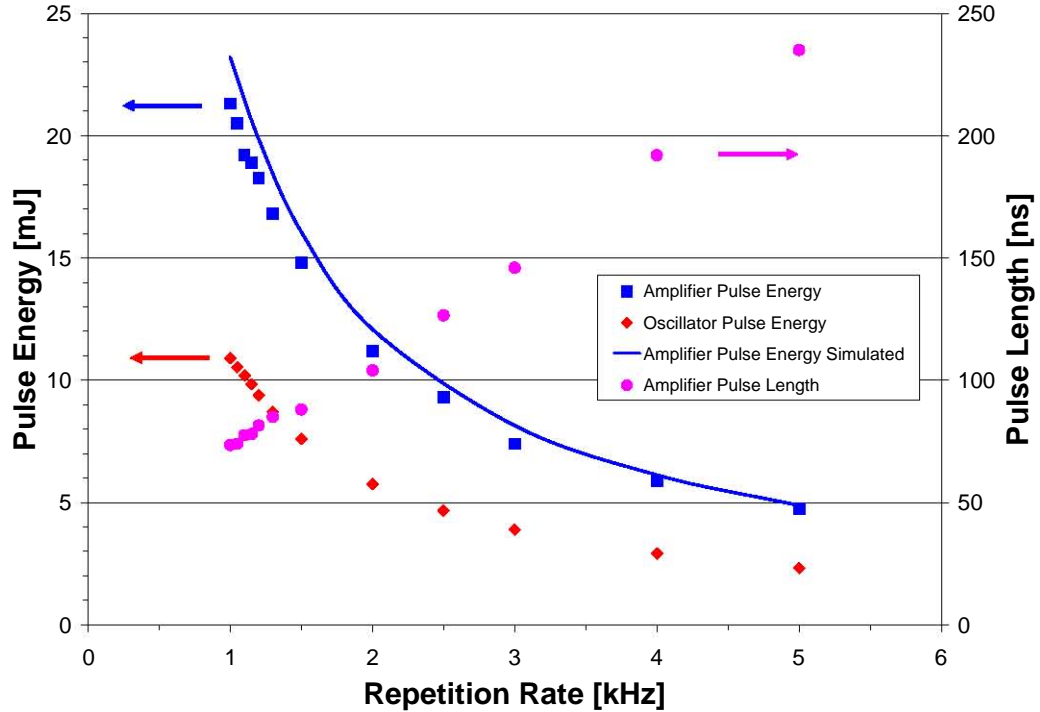
Figure 3.18: Oscillator and amplifier output energy and FWHM pulse lengths as a
function of the repetition rate at full pump power (dots) together with the results of a
numerical simulation (solid line).

the tolerance of the fibre laser to back reflection was. Additionally, a two dimensional
rotational symmetric amplifier model was developed by Dr Shellhorn (Koen *et al.*,
2009), the full details of which are available in the published paper attached to this
dissertation as an appendix. In brief, the model considered upconversion losses and
ground-state depletion, as well as the spatial distribution of the pump and laser beams.
Taking into account the measured transmitted pump power through the laser crystal,
the amplified laser power is calculated assuming a pump and laser spot radius of $550\,\mu$m
(see Table 1 in the Appendix) at the position of the amplifier crystal. The solid lines
in Figures 3.17, 3.18, and 3.19 indicate the results of these calculations which agree
well with the experimental values. It also indicated that upconversion can be ignored
as it is negligible in the $0.5\,\%$ doped Ho:YLF crystals used.
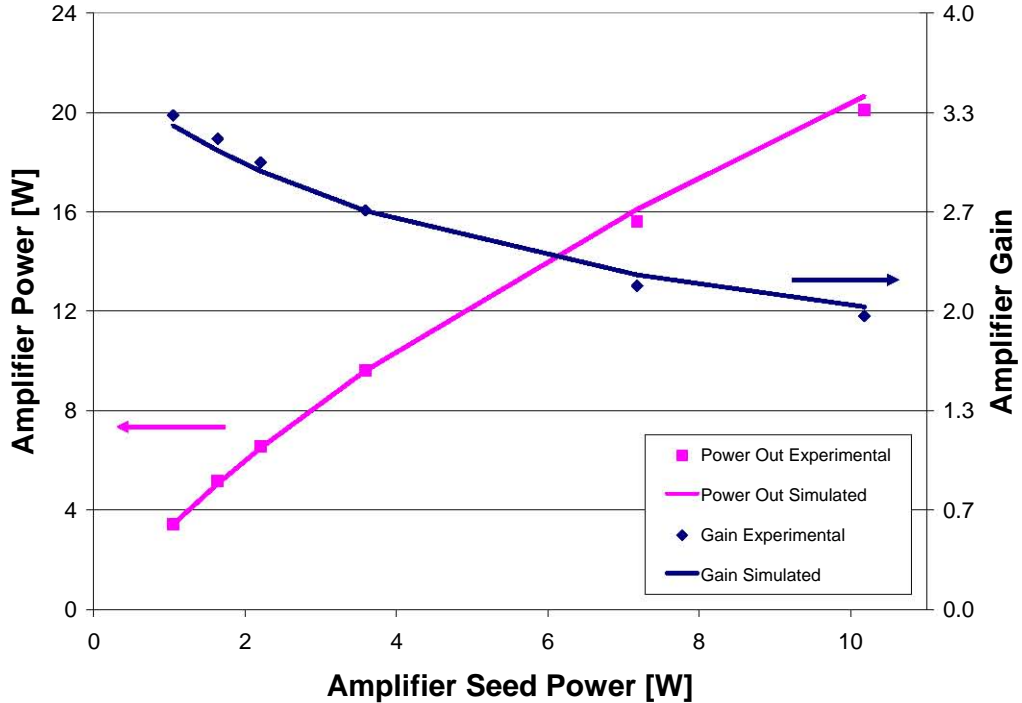
Figure 3.19: Amplifier output power and gain under cw operation (dots) for different
seed powers, together with the results of a numerical simulation (solid lines).

3.5.6   Amplifier Small Signal Gain

The amplifier small signal gain was measured under cw operation at a fixed pump
power of 75 W of the fibre laser. The oscillator output power was attenuated with
different partial reflectors to vary the seed power of the amplifier. The amplifier was
pumped with the transmitted pump power of 40 W. Figure 3.19 shows the measured
amplifier small signal output power and gain under cw operation (dots) together with
the results of the numerical simulation (solid lines). Assuming a pump and laser spot
radius of $550\,\mu$m (see Table 1 in the Appendix) the results of the simulation show good
agreement with the experiment and the small signal gain of approximately 3.3 implies
that the amplifier is operated nearly in saturation at full cw power.
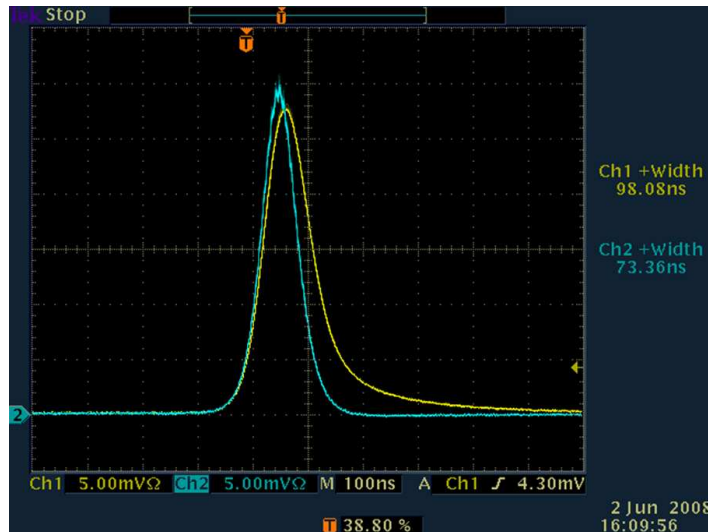
Figure 3.20: Amplifier pulse shape measured with a PEM (cyan line) and an extended
InGaAs (yellow line) detector at 1 kHz pulse repetition rate. The PEM detector gives
the more accurate reading as the extended InGaAs detector is slower.

3.5.7   Pulsed System Performance

Finally, the oscillator was Q-switched between 5 kHz and 1 kHz to test the performance
of the complete system.   The pulse energies of the oscillator and amplifier and the
FWHM pulse lengths as a function of the repetition rate are shown in Figure 3.18 at
full pump power together with the results of a numerical simulation. The highest pulse
energies for the system in our operating regime were achieved at a repetition rate of
1 kHz with the oscillator delivering 10.9 mJ per pulse and an amplified pulse energy
of 21.3 mJ with a FWHM pulse length of 74 ns (Figure 3.20). This corresponds to a
gain of 2.2. The results of the simulation show good agreement with the experiment
and the calculated small signal gain of 3.85 at 1 kHz repetition rate is slightly higher
than that measured in cw mode. The amplifier did not change the pulse length in any
measurable way compared to the oscillator.

The beam quality of the oscillator as well as the amplifier was measured by using
a knife edge. It was subsequently found that both the oscillator and amplifier had an
M^2 value of better than 1.1 at full power. The intensity profile of the amplifier beam
is shown in Figure 3.21.
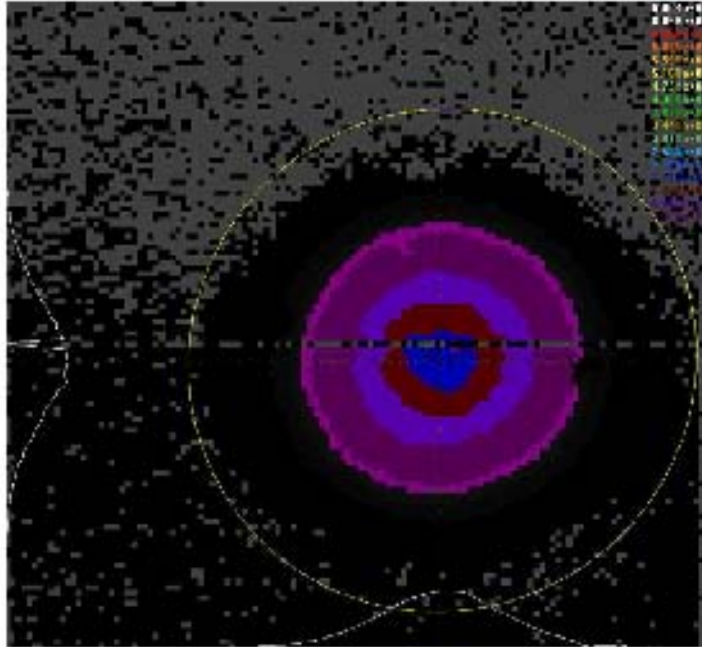
Figure 3.21: Amplifier beam profile at 1 kHz pulse repetition rate.

3.6 Conclusion

A novel oscillator-amplifier scheme was developed and successfully demonstrated, where
the unused pump light transmitted by the oscillator was utilised to pump an amplifier
crystal. The system produced more than 21 mJ of energy per pulse at 1 kHz, with
an M^2 better than 1.1. The amplified energies agreed well with the predicted values
from a two dimensional rotational symmetric amplifier model that was developed. The
model considered upconversion losses and ground-state depletion, as well as the spatial
distribution of the pump beam.

Future work entails building a single-frequency system with higher output energies
at low pulse repetition rates. This is elaborated upon in the next chapter.

Chapter 4

Conclusion

Through the demonstration of the two laser systems presented in this dissertation YLF has been shown to be an excellent host material for high-power laser systems in both the near- and the mid-infrared regime, provided that the thermal issues of YLF are correctly addressed.

In both these systems end-pumping, as discussed in Chapter 1, was implemented, resulting in high efficiencies and excellent beam quality which demonstrated the benefits of end-pumping solid-state lasers.

In Chapter 2 two scaling techniques for a Nd:YLF laser were demonstrated successfully. The novel mounting technique used for the Nd:YLF rods improved the cooling of the crystal, while pumping the crystals from their low-doped end resulted in a more uniform heat distribution along the optical axis. Both these techniques resulted in lower maximum temperatures at the pump face of the crystal, thus decreasing thermally induced stress in the crystals. This scaling approach subsequently led to the highest reported power from a diode-end-pumped Nd:YLF laser (Bollig *et al.*, 2008).

With these results limited solely by the available pump power, and not by thermal fracture of the laser crystals used, power scaling should be possible with the use of higher powered laser diodes of similar beam quality. Additionally, the longer crystals mentioned in Section 2.6 (75 mm vs. 45 mm) of lower doping could be used should the increased heat load prove too much for the current crystals.

In Chapter 3 a novel oscillator-amplifier scheme was developed and successfully demonstrated where the unused pump light transmitted by the oscillator was utilised

to pump an amplifier crystal. This pump scheme had two advantages:

Firstly, the compact design minimised the pump beam path in air. This decreased pump beam distortions and beam wandering caused by laser light absorption by water vapour in air, a common problem for lasers operating in this wavelength regime. It eliminated the need for the laser to be enclosed and flushed with dry air - the solution mostly used to solve this problem.

Secondly, the unpolarised pump light was absorbed efficiently despite the highly polarisation dependent pump light absorption of the Ho:YLF crystals. The improved pump light absorption led to a higher overall efficiency when compared to the conventional pump schemes where the unpolarised pump light is split into two using a polarising beam splitter to pump the laser crystal and the amplifier crystal separately (Dergachev *et al.*, 2007).

This pumping scheme has subsequently also been used successfully in a high-energy single-frequency Ho:YLF system which delivered the highest reported pulse energies (Bollig *et al.*, 2009).

References

Bagdasarov Crystals Group. 2009. *YAG crystal specifications page.* Tech. rept. Bagdasarov Crystals Group. Accessed June 2009.

Bai, Y., Yui, J., Petros, M., Petzar, P., Trieu, P., Lee, H., & Singh, U. 2007. Highly efficient Q-switched Ho:YLF laser pumped by Tm:fiber laser. *CLEO/QELS Conference. May 6-11, paper CtuN5. Baltimore Convention Center, Baltimore, Maryland, USA.*

Barnes, N.P., & Gettemy, D.J. 1980. Temperature variation of the refractive indices of yttrium lithium fluoride. *J. Opt. Soc. Am.,* **70**(10), 1244.

Barnes, N.P., Rodriguez, W.J., & Walsh, B.M. 1996. Ho:Tm:YLF laser amplifier performance. *J. Opt. Soc. Am. B,* **13**, 2872–2882.

Barnes, N.P., Walsh, B.M, & Filer, E.D. 2003. Ho:Ho upconversion: applications to Ho lasers. *J. Opt. Soc. Am. B,* **20**(6), 1212–1219.

Bernhardi, E.H. 2008. *Modelling Diode-Pumped Solid-State Lasers.* M.Phil. thesis, University of Kwazulu-Natal.

Bollig, C. 2006. *Personal Communication.*

Bollig, C., Hayward, R.A., Clarkson, W.A., & Hanna, D.C. 1998. 2-W Ho:YAG laser intracavity-pumped by a diode-pumped Tm:YAG laser. *Opt. Lett.,* **23**(22), 1757–1759.

Bollig, C., Jacobs, C., Esser, M.J.D., & von Bergmann, H.M. 2005. Elimination of Lifetime Quenching through Gain Optimization in a Q-switched high-power end-pumped Nd:YLF Laser. *CLEO/Europe (invited).*

REFERENCES

Bollig, C., Koen, W., Strauss, H., Bernhardi, E.H., Botha, R., Esser, M.J.D., & Preussler, D. 2008. Exploiting the natural doping gradient of Nd:YLF crystals for high power end-pumped lasers. *In Proceedings of the 3rd EPS-QEOD Europhoton Conference, Paris, France, 31 August - 5 September.*

Bollig, C., Esser, M.J.D., Jacobs, C., Koen, W., Preussler, D., Nyangaza, K., & Schellhorn, M. 2009. 70 mJ Single-Frequency Q-Switched Ho:YLF Ring Laser - Amplifier System Pumped by a Single 82-W Tm Fibre Laser. *Middle-Infrared Coherent Sources, Trouville, France, 8-12 June 2009 (invited).*

Budni, P.A., Lemons, M.L., Mosto, J.R., & Chicklis, E.P. 2000. High-Power/High-Brightness Diode-Pumped 1.9-um Thulium and Resonantly Pumped 2.1-um Holmium Lasers. *IEEE J. Sel. Top. in Quantum Electron*, **6**(4), 629–635.

Clarkson, W.A. 1998. High-power diode-bar end-pumped Nd:YLF laser at 1053 nm. *Optics Letters*, **23**, 1363–1365.

Clarkson, W.A. 2001. Thermal effects and their mitigation in end-pumped solid-state lasers. *J. Phys. D: Appl. Phys.*, **34**, 2381–2395.

Coherent. 2009. Laser TV. *www.coherent.com/flash/LaserTV KRON*.

Cross, P.L. 2005. Database of laser materials. *http://aesd.larc.nasa.gov/gl/laser/dbmain.htm*. Accessed March 2005.

Czeranowsky, C. 2002. *Resonatorinterne Frequenzverdopplung von diodengepumpten Neodym-Lasern mit hohen Ausgangsleistungen im blauen Spektralbereich*. Ph.D. thesis, University of Hamburg.

Dergachev, A., Armstrong, D., Smith, A., Drake, T., & Dubois, M. 2007. 3.4-um ZGP RISTRA nanosecond optical parametric oscillator pumped by a 2.05-um Ho:YLF MOPA system. *Opt. Express*, **15**, 14404.

Eichorn, M. 2008. Quasi-three-level solid-state lasers in the near and mid infrared based on trivalent rare earth ions. *Applied Physics B*, **93**, 269–316.

Einstein, A. 1917. Zur Quantentheorie der Strahlung. *Physikalische Zeitschrift XVIII*.

REFERENCES

Esser, M.J.D. 2004. *Diode-End-Pumped Solid-State Lasers.* M.Phil. thesis, University of Stellenbosh.

Fan, T.Y., & Byer, R.L. 1988. Diode Laser-Pumped Solid-state Lasers. *IEEE J. Quantum Electron.*, **24**, 895–912.

Fan, T.Y., Huber, G., Byer, R.L., & Mitzscherlich, P. 1988. Spectroscopy and diode laser-pumped operation of Tm,Ho:YAG. *IEEE J. Quantum Electron*, **24**(6), 924–933.

Findlay, D., & Clay, R.A. 1966. The measurement of internal losses in 4-level lasers. *Physics Letters*, **20**, 277.

Geusic, J.E., Marcos, L.G., & van Uitert, L.G. 1964. Laser Oscillations in Nd-doped Yttrium Aluminum, Yttrium Gallium and Gadolinium garnets. *Appl. Phys. Lett.*, **4**, 182.

Hardman, P.J., Clarkson, W.A., Friel, G.J., Polnau, M., & Hanna, D.C. 1999. Energy-Transfer Upconversion and Thermal Lensing in High-Power End-Pumped Nd : YLF Laser Crystals. *IEEE J. Quantum Electron.*, **35**(4), 647–655.

Johnson, L.F., & Nassau, K. 1961. Proc IRE 49 (1704). *IRE.*

Koechner, W. 1970. Analytical model of a cw Nd:YAG laser. *Laser Focus.*

Koechner, W. 1999. *Solid-State Laser Engineering.* 5th edn. Heidelberg, Germany: Springer-Verlag.

Koen, W., Bollig, C., Strauss, H., Schellhorn, M., Jacobs, C., & Esser, M.J.D. 2009. Compact fibre-laser-pumped Ho:YLF oscillator-amplifier system. *Applied Physics B*, November.

Lippert, E., Arisholm, G., Rustad, G., & Stenersen, K. 2003. Fiber laser pumped mid-IR source. *Advanced Solid State Photonics of OSA Trends in Optics and Photonics Series*, **83**, 292–297.

Lippert, E., Nicolas, S., Arisholm, G., Stenersen, K., & Rustad, G. 2006. Midinfrared laser source with high power and beam quality. *Appl. Opt*, **45**, 3839–3845.

REFERENCES

Magni, V. 1986. Resonators for solid-state lasers with large-volume fundamental mode and high alignment stability. *Applied Optics*, **25**, 107–117.

Maiman, A.H. 1960. Stimulated Optical Radiation in Ruby. *Nature*, **187**, 493–494.

Northrop Grumman Space Technology. 2009. Nd:YLF Data Sheet. *http : //www.optoscience.com/maker/northrop/pdf/NdYLF.pdf*. Accessed 2009.

Pachotta, R. 2008. *Field Guide to Lasers.* SPIE.

Pachotta, R. 2009. *Encyclopedia of Laser Physics and Technology.*

Payne, S.A., Chase, L.L., Smith, L.K., Kway, W.L., & Krupke, W.F. 1992. Infrared cross-section measurements for crystals doped with Er3+, Tm3+, and Ho3+. *IEEE J. Quantum Electron.*, **28**(11), 2619–2630.

Pfistner, C., Weber, R., Weber, H.P., Merazzi, S., & Gruber, R. 1994. Thermal Beam Distortions in End-Pumped Nd:YAG. Nd:GSGG and Nd:YLF Rods. *IEEE J. Quantum Electron.*, **30**, 1605–1615.

Pollak, T.M., Wing, W.F., Grasso, R.J., Chicklis, E.P., & Jenssen, H.P. 1982. CW Laser Operation of Nd:YLF. *IEEE J. Quantum Electron.*, **18**, 159–163.

Pollnau, M., Hardman, P.J., Kern, M.A., Clarkson, W.A., & Hanna, D.C. 1998. Upconversion-induced heat generation and thermal lensing in Nd:YLF and Nd:YAG. *Physical Review B*, **58**, 16076–16092.

Rothman, L.S., Barbe, A., Benner, D.C., Brown, L.R., Camy-Peyret, C., Carleer, M.R., Chance, K., Clerbaux, C., Dana, V., Devi, V.M., Fayt, A., Flaud, J.M., Gamache, R.R., Goldman, A., Jacquemart, D., Jucks, K.W., Lafferty, W.J., Mandin, J.Y., Massie, S.T., Nemtchinov, V., Newnham, D.A., Perrin, A., Rinsland, C.P., Schroeder, J., Smith, K.M., Smith, M.A.H., Tang, K., Toth, R.A., Vander Auwera, J., Varanasi, P., & Yoshino, K. 2003. The HITRAN Molecular Spectroscopic Database: Edition of 2000 Including Updates through 2001. *J. Quant. Spectrosc. and Rad. Transfer.*

Ryan, J.R., & Beach, R. 1992. Optical absorption and stimulated emission of neodymium in yttrium lithium fluoride. *J. Opt. Soc. Am. B*, **9**, 1883.

84

REFERENCES

SCIOPT. 2010. Paraxia Plus Software. *http://www.sciopt.com/paraxpls.htm [accessed Aug 2010]*.

Shen, D.Y., Abdolvand, A., Cooper, L.J., & Clarkson, W.A. 2004. Efficient Ho:YAG laser pumped by a cladding-pumped tunable Tm: silica-fibre laser. *Appl. Phys. B*, **79**, 559–561.

Siegman, A.E. 1986. *LASERS*. Mill Valley, California: University Science Books.

Strauss, H.S. 2009. *Thermo-optical effects in high-power end-pumped vanadate lasers.* Ph.D. thesis, University of Stellenbosch.

VLOC YAG Brochure. 2008. YAG Brochure. *www.vloc.com/PDFs/YAGBrochure.pdf*, February.

Walsh, B.M. 2009. Review of Tm and Ho materials; spectroscopy and lasers. *Laser Physics*, **19**(4), 855–866.

Walsh, B.M., Barnes, N.P., & Di Bartolo, B. 1998. Branching ratios, cross sections, and radiative lifetimes of rare earth ions in solids: Application to Tm3+ and Ho3+ ions in LiYF4. *Journal of Applied Physics*, **83**(5), 2772– 2787.

Weber, M.J. 2001. *Handbook of Lasers*. CRC Press.

Weber, R., Neuenschwander, B., & Weber, H.P. 1999. Thermal effects in solid-state laser materials. *Optical Materials*, **11**, 245–254.

List of Publications

Peer-Reviewed Journal Papers

1. **W. Koen**, C. Bollig, H. Strauss, M. Schellhorn, C. Jacobs, and M.J.D. Esser, "Compact Fibre-Laser-Pumped Ho:YLF Oscillator-Amplifier System," *Journal of Applied Physics B*, 21 November, 2009,

   URL: *http://www.springerlink.com/content/m823265551470079*

   DOI: *10.1007/s00340-009-3819-y*

International Conference Papers

1. C. Bollig, H.J. Strauss, M.J.D. Esser, **W. Koen**, M. Schellhorn, D. Preussler, K. Nyangaza, C. Jacobs, E.H. Bernhardi and L.R. Botha, "Compact Fibre-Laser-Pumped Ho:YLF Oscillator-Amplifier System," CLEO Europe, Munich, Germany, 14-19 June, 2009.

2. C. Bollig, M. J. D. Esser, C. Jacobs, **W. Koen**, D. Preussler, K. Nyangaza and M. Schellhorn, "70 mJ Single-Frequency Q Switched Ho:YLF Ring Laser - Amplifier System Pumped by a Single 82 W Tm Fibre Laser," Middle-Infrared Coherent Sources, Trouville, France, 8-12 June, 2009 **(invited)**.

3. M. J. Daniel Esser, H. Strauss, **W. S. Koen**, D. Preussler, K. Nyangaza and C. Bollig, "Q-switched Ho:YLF Laser Pumped by a Tm:GdVO4 Laser," Middle-Infrared Coherent Sources, Trouville, France, 8-12 June, 2009.

4. H. J. Strauss, **W. Koen**, C. Bollig, M. J. D. Esser, D. Preussler, K. Nyangaza and C. Jacobs, "Efficient Fiber-Laser-Pumped Ho:YLF Oscillator and Amplifier Utilizing the Transmitted Pump Power of the Oscillator," CLEO, Baltimore, USA, 31 May - 5 June, 2009.

5. C. Bollig, **W. Koen**, H. Strauss, E.H. Bernhardi, R. Botha, M.J.D. Esser and D. Preussler, "Exploiting the natural doping gradient of Nd:YLF crystals for high power end-pumped lasers," In Proceedings of the *3rd EPS-QEOD Europhoton Conference*, Paris, France, 31 August - 5 September, 2008.

6. M.J.D. Esser, C. Bollig, D. Preussler, C. Jacobs, **W. Koen** and E.H. Bernhardi, "High power diode end pumped Tm:GdVO$_4$ laser operating at 1818 nm and 1915 nm," In Proceedings of the *Marie Curie Chair Conference Recent advances in laser spectroscopy and laser technology*, Lodz, Poland, 29-31 May, 2007.

National Conference Papers

1. C. Bollig, M. J. D. Esser, C. Jacobs, **W. Koen**, D. Preussler and K. Nyangaza, "High-energy single-frequency Q switched 2-μm Ho:YLF oscillator - amplifier system pumped by a thulium fibre laser" in South African Institute of Physics 54th annual conference, University of KwaZulu-Natal, KwaZulu-Natal, July, 2009.

2. C. Jacobs, C. Bollig, M. J. D. Esser and **W. Koen**, "Electronic feedback control to stabilise a high-energy Ho:YLF ring laser" in South African Institute of Physics 54th annual conference, University of KwaZulu-Natal, KwaZulu-Natal, July, 2009.

3. M. J. D. Esser, C. Jacobs, S. Ngcobo, **W. Koen**, H. Strauss, D. Preussler, L.R. Botha and C. Bollig, "Development of high-energy 2 m solid-state lasers" in South African Institute of Physics 54th annual conference, University of KwaZulu-Natal, KwaZulu-Natal, July, 2009.

4. M.J.D. Esser, C. Bollig, D. Preussler, **W.S. Koen**, E. H. Bernhardi, H.J. Strauss, and M. Schellhorn "Tm:GdVO4 Laser as Pump Source For a Ho:YLF Laser Oscillator" in South African Institute of Physics 53srd annual conference, University of Limpopo, Polokwane, July, 2008.

5. **W. Koen**, C. Bollig, H. Strauss, R. Botha, E. Bernhardi, and M. J. D. Esser, "Power Scaling of a High-Power End-Pumped Nd:YLF Laser" in South African Institute of Physics 53srd annual conference, University of Limpopo, Polokwane, July, 2008.

6. H. J. Strauss, C. Bollig, M. J. D. Esser, M. Schellhorn, D. Preussler, C. Jacobs, K. Nyangaza1 and **W. Koen**, "High energy fibre laser pumped Ho:YLF 2μm laser" in South African Institute of Physics 53srd annual conference, University of Limpopo, Polokwane, July, 2008.

7. C. Bollig, D. Preussler, M. J. D. Esser, S. Ngcobo, C. Jacobs, R. C. Botha, **W. S. Koen**, E. H. Bernhardi, A. R. Sarmani and L. R. Botha, "Solid-state laser source research at the CSIR - National Laser Centre" in South African Institute of Physics 52nd annual conference, University of the Witwatersrand, Johannesburg, July, 2007.

8. M.J.D. Esser, C. Bollig, D. Preussler, C. Jacobs, **W. Koen** and E.H. Bernhardi, "Diode-end-pumped Tm:GdVO$_4$ laser at selected wavelengths" in Proceedings of the *52nd South African Institute of Physics Conference*, University of the Witwatersrand, Johannesburg, South Africa, July, 2007

9. **W. S. Koen**, C. Bollig, A. Forbes, A. R. Sarmani, R. C. Botha and M. J. D. Esser, "Ultra short-pulse (USP) laser development" in South African Institute of Physics 52nd annual conference, University of the Witwatersrand, Johannesburg, July, 2007.

10. R. C. Botha, C. Bollig, **W. S. Koen**, A. R. Sarmani, L. R. Botha and C. Jacobs, "Energy scaling techniques in ultra-short pulse lasers" in South African Institute of Physics 52nd annual conference, University of the Witwatersrand, Johannesburg, July, 2007.

11. R. C. Botha, C. Bollig, **W. S. Koen** and N. V. Kuleshov, "High-Power Continuous-Wave and Passively Q-switched 1314 nm Nd:YLF laser" in South African Institute of Physics 50th annual conference, Pretoria, 2005.

Appendix A

Appendix: Publications

Compact fibre-laser-pumped Ho:YLF oscillator–amplifier system

W. Koen · C. Bollig · H. Strauss · M. Schellhorn ·
C. Jacobs · M.J.D. Esser

Abstract We developed a compact Ho:YLF oscillator–amplifier system in a novel setup to utilise the unpolarised pump power from a fibre laser efficiently, and produced 21.3 mJ at 1 kHz, with an M^2 better than 1.1. The amplified energies agreed well with the predicted values from a two dimensional rotational symmetric amplifier model that we developed. The model considers upconversion losses and ground-state depletion, as well as the spatial distribution of the pump beam.

PACS 42.55.Xi · 42.60.Gd · 42.60.Da

1 Introduction

Q-switched lasers operating in the eye-safe 2 µm wavelength region have applications in a number of areas, including remote sensing, defence, materials processing and medical applications. Some of these require reliable and efficient operation in a compact device. Initial work on 2-µm holmium

W. Koen (✉) · C. Bollig · H. Strauss · C. Jacobs · M.J.D. Esser
National Laser Centre, Council for Scientific and Industrial
Research, P.O. Box 395, Pretoria 0001, South Africa
e-mail: wkoen@csir.co.za
Fax: +27-12-8413152

W. Koen
University of KwaZulu-Natal, Durban 4041, South Africa

H. Strauss · C. Jacobs
University of Stellenbosch, Private Bag X1 Matieland, 7602
South Africa

M. Schellhorn
French–German Research Institute, ISL, 5 rue du Général
Cassagnou, 68301 Saint-Louis, France

lasers concentrated on thulium–holmium co-doped operation [1]. More recently, work has concentrated on Ho lasers resonantly pumped by Tm lasers, both intra-cavity [2] and extra-cavity [3] pumped. With the emergence of high-power Tm-doped fibre lasers, efficient and robust Ho:YAG lasers pumped by Tm-fibre-lasers were demonstrated [4–6].

However, in order to achieve high-energy Q-switched operation, Ho:YLF is a more attractive laser material than Ho:YAG since it has a much longer upper laser level life-time (~14 ms) and higher emission cross section (1.8 × 10^{-20} cm^2 at 2050 nm versus 1.0×10^{-20} cm^2 at 2091 nm for Ho:YAG) [7, 8]. In addition, the very weak thermal lens on the σ-polarisation helps to deliver diffraction limited beams even under intense end-pumping. However, Ho:YLF has a somewhat stronger quasi-three-level nature than Ho:YAG. In order to reach gain at the 2065 nm line, 22% of the Ho ions need to be pumped into the upper laser level (at room temperature), but it already reaches transparency at the 1940 nm pump wavelength with only 56% of the Ho ions in the upper laser level (see Appendix). In addition, the pump absorption at 1940 nm is relatively weak and strongly polarised. Subsequently, the laser design requires a trade-off between efficient pump absorption and low laser threshold.

Efficient fibre-laser-pumped Ho:YLF oscillators have previously been demonstrated [9], but to scale the output energy further, an oscillator–amplifier system can be employed. The traditional approach when pumping an oscillator–amplifier system with one fibre laser pump source is to split the unpolarised pump beam into two polarised beams in order to pump the oscillator and amplifier crystals separately [10]. In our approach, we use the full unpolarised beam from the fibre laser to pump the oscillator, and then use the partially polarised transmitted pump light from the oscillator to pump the amplifier with its crystal rotated by

90° around the laser beam axis. This leads to a small system footprint and keeps the path length of the pump light short, reducing adverse effects of water absorption [11].

Figure 1 shows the emission and absorption spectra of Ho:YLF. The emission is stronger on the π-polarisation than on the σ-polarisation. However, the σ-polarisation has a much weaker thermal lens in YLF than the π-polarisation and is thus preferred for a high-power oscillator. In an amplifier, on the other hand, gain is the most important factor while the thermal lens is not as problematic as in an oscilla-

tor. Therefore, we chose to utilise the σ-polarisation for the laser oscillator and the π-polarisation for the amplifier.

2 Experimental set-up

The layout of the Ho:YLF oscillator/amplifier is shown in Fig. 2. A single 82 W Tm-fibre laser (Model TLR-80-1940, from IPG Photonics) was used as pump source. The fibre-laser's wavelength was selected to match the Ho:YLF absorption peak at 1940 nm. The pump light was collimated and sent through a telescope consisting of two lenses with respective focal lengths of 100 mm and −50 mm. The spot radius w_p of the pump beam was measured to be ∼600 μm.

We used the full unpolarised pump beam from the Tm-fibre laser to pump the oscillator crystal, which was a 0.5 at.% doped, a-cut Ho:YLF crystal with a length of 30 mm and a diameter of 6 mm. The crystal was mounted in a water cooled copper mount. The water temperature was kept constant at 20°C. The resonator was 370 mm long with a 500 mm concave back-reflector and a flat output coupler with a reflectivity of 50%. To keep the optical path of the pump light to the amplifier crystal to a minimum, the resonator was folded using 45° dichroic mirrors with high transmission for the pump light (s- and p-polarisation), high reflection for s-polarised laser light, and 20% transmission for π-polarised laser light, forcing the oscillator to operate vertically polarised. Having the c-axis of the crystal horizontal, we insured lasing on the σ-polarisation. A plane cut, AR coated crystal quarts acousto-optic modulator manufactured by *Gooch & Housego* (Model QS027-10M-NL5) was inserted for Q-switched operation. It delivered a loss modulation of approximately 80% at the maximum recommended RF power of 100 W. It was subsequently used with a gate time of 6 μs at 95 W of RF power. Neglecting thermal lensing, the calculated TEM$_{00}$ beam radius in the YLF crystal was 580 μm, which was assumed to increase at higher pump power due to the effect of the weak negative thermal lensing in Ho:YLF.
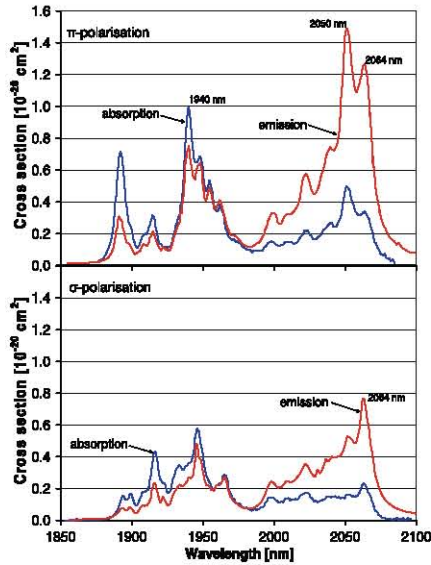
Fig. 1 Ho:YLF absorption and emission cross-sections [8]
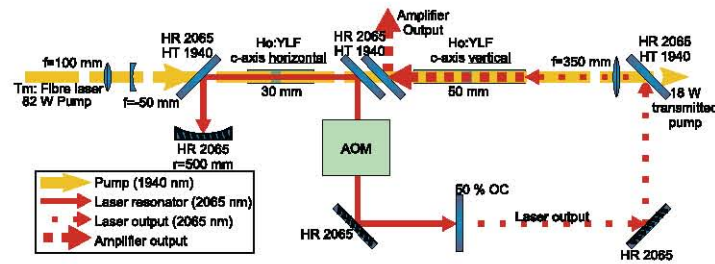
Fig. 2 A schematic diagram of the fibre-laser-pumped Ho:YLF oscillator–amplifier system

Compact fibre-laser-pumped Ho:YLF oscillator–amplifier system
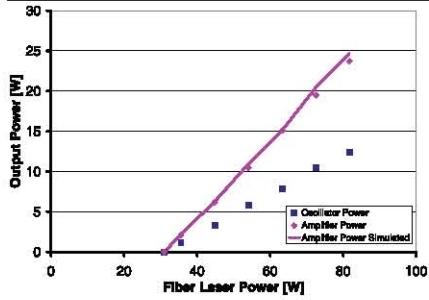
Fig. 3 Oscillator and amplifier output power versus fibre pump power under cw lasing conditions (*data points*) together with the results of a numerical simulation (*solid line*)
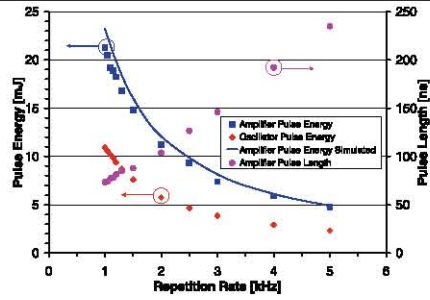
Fig. 5 Oscillator and amplifier output energy and FWHM pulse lengths as a function of the pulse repetition rate at full pump power (*data points*) together with the results of a numerical simulation (*solid line*)

Fig. 4 Amplifier small signal output power and gain under cw operation (*data points*) together with the results of a numerical simulation (*solid lines*)

Fig. 6 View of the energy levels of Ho:YLF taken into account in the presented amplifier model [12]

The transmitted pump power was subsequently used to pump the amplifier crystal (50 mm long, also 0.5 at.% doped) which was placed as close to the resonator as possible to minimise atmospheric water absorption of the 1940 nm pump light which would lead to heating of the air and subsequent thermal turbulence. This negated the need for any enclosure or dry-air flushing typically used for such setups to prevent pump-beam distortions caused by thermal turbulence. Since the absorption in Ho:YLF is strongly polarisation dependent, there is a difference between the transmissions of the two polarisations. This makes the transmitted light partially polarised. Therefore, in order to achieve maximum absorption in the amplifier crystal, it was orientated with its c-axis rotated by 90° with respect to the c-axis of the oscillator crystal. This effectively "swapped" the polarisations for the amplifier crystal. Thus, the π-polarisation, with the higher emission cross-section [8] but stronger thermal lens, was used for amplification

while the σ-polarisation, with the very weak thermal lens but lower cross section, was used in the oscillator.

The laser output was coupled into the amplifier crystal using a lens with a focal length of 350 mm.

3 Experimental results

The oscillator and amplifier were first operated in cw mode. The output power as a function of the fibre laser pump diode power incident on the crystal is shown in Fig. 3. The oscillator had a threshold of 31 W (17 W absorbed) of pump power, with an overall slope efficiency of 25% (47% vs. absorbed power). At full pump power (82 W), the oscillator power was 12.4 W and the amplified power was 23.7 W at a centre wavelength of 2065 nm. This corresponds to a gain of the

amplifier of 1.9. The total pump power transmitted through the oscillator crystal was 47 W (57% of the pump power) at full power. The amplifier crystal absorbed 62% (29 W) of this transmitted pump light, which left 22% (18 W) of the total pump light unused. The slope efficiency of the amplified beam versus total fibre pump power was 47% with an overall optical-to-optical efficiency of 29%. With respect to the total absorbed power ($35 + 29$ W), the slope efficiency was 60% and the overall efficiency was 37%. The efficiency with respect to incident pump power could be further increased by reflecting the 18 W transmitted pump light back into the amplifier and oscillator. This was not attempted as it was unclear at the time what the fibre-laser's tolerance to back reflection was.

A two dimensional rotational symmetric amplifier model was developed. The model considers upconversion losses and ground-state depletion, as well as the spatial distribution of the pump and laser beam and is described in detail in the Appendix. The parameter values used in the simulation are listed in Table 1. Taking into account the measured transmitted pump power through the laser crystal, the amplified cw laser power is calculated. The solid line in Fig. 3 shows the results of this calculation which agree well with the experimental data, if we assume a pump and laser spot radius of 550 μm, which is slightly smaller than the measured pump spot at the oscillator crystal of 600 μm. The total upconversion loss constant k_Σ must be set to zero in the simulation. If a small amount of upconversion is considered in the amplifier model (e.g. $k_\Sigma = 1 \times 10^{-18}$ cm^3/s) the gain decreases and the pump and laser spot size must be set to 475 μm to get good agreement with the experimental data, which was not the case in the experiments. Therefore, it can concluded from the amplifier model, that upconversion at the low dopant level of 0.5% in Ho:YLF is negligible.

The amplifier small signal gain was measured under cw operation at a fixed pump power of 75 W of the fibre laser. The oscillator output power was attenuated with different partial reflectors to vary the seed power of the amplifier. The amplifier was pumped with the transmitted pump power of 40 W. Figure 4 shows the measured amplifier small signal output power and gain under cw operation (data points) togethe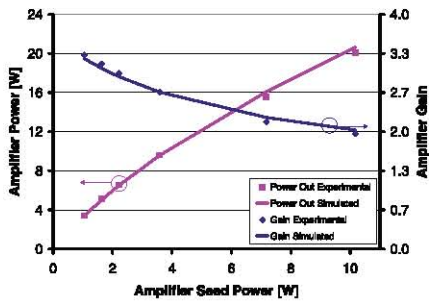r with the results of the numerical simulation (solid lines). The results of the simulation show good agreement with the experiment and the small signal gain of ~3.6 implies that the amplifier is operated nearly in saturation at full cw power.

The oscillator was subsequently Q-switched with an acousto-optic modulator at repetition rates between 5 kHz and 1 kHz. The pulse energies of the oscillator and amplifier and the FWHM pulse lengths as a function of the repetition rate are shown in Fig. 5 at full pump power together with the results of a numerical simulation. Repetition rates below 1 kHz were not attempted in order to keep the intra-cavity

Table 1 List of parameter values used in the simulation unless otherwise stated

Description, symbol [unit]	Ho:YLF
Dopant concentration	0.5%
Length of crystal, L [cm]	5
Upper level lifetime, τ_2 [ms] [7]	14
Pump wavelength, λ_p [μm]	1.94
Laser wavelength, λ_l [μm]	2.065
Eff. Stim. em. cross-section, σ_{eff} [10^{-21} cm^2]	12.5
Eff. pump abs. cross-section, σ_{abs} [10^{-21} cm^2]	7
Refractive index, n	1.44
Temperature, T [K]	300
Ratio of Boltzmann factors, F_p	1.2576
Ratio of Boltzmann factors, F_l	0.2845
Pump beam radius, w_p [μm]	550
Super-Gaussian pump parameter, sgp	2
Laser beam radius, w_l [μm]	550
Super-Gaussian pump parameter, sgl	2
Eff. pump quantum efficiency, η_p	1
Total UC loss constant, k_Σ [10^{-18} cm^3/s]	0

energy density below the damage threshold of the 45° pump mirrors. As expected, the highest pulse energies for the system in our operating regime was achieved at a repetition rate of 1 kHz with the oscillator delivering 10.9 mJ per pulse and an amplified pulse energy of 21.3 mJ with a FWHM pulse length of 74 ns. This corresponds to a gain of 2.2. Assuming a pump and laser spot radius of 550 μm (see Table 1) the results of the simulation show good agreement with the experiment and the calculated small signal gain of ~3.85 at 1 kHz repetition rate is slightly higher than in cw mode. The amplifier did not change the pulse length in any measurable way compared to the oscillator. The beam quality of the amplified beam was measured to be better than an M^2 of 1.1.

4 Conclusion

A novel oscillator–amplifier scheme was developed and successfully demonstrated, where the unused pump light transmitted by the oscillator was utilised to pump an amplifier crystal. The system produced more than 21 mJ energy per pulse at 1 kHz, with an M^2 better than 1.1. The amplified energies agreed well with the predicted values from a two dimensional rotational symmetric amplifier model that we developed. The model considers upconversion losses and ground-state depletion, as well as the spatial distribution of the pump beam. From the good agreement between simulation and experiment it can be concluded that upconversion at

93

the low dopant level of 0.5% in Ho:YLF is negligible. Further work entails building a single-frequency system with higher output energies at low pulse repetition rates.

Appendix: Amplifier model

We consider a cylindrical amplifier crystal which is end-pumped from one or both sides with a pump laser beam. The beam quality of the fibre laser is excellent ($M^2 < 1.1$). Assuming a spot radius of the pump beam $w_p = 550$ µm the Rayleigh range z_R ($z_R = \pi w_p^2 n / \lambda_p M^2$) is ~640 mm inside the crystal with refraction index $n = 1.44$ (λ_p is the wavelength of the pump beam). Therefore, the amplifier model is treated in a plane wave approximation. For the pump laser, a super-Gaussian intensity distribution is assumed which is given by

$$I_p(r) = \frac{P_p}{\pi w_p^2} \frac{sgp}{2^{1-\frac{2}{sgp}} \Gamma(\frac{2}{sgp})} \exp\left[-2\left(\frac{r}{w_p}\right)^{sgp}\right], \qquad (1)$$

where P_p is the pump power, sgp is the super-Gaussian exponent of the pump light and r is the radial position. The launched pump photon density at the entrance surface is thus given by

$$P_{\text{launched}}(r, z = 0) = \frac{I_p(r) n}{c_0 h \nu_p}, \qquad (2)$$

where c_0 is the speed of light and $h\nu_p$ is the pump photon energy.

When the YLF amplifier crystal is pumped with the 1940 nm fibre laser, the ground state ions in the $^5I_8$ Ho manifold can be excited to the upper lasing level of the $^5I_7$ Ho manifold as can be seen in Fig. 6. According to [13], the rate equations for the local population densities of the Ho manifolds read as:

$$\frac{dN_2(r, z, t)}{dt} = \frac{c_0}{n} \sigma_{\text{abs}}(\lambda_p) \eta_p \left[P^+(r, z, t) + P^-(r, z, t)\right]$$
$$\times \left[N_1(r, z, t) - \frac{N_2(r, z, t)}{F(\lambda_p, T)}\right]$$
$$- k_\Sigma N_2^2(r, z, t) - \frac{N_2(r, z, t)}{\tau_2}, \qquad (3)$$

$$N_1 = N_{\text{tot}} - N_2, \qquad (4)$$

where $\sigma_{\text{abs}}(\lambda_p)$ is the absorption cross-sections at the pump wavelength, η_p is the effective pump efficiency of the upper lasing level, P^+ and P^- are the local photon densities of the pump laser fields (the superscripts $+$ and $-$ refer to the forward and backward propagation directions), N_i are the population densities of the Ho ions of manifold i, N_{tot} is the holmium dopant concentration, k_Σ is the total upconversion

loss constant [14] and $F(\lambda_p, T)$ is the ratio $(f_1 g_2)/(f_2 g_1)$ of Boltzmann population distributions of Ho, which can be written as [15]

$$F(\lambda_p, T) = \frac{f_1}{f_2} \frac{g_2}{g_1} = \frac{Z_2(T)}{Z_1(T)} \exp\left[\frac{hc_0}{kT}\left(\frac{1}{\lambda_p} - E_0\right)\right], \quad (5)$$

where $Z_1(T)$ and $Z_2(T)$ are the partition functions of the $^5I_8$ and $^5I_7$ manifolds of Ho as function of the temperature T, and E_0 is the energy of the lowest energy level of the $^5I_7$ Ho manifold.

The forward and reverse propagating pump fields P^+ and P^- are iterated along the length of the amplifier crystal according to

$$\frac{dP^\pm(r, z, t)}{dz} = \mp P^\pm(r, z, t) \sigma_{\text{abs}}(\lambda_p)$$
$$\times \left[N_1(r, z, t) - \frac{N_2(r, z, t)}{F(\lambda_p, T)}\right]. \qquad (6)$$

Note that the negative sign in (6) relates to the forward $(+z)$-direction and the positive sign to the reverse $(-z)$-direction.

The treatment considers either a cw or a Q-switched laser beam to be amplified in a single or double pass through the crystal. For cw, a super-Gaussian intensity distribution is assumed:

$$I_l(r) = \frac{P_l}{\pi w_l^2} \frac{sgl}{2^{1-\frac{2}{sgl}} \Gamma(\frac{2}{sgl})} \exp\left[-2\left(\frac{r}{w_l}\right)^{sgl}\right]. \qquad (7)$$

For Q-switching a Gaussian temporal pulse shape according to

$$I_l(r, t) = \frac{E_l}{\pi^{3/2} t_0 w_l^2} \frac{sgl}{2^{1-\frac{2}{sgl}} \Gamma(\frac{2}{sgl})}$$
$$\times \exp\left[-2\left(\frac{r}{w_l}\right)^{sgl} - \left(\frac{t}{t_0}\right)^2\right] \qquad (8)$$

with

$$t_0 = \frac{t_{\text{FWHM}}}{2\sqrt{\ln(2)}} \qquad (9)$$

is assumed, where P_l is the incident laser power (cw mode), E_l is the energy (Q-switched mode) of the incident laser pulse, w_l is the laser spot radius, sgl is the super-Gaussian exponent of the laser light and t_{FWHM} is the full width at half maximum pulse duration of the incident pulse. The launched laser photon density at the entrance surface is therefore given by

$$S_{\text{launched}}(r, z = 0, t) = \frac{I_l(r, t) n}{c_0 h \nu_l}, \qquad (10)$$

where $h\nu_l$ is the laser photon energy.

Inside the crystal the forward and reverse propagating amplified laser fields S^+ and S^- (photon densities) are iterated along the length of the crystal according to

$$\frac{dS^{\pm}(r,z,t)}{dz} = \pm S^{\pm}(r,z,t)\sigma_{\text{eff}}(\lambda_l)$$
$$\times \left[N_2(r,z,t) - F(\lambda_l,T)N_1(r,z,t) \right]$$
$$+ \frac{\Delta\Omega}{4\pi} \frac{N_2(r,z,t)}{\tau_2 c_0}. \tag{11}$$

Note that the positive sign in (11) relates to the forward $(+z)$-direction and the negative sign to the reverse $(-z)$-direction. $\sigma_{\text{eff}}(\lambda_l)$ is the effective stimulated emission cross-section at the Ho wavelength λ_l, $F(\lambda_l,T)$ is the ratio $(f_1 g_2)/(f_2 g_1)$ of Boltzmann population distributions of Ho at the lasing wavelength λ_l given by (5) (by replacing λ_p with λ_l). The last term in (11) is amplified spontaneous emission, where $\Delta\Omega$ is the solid angle given by the length of the amplifier crystal L and the pump spot radius w_p ($\Delta\Omega = 2\pi \cdot (1 - \cos\beta)$, with $\beta = \tan^{-1}(\frac{w_p}{L})$).

Calculating the local population in (3) and iterating (6) and (11) along the length of the amplifier crystal, we obtain the extracted photon densities of the laser field after amplification. The simulations have been done using the parameters listed in Table 1.

A positive gain could be deduced from setting the first term in (11), i.e. $N_2 - F(\lambda_l,T)N_1 > 0$, which results in $N_2/N_{\text{tot}} = F(\lambda_l,T)/(1 + F(\lambda_l,T)) = 0.22$. The amplifier becomes transparent if (6) is set to zero, which results in $N_2/N_{\text{tot}} = F(\lambda_p,T)/(1 + F(\lambda_p,T)) = 0.56$.

References

1. T.Y. Fan, G. Huber, R.L. Byer, P. Mitzscherlich, Spectroscopy and diode laser-pumped operation of Tm,Ho:YAG. IEEE J. Quantum Electron. **24**(6), 924 (1988)
2. C. Bollig, R.A. Hayward, W.A. Clarkson, D.C. Hanna, 2-W Ho:YAG laser intracavity-pumped by a diode-pumped Tm:YAG laser. Opt. Lett. **23**(22), 1757 (1998)
3. P.A. Budni, M.L. Lemons, J.R. Mosto, E.P. Chicklis, High-power/high-brightness diode-pumped 1.9-µm thulium and resonantly pumped 2.1-µm holmium Lasers. IEEE J. Sel. Top. Quantum Electron. **6**(4), 629 (2000)
4. E. Lippert, G. Arisholm, G. Rustad, K. Stenersen, Fiber laser pumped mid-IR source, in *Advanced Solid State Photonics*, ed. by J.J. Zayhowski. OSA Trends in Optics and Photonics Series, vol. 83 (2003), pp. 292–297
5. D.Y. Shen, A. Abdolvand, L.J. Cooper, W.A. Clarkson, Efficient Ho:YAG laser pumped by a cladding-pumped tunable Tm: silica-fibre laser. Appl. Phys. B **79**, 559 (2004)
6. E. Lippert, S. Nicolas, G. Arisholm, K. Stenersen, G. Rustad, Mid-infrared laser source with high power and beam quality. Appl. Opt. **45**, 3839 (2006)
7. S.A. Payne, L.L. Chase, L.K. Smith, W.L. Kway, W.F. Krupke, Infrared cross-section measurements for crystals doped with Er^{3+}, Tm^{3+}, and Ho^{3+}. IEEE J. Quantum Electron. **28**(11), 2619 (1992)
8. B.M. Walsh, N.P. Barnes, B. Di Bartolo, Branching ratios, cross sections, and radiative lifetimes of rare earth ions in solids: Application to Tm^{3+} and Ho^{3+} ions in $LiYF_4$. J. Appl. Phys. **83**(5), 2772 (1998)
9. Y. Bai, J. Yui, M. Petros, P. Petzar, P. Trieu, H. Lee, U. Singh, Highly efficient Q-switched Ho:YLF laser pumped by Tm:fiber laser, in *CLEO/QELS Conference*, paper CtuN5 (2007)
10. A. Dergachev, D. Armstrong, A. Smith, T. Drake, M. Dubois, 3.4-µm ZGP RISTRA nanosecond optical parametric oscillator pumped by a 2.05-µm Ho:YLF MOPA system. Opt. Express **15**, 14404 (2007)
11. L.S. Rothman, A. Barbe, D.C. Benner, L.R. Brown, C. Camy-Peyret, M.R. Carleer, K. Chance, C. Clerbaux, V. Dana, V.M. Devi, A. Fayt, J.-M. Flaud, R.R. Gamache, A. Goldman, D. Jacquemart, K.W. Jucks, W.J. Lafferty, J.-Y. Mandin, S.T. Massie, V. Nemtchinov, D.A. Newnham, A. Perrin, C.P. Rinsland, J. Schroeder, K.M. Smith, M.A.H. Smith, K. Tang, R.A. Toth, J. Vander Auwera, P. Varanasi, K. Yoshino, The HITRAN molecular spectroscopic database: edition of 2000 including updates through 2001. J. Quantum Spectrosc. Radiat. Transfer **82**, 5 (2003)
12. P.L. Cross, Database of laser materials. Laser Systems Branch, NASA Langley Research Center, USA (2004). Previously available from: http://aesd.larc.nasa.gov/gl/laser/dbmain.htm (Accessed March 2005)
13. M. Schellhorn, A. Hirth, Modelling of intracavity-pumped quasi-three-level lasers. IEEE J. Quantum Electron. **38**, 1455 (2002)
14. G. Rustad, K. Stenersen, Modelling of laser-pumped Tm and Ho lasers accounting for upconversion and ground-state depletion. IEEE J. Quantum Electron. **32**, 1645 (1996)
15. R.C. Stoneman, L. Esterowitz, Efficient 1.94-µm Tm:YALO laser. IEEE J. Sel. Top. Quantum Electron. **1**, 78 (1995)

Compact Fibre-Laser-Pumped Ho:YLF Oscillator-Amplifier System

C. Bollig[1], H.J. Strauss[1], M.J.D. Esser[1], W. Koen[1], M. Schellhorn[2], D. Preussler[1], K. Nyangaza[1], C. Jacobs[1], E.H. Bernhardi[1,3] and L.R. Botha[1]

1. National Laser Centre, Council for Scientific and Industrial Research, PO Box 395, Pretoria, 0001, South Africa

2. French-German Research Institute, ISL, 5, rue du Général Cassagnou, 68301, Saint-Louis, France

3. Integrated Optical MicroSystems (IOMS), MESA+ Institute for Nanotechnology, University of Twente, Enschede, The Netherlands

Ho:YLF is an attractive laser material for 2 µm high energy sources since it has a much longer upper laser level lifetime (~14 ms) and higher emission cross section than Ho:YAG. In addition, the very weak thermal lens on the σ-polarisation helps to deliver diffraction limited beams even under intense end-pumping. However, Ho:YLF has a somewhat stronger quasi-three-level nature, which implies that in order to reach transparency at the 2065 nm line, 22% of the Ho ions need to be pumped into the upper laser level (at room temperature), but it already reaches transparency at the 1940 nm pump wavelength with only 56% of the Ho ions in the upper laser level. In addition, the pump absorption cross section at 1940 nm is relatively low and strongly polarised. Therefore, the laser design requires a trade-off between efficient pump absorption and low laser threshold.

Efficient fibre-laser-pumped Ho:YLF oscillators have previously been demonstrated [1], but to scale the output energy further, an oscillator-amplifier system can be employed. The traditional approach when pumping an oscillator-amplifier system with one fibre laser pump source is to split the unpolarised pump beam into two polarised beams in order to pump the oscillator and amplifier crystals separately [2]. In our novel approach, we used the full unpolarised pump beam from our 82 W Tm-fibre laser to pump a relatively short oscillator crystal (30 mm long, 0.5% doped), which absorbs roughly half the pump power under lasing conditions, mainly on its π-polarisation . The transmitted pump power is subsequently used to pump the amplifier crystal (50 mm long, also 0.5% doped), as illustrated in Figure 1. We orientated the c-axis of the two crystals perpendicular to each other, in order to optimally utilise the unpolarised pump light and to facilitate lasing on the σ-polarisation (with the weak thermal lens) in the oscillator, while amplifying on the stronger π-polarisation. The distances between the pump fibre collimator and the crystals were kept short to minimise atmospheric water absorption at 1940 nm. This enabled us to work without any enclosure or dry-air flushing.
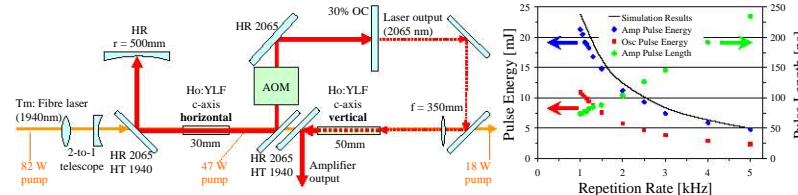

Fig. 1 A schematic diagram of the compact fibre-laser-pumped Ho:YLF oscillator-amplifier system.
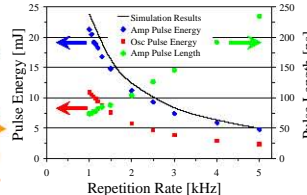
Fig. 2 Output energy of the Ho:YLF oscillator, and of the oscillator-amplifier system.

The 370 mm long oscillator, initially operated CW, had a threshold of 31 W (17 W absorbed) of pump power, an overall slope efficiency of 25% (47% vs. absorbed power), and a maximum average output power of 12.4 W at a centre wavelength of 2065 nm. The oscillator was subsequently Q-switched with an acousto-optic modulator at repetition rates of 5 kHz down to 1 kHz, which resulted in a maximum pulse energy of 10.9 mJ, as indicated in Figure 2. Lower repetition rates were not attempted in order to keep the intra-cavity energy density below the damage threshold of the two 45° dichroic pump mirrors.

After passing the laser output through the amplifier crystal, the slope efficiency of the system increased to 47%. The maximum pulse energy at 1 kHz was 23.7 mJ in a FWHM pulse length of 74 ns. This gain factor of 2.2 was not much less than the measured maximum small-signal gain of 3.3. The beam quality of the amplified beam had an M^2 of better than 1.1. The amplified energies agreed well with the predicted values from a two dimensional rotational symmetric amplifier model that we have developed (solid line in Figure 2). The model considers upconversion losses and ground-state depletion, as well as the spatial distribution of the pump beam.

In conclusion, we demonstrated a Ho:YLF oscillator-amplifier system in a compact setup which efficiently utilises the unpolarised power from a fibre laser. The system produced more than 23 mJ energy per pulse at 1 kHz, while maintaining an M^2 of better than 1.1. These results agreed well with our amplifier model.

References

[1] Y. Bai, J. Yui, M. Petros, P.Petzar, P. Trieu, H. Lee, and U. Singh, "Highly efficient Q-switched Ho:YLF laser pumped by Tm:fiber laser." CLEO/QELS Conference. May 6–11 (2007) paper CtuN5. Baltimore Convention Center, Baltimore, Maryland, USA

[2] A. Dergachev, D. Armstrong, A, Smith, T. Drake, and M. Dubois, "3.4-µm ZGP RISTRA nanosecond optical parametric oscillator pumped by a 2.05-µm Ho:YLF MOPA system" Opt. Express **15**, 14404 (2007).

70 mJ Single-Frequency *Q*-Switched Ho:YLF Ring Laser - Amplifier System Pumped by a Single 82-W Tm Fibre Laser

C. Bollig[*1], M. J. D. Esser[1], C. Jacobs[1], W. Koen[1], D. Preussler[1], K. Nyangaza[1] and M. Schellhorn[2],

1. National Laser Centre, Council for Scientific and Industrial Research (CSIR), PO Box 395, Pretoria 0001, South Africa (* cbollig@csir.co.za),

2. French-German Research Institute, ISL, 5, rue du Général Cassagnou, 68301 Saint-Louis, France

1 INTRODUCTION

High energy 2-µm solid state lasers have applications in a number of areas, including remote sensing, medicine and defence. Furthermore, single-frequency operation is often required for applications such as remote trace gas monitoring and wind detection using coherent lidar. Traditionally, high-energy single-frequency *Q*-switched operation in the 2-µm region is achieved with side-pumped Tm,Ho:YLF or Tm,Ho:LuLF lasers.[1] However, due to the high complexity and relatively low efficiency of these systems, recent work has focussed on Ho-doped solid-state lasers pumped by Tm fibre lasers, especially on Ho:YLF lasers.[2,3] However, a single-frequency *Q*-switched fibre-laser-pumped Ho laser has, to our knowledge, not yet been reported. In this paper, we present an injection-seeded single-frequency *Q*-switched Ho:YLF oscillator-amplifier system pumped by a single 82-W Tm fibre laser, which delivers 70 mJ per pulse at 50 Hz repetition rate.

2 PUMPING SCHEME

Commercial high-power Tm fibre lasers are typically unpolarised. However, the 1940-nm absorption line of Ho:YLF is strongly polarisation dependent. At this wavelength, the absorption cross section on the π-polarisation is more than twice as high as the absorption cross section on the σ-polarisation. In addition, the crystal needs to be kept short due to the quasi-3-level nature of Ho:YLF, requiring a trade-off between efficient absorption and low laser threshold.

It is possible to improve the absorption by forcing the fibre laser onto a single polarisation through optical feedback.[2] However, this results in a ~25% reduction of available power from the fibre laser.[2] Another approach, which is more widely used, is to split the unpolarised pump beam into two polarised beams in order to pump the oscillator and amplifier crystals separately.[3]

We recently reported an alternative approach,[4] where the full unpolarised pump beam from our 82-W Tm-fibre laser was used to pump a relatively short oscillator crystal, which absorbed roughly half the pump power under lasing conditions. The transmitted pump power was subsequently used to pump the amplifier crystal. We orientated the c-axis of the two crystals perpendicular to each other, in order to optimally utilise the unpolarised pump light and to facilitate lasing on the σ-polarisation (with the weak thermal lens) in the oscillator, while amplifying on the stronger π-polarisation.[4]

In the experiments reported here, a similar approach was used, with the main difference that the oscillator was a seeded single-frequency ring laser instead of the standing-wave laser reported in Ref. 4. As previously, the distances between the pump fibre collimator and the crystals were kept short to minimise atmospheric water absorption at 1940 nm.

3 Ho:YLF RING LASER

3.1 Setup

The achievable energy at low repetition rates is often limited by either a too high gain or damage to coatings or the crystal. This can be avoided by increasing the laser mode size. On the other hand, a large mode size in the gain crystal leads to an increased laser threshold and reduced efficiency. Therefore, a careful trade-off between these two effects is required. Since the threshold depends only on the mode size in the crystal, the resonator design should ensure that the laser mode is at least as large on all mirrors and other optical surfaces as it is in the gain crystal.

For the experiments reported here, a pump and laser mode radius of w = ~1 mm in the 40-mm long, 0.5%-doped Ho:YLF crystal was chosen. In order to achieve relatively long *Q*-switched pulses, a 2.4 m long ring resonator was used, which had the minimum mode size in the gain crystal (see Fig. 1). The ~125 mm distance between the convex mirror M6

(500 mm ROC) and the concave mirror M5 (-300 mm ROC) could be adjusted to fine tune the resonator mode size in the Ho:YLF crystal and to compensate for thermal lensing. The R = 80% output coupler proved to be the best compromise between efficient operation and intra-cavity fluence.
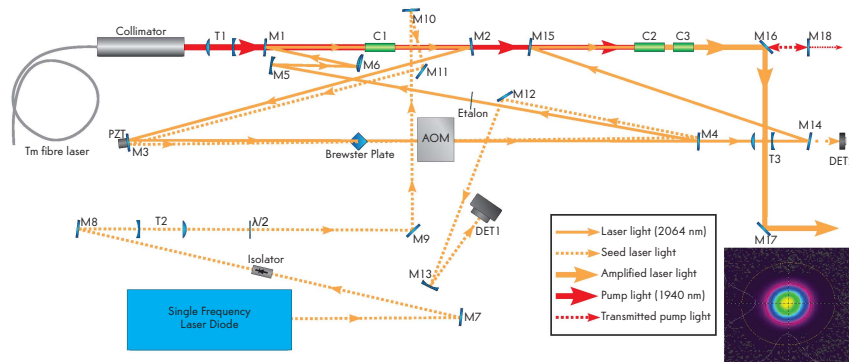

Figure 1: Setup of the Ho:YLF ring laser and amplifier with beam profile of the *Q*-switched amplified beam in the insert.

In order to enforce operation on the σ-polarisation, a 4-mm thick crystalline quartz plate was inserted as Brewster plate and orientated for minimum loss. A 400-µm thick fused-silica etalon was used to fine-tune the oscillator wavelength to be close to the 2064 nm seeding wavelength.

3.2 Injection seeding

The single frequency diode laser emitted 13 mW cw power at 2064 nm. Seeding was performed through the first order of the 27 MHz acousto-optic modulator. The diode laser current was modulated with a 20 MHz RF signal, so that the Pound-Drever-Hall technique could be used for resonator locking.[5] The detector DET1 was used to detect the oscillator resonance of the seed laser, with electronic feedback to the piezo-controlled mirror M3. Once locked, the seeding was stable and in resonance, ensuring reliable unidirectional, single-frequency operation.

3.3 Oscillator performance

Roughly 40 W of the 82 W Tm fibre laser pump power was absorbed in the Ho:YLF oscillator crystal in a single pass. At this pump power level, the oscillator delivered 31 mJ of single-frequency energy per pulse at 50 Hz repetition rate. This increased to 35 mJ when the double-pass pumping scheme was implemented, despite the fact that it added less than 1 W of absorbed pump power to the oscillator crystal. The pulse length was ~320 ns.

4 AMPLIFIER

4.1 Amplifier modelling

The amplifier performance was predicted with a two dimensional rotational symmetric amplifier model that we developed. The model considers upconversion losses and ground-state depletion, as well as the spatial distribution of the pump beam. In the model, we simulated a 30 mJ seed pulse at 50 Hz pulse repetition frequency, amplified in a single 50 mm long, 0.5% doped Ho:YLF crystal pumped by 40 W of 1940-nm pump power. Figure 2 shows the results for single-pass pumping and for double-pass pumping.

It was decided to use a $w = 1$ mm seed beam in order to keep the peak fluence as low as possible. The pump beam at the amplifier crystal C2 was measured to also have a size of $w = 1$ mm and therefore it was decided not to insert any further beam shaping optics into the pump beam.
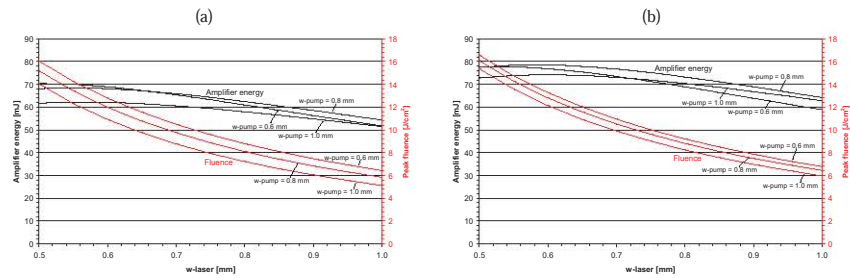
Figure 2: Simulated amplifier output energy and peak fluence for (a) single-pass pumping and (b) double-pass pumping as function of the laser beam size for various pump beam sizes.

4.2 Amplifier setup

After amplification with a single 50 mm Ho:YLF crystal (C2, inserted with its c-axis vertical), the remaining transmitted pump power was still 16.5 W. Since the maximum safe back reflection into the fibre laser was specified at 5%, a third 30mm crystal (C3) was added before back-reflecting the pump for double pass absorption. The output energy was nearly independent of the rotation of the C3. However, with its c-axis horizontal (amplifying on the σ-polarisation), the beam profile was significantly better. With all three crystals inserted, the transmitted pump power was 6 W, so that it was safe to reflect the pump back.

4.3 Amplifier performance

At 50 Hz, the output of a single 50-mm amplifier crystal with single-pass pump was 52 mJ. With both 50 and 30 mm crystals, but single-pass pumping the output energy was 54 mJ and with double-pass pumping the output energy was 70 mJ. The big increase in performance is probably due to an increased performance of both the oscillator and the amplifier under double-pass pumping. So far, an M^2-measurement was only performed cw under full pump power with the AOM constantly on to maintain unidirectional operation, which yielded a value of $M^2 < 1.1$. However, the beam profile measured with a Pyrocam looks similar both for the cw case and under pulsed operation (see insert in Fig. 1).

5   CONCLUSIONS

A single-frequency Q-switched oscillator-amplifier system was demonstrated, with 70 mJ output energy. The laser system was operated daily over several weeks with robust locking at all times. During the time, the output energy varied between 60 and 80 mJ. To our knowledge, this is the first report of a fibre-laser pumped single-frequency Q-switched Ho laser and the highest energy ever reported of any Ho oscillator-amplifier system pumped by a single Tm fibre laser.

REFERENCES

1.   M. Petros, J. Yu, B. Trieu, Y. Bai, P. Petzar and U. N. Singh, "300mJ, injection seeded, compact 2µm coherent Lidar transmitter," *Lidar Remote Sensing for Environmental Monitoring VII*, Proc. of SPIE 6409, 64091A, (2006).
2.   Y. Bai, J. Yui, M. Petros, P.Petzar, P. Trieu, H. Lee and U. Singh, "Highly efficient Q-switched Ho:YLF laser pumped by Tm:fiber laser." CLEO/QELS Conference, paper CtuN5, Baltimore, Maryland, USA (May 2007)
3.   A. Dergachev, D. Armstrong, A, Smith, T. Drake and M. Dubois, "3.4-µm ZGP RISTRA nanosecond optical parametric oscillator pumped by a 2.05-µm Ho:YLF MOPA system," Opt. Express **15** (22) pp 14404-14413 (2007)
4.   H. J. Strauss, W. Koen, C. Bollig, M. J. D. Esser, D. Preussler, K. Nyangaza and C. Jacobs, "Efficient Fiber-Laser-Pumped Ho:YLF Oscillator and Amplifier Utilizing the Transmitted Pump Power of the Oscillator," CLEO/QELS Conference, paper CWH3, Baltimore, Maryland, USA (June 2009)
5.   E. D. Black, "An introduction to Pound-Drever-Hall laser frequency stabilization," Am. J. Phys. **69** (1) pp 79-87 (2001)

Q-switched Ho:YLF Laser Pumped by a Tm:GdVO$_4$ Laser

M. J. Daniel Esser,* H. Strauss, W. S. Koen, D. Preussler, K. Nyangaza and C. Bollig

National Laser Centre, Council for Scientific and Industrial Research, PO Box 395, Pretoria, 0001,
South Africa (*desser@csir.co.za)

INTRODUCTION

Orthovanadates are attractive host crystals for rare-earth doped diode-pumped solid-state lasers. This is also the case when doped with Tm^{3+} or Ho^{3+}, which have been shown to exhibit certain advantages over other host crystals for Mid-IR lasers.[1,2] In particular, it has been shown that Tm:GdVO$_4$ has strong and broad absorption features at the emission wavelength of commercially available high power laser diodes at ~800 nm.[1] In addition, the broad emission peak at 1.9 µm in Tm:GdVO$_4$ can be utilised for laser operation over a wide wavelength tuning range, including wavelengths which can be used to pump Ho^{3+} and Cr^{2+}:ZnSe lasers.[3] The highest laser output power was reported by Li *et al* who achieved a maximum continuous-wave output power of 2.8 W from a diode-end-pumped Tm:GdVO$_4$ laser.[4] In addition, with the use of an intra-cavity birefringence filter, they demonstrated a tuning range of 126 nm (1820 to 1946 nm). More recently, a comparative study of the tuning ranges of Tm:YVO$_4$, Tm:LuVO$_4$ and Tm:GdVO$_4$ was conducted by Šulc *et al*, both in continuous wave (CW) and quasi-continuous wave (QCW) mode.[5] Also, we have previously demonstrated a diode-end-pumped QCW Tm:GdVO$_4$ laser operating at 1818 nm or at 1915 nm by appropriate selection of the resonator output coupling value.[6] Thus, even though significant wavelength tuning has been demonstrated for Tm:GdVO$_4$, to our knowledge, there has been no report of a Tm:GdVO$_4$ laser pumping a Ho^{3+} laser. In this paper we report on the design and operation of a diode-end-pumped QCW Tm:GdVO$_4$ laser selected to lase at 1892 nm, which was used to pump a *Q*-switched Ho:YLF laser.

SPECTRAL ANALYSIS

To design a high-power diode-pumped Tm:GdVO$_4$ laser for pumping a Ho:YLF laser, detailed spectroscopic studies of the laser materials are required. The absorption cross section data (σ_{abs}) of Ho:YLF for the $^5I_8$ – $^5I_7$ transition is shown in Figure 1.[7] The absorption is highly polarised and it would be preferential to pump on either of the two absorption peaks of the π-polarisation (*E*||*c*), located at 1892 nm (0.72 x 10^{-20} cm^2), and at 1940 nm (0.99 x 10^{-20} cm^2).[7] When pumped at either of these two wavelengths, the Ho:YLF laser can emit at 2.05 µm, (on π-polarisation) or at 2.06 µm when forced to lase on the weaker σ-polarisation (*E*⊥*c*).
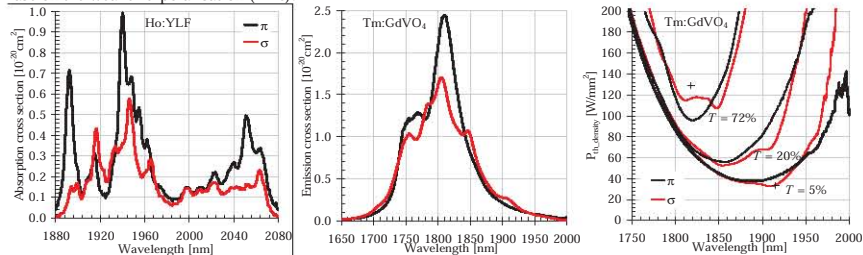
Figure 1: The absorption cross section of Ho:YLF; the emission cross section of Tm:GdVO$_4$, and the calculated threshold power density of the Tm:GdVO$_4$ laser with different transmission *T* output coupler mirrors.

We have previously measured the absorption cross section (σ_{abs}) of our Tm:GdVO$_4$ laser crystals at 1.9 µm to enable accurate predictions of the laser performance[8]. Based on the measurements, we calculated with the reciprocity method[9] the emission cross section (σ_{em}) of Tm:GdVO$_4$ for the $^3F_4$ – $^3H_6$ laser transition, also shown in Figure 1. From this graph it is evident that the Tm:GdVO$_4$ laser emission will be stronger at the 1892 nm pump wavelength of Ho:YLF, compared to the 1940 nm absorption line.

The wavelength of the quasi-three level Tm:GdVO$_4$ laser can be roughly selected by choosing the correct output coupling value. To determine the output coupler transmission to operate at 1892 nm, we calculated the expected

threshold power and the operational wavelength of the Tm:GdVO$_4$ laser for different output coupling values T. The calculations were made using the expression,[10, 11]

$$P_{\text{th\_density}}(\lambda) = \frac{P_{\text{th}}}{\pi w^2} = \frac{h\nu_{\text{p}}\left[L + T + 2Nl\sigma_{\text{abs}}(\lambda)\right]}{2\tau\eta_{\text{p-q}}\sigma_{\text{em}}(\lambda)}$$

where L represents additional resonator losses, assumed to be 1%; $w_l \approx w_p \approx w$ is the laser mode and pump beam radius in the laser crystal, assumed to be equal for the end-pumped laser developed; N is the concentration of Tm^{3+} ions in the laser crystal (3% at. doping x 1.21×10^{22} cm^3);[12] ν_{p} is the frequency of the pump light; $\eta_{\text{p-q}}$ is the pump quantum efficiency, typically assumed to be 1.5 for diode-pumped Tm^{3+} lasers to incorporate the 2-for-1 pumping process; τ is the lifetime of the ^{3}F$_4$ upper laser manifold, taken as 1.85 ms);[1] and l is the length of the laser crystal, which was 3 mm.

The result of the calculations for three output coupling values is shown in Figure 1. For a particular output coupling value T, continuous-wave laser oscillation will occur at the wavelength and polarisation for which the threshold power density is a minimum. This method of analysing a laser material for laser performance is complimentary to the "effective emission cross section" method used by other authors.[1,13] The calculation method we used provides a clear indication on what polarisation and output coupling loss to select in order to operate the Tm:GdVO$_4$ laser at 1892 nm. By selecting an output coupler transmission $T = 5\%$ (reflectivity 95%), and by inserting a Brewster plate inside the laser to force it to operate on π-polarisation, the Tm:GdVO$_4$ wavelength will be approximately at 1890 nm. To further fine-tune the output wavelength of the Tm:GdVO$_4$ laser onto the absorption peak of Ho:YLF at 1892 nm, we inserted an uncoated fused-silica etalon of thickness 100 µm in the Tm:GdVO$_4$ laser resonator.

EXPERIMENTAL SETUP

The 3% at. doped Tm:GdVO$_4$ crystal (2.5 x 2.5 x 3 mm^3) was end-pumped with two fibre-coupled laser diodes, as indicated in Figure 2. The laser diodes were operated in a quasi-continuous-wave (QCW) mode with the pump pulse on-time set to 20 ms at 5 Hz repetition rate (10% duty cycle). The duty cycle was limited, as well as the launched pump power (maximum 30 W from each diode), to avoid thermal fracture of the Tm:GdVO$_4$ crystal. The Tm:GdVO$_4$ resonator was based on a compact design, with a concave high-reflector (HR) end-mirror with r = 200 mm, which was also coated for high transmission (HT) at the pump wavelength (804 nm). The plane output coupler reflectivity was 95% at 1.9 µm (unspecified at 804 nm). The Tm:GdVO$_4$ resonator, containing a Brewster plate and a 100 µm etalon, had an optical length of approximately 73 mm.
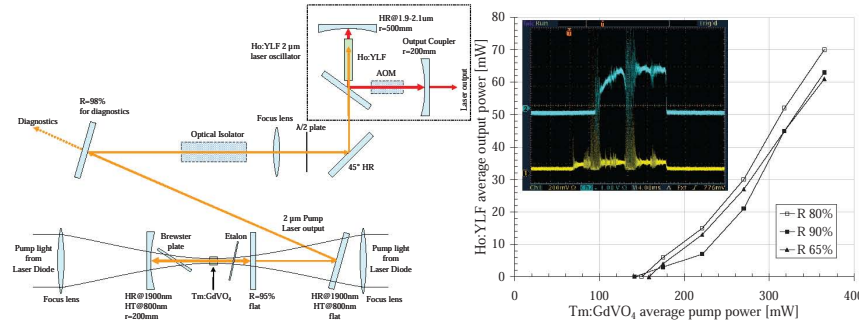

Figure 2: Experimental setup of the Tm:GdVO$_4$ pumped Ho:YLF laser. Figure 3: QCW output of the Ho:YLF laser.

The output beam of the Tm:GdVO$_4$ laser was transmitted through an optical isolator to protect the Tm:GdVO$_4$ laser from back reflections from the Ho:YLF resonator. A lens with focal length 350 mm was used to produce a spot size of 480 µm diameter inside the 40 mm long, 0.5% doped Ho:YLF crystal. The folded Ho:YLF resonator was formed between the 500 mm curved end-mirror and the 200 mm curved output coupler mirror. The fold mirror had a 25-30% loss for the p-polarisation and a high reflection for the s-polarisation at the Ho:YLF laser wavelengths, and a high transmission for the pump light at 1892 nm. Due to this fold mirror, the Ho:YLF laser could be operated on either π-polarisation (2.05 µm) or σ-polarisation (2.06 µm) by the appropriate orientation of the Ho:YLF crystal axis. The pump polarisation was controlled

with the $\lambda/2$ plate at 1892 nm to ensure that the Ho:YLF crystal was pumped on the π-polarisation. The laser back mirror also reflected the pump beam to realise a double-pass pump scheme. The etalon inside the Tm:GdVO$_4$ cavity was adjusted during lasing conditions to set its wavelength to the maximum absorption in Ho:YLF. An acoustic-optical modulator (AOM) was used as Q-switch for the Ho:YLF laser, which was synchronised to the QCW output pulse of the Tm:GdVO$_4$ laser.

RESULTS

Three Ho:YLF output coupler mirrors with reflectivity R80%, R90% and R65% at 2 µm were used during the initial QCW experiments, the result of which is shown in Figure 3. Also shown in Figure 3 is the measured QCW pump pulse at 1892 nm (Channel 1), and the free-running Ho:YLF laser pulse (Channel 2) that followed the pump pulse after a delay of approximately 5 ms. The severe spiking behaviour of the Tm:GdVO$_4$ pulse was attributed to instabilities caused by strong atmospheric water absorption at 1892 nm. The maximum average pump power from the Tm:GdVO$_4$ laser incident on the Ho:YLF resonator was 365 mW, or 3.65 W peak power during the on-time of the 20 ms QCW pulse. With the R80% output coupler, the Ho:YLF laser produced a maximum of 70 mW average power, with pulse duration of approximately 15 ms. The Ho:YLF crystal was orientated to lase on σ-polarisation, the measured centre wavelength of which was 2064 nm. Next, the AOM was inserted in the cavity to Q-switch the Ho:YLF laser. The output coupler reflectivity was R65%, and the Ho:YLF crystal axis was orientated to lase on the stronger π-polarisation. The laser threshold was slightly higher with the AOM inserted, at 200 mW of average pump power. The maximum output energy of 1.9 mJ in an 18 ns pulse, as shown in Figure 4, was achieved with only 270 mW of average pump power. Increasing the pump power beyond this point resulted in the Q-switched Ho:YLF laser to have unstable output and pre-lasing, since the AOM could not hold-off lasing with such high gain inside the resonator. The wavelength output of the Q-switched Ho:YLF laser was centred at 2050 nm.
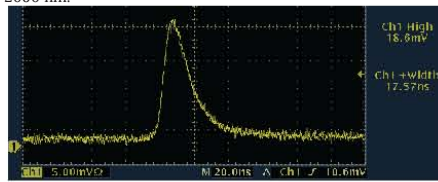

Figure 4: The 1.9 mJ output pulse of the Q-switched Ho:YLF laser pumped by the Tm:GdVO$_4$ laser.

CONCLUSION

We have shown that the Tm:GdVO$_4$ laser wavelength can be operated at an absorption peak of Ho:YLF through careful analysis of the spectroscopic data of these laser materials. A diode-end-pumped QCW Tm:GdVO$_4$ laser operating at 1892 nm was demonstrated by implementing an output coupler transmission of 5%, and by inserting a Brewster plate and a 100 µm etalon. This laser was used to pump a Ho:YLF laser with a resonator design that enabled double-pass pumping and polarisation selection of the Ho:YLF laser output. Both the free-running and Q-switched performances of the Ho:YLF laser were evaluated, the best result of which was an energy of 1.9 mJ in an 18 ns pulse, at a wavelength output of 2050 nm. This is the first time to our knowledge that a Tm:GdVO$_4$ laser has been used to pump a Ho^{3+} laser.

REFERENCES

1. R. Lisiecki, *et al*, Phys. Rev. B **74**, 035103 (2006).
2. A. Sato, K. Asai and K. Mizutani, Optics Letters **29** (8) 836-838 (Apr 2004).
3. E. Sorokin, I. T. Sorokina, A. N. Alpatiev, A. I. Zagumennyi, and I. A. Shcherbakov, ASSL, WA2 (2002).
4. Yu-Feng Li, *et al*, Chinese Phys. Lett. **24**, 724-726 (2007).
5. J. Šulc, *et al*, Proc. SPIE **6998**, 69980T, (2008).
6. M. J. D. Esser, C. Bollig and D. Preussler, ASSP, WB6 (2008).
7. B. M. Walsh, N. P. Barnes, Di Bartolo, J. Appl. Phys **83** (5) (1998).
8. M. J. D. Esser, D. Preussler, E. H. Bernhardi, C. Bollig, and M. Posewang, submitted to Appl. Phys B. (2009).
9. S. A. Payne, L. L. Chase, L. K. Smith, W. L. Kway and W. F. Krupke, IEEE JQE **28** (11) 2619-2630 (1992).
10. T.Y. Fan, and R.L. Byer, IEEE JQE **23** (5) 605–612 (1987).
11. R. C. Stoneman and L. Esterowitz, IEEE JSTQE **1** (1) 78-81 (1995).
12. J. Šulc, *et al*, Proc. SPIE **6871**, 68711V (2008).
13. A.A. Lagatsky, N.V. Kuleshov, and V.P. Mikhailov, Opt. Comm. **165**, 71–75 (1999).

Efficient Fiber-Laser-Pumped Ho:YLF Oscillator and Amplifier Utilizing the Transmitted Pump Power of the Oscillator

H. J. Strauss, W. Koen, C. Bollig, M. J. D. Esser, D. Preussler, K. Nyangaza and C. Jacobs
National Laser Centre, CSIR, Pretoria, 0001, South Africa
Phone: +27 841 3826 Fax: +27 841 3152
E-Mail: hstrauss@csir.co.za

Abstract: We present a novel scheme for a compact and robust pulsed fiber-laser-pumped Ho:YLF oscillator and amplifier system, where the pump power transmitted by the oscillator is utilized to pump the amplifier.
OCIS codes: 140.0140, 140.3070, 140.3480, 140.3580, 140.5680s

1. Introduction

High energy 2 μm laser sources are of great interested for applications in remote sensing, medicine and defense. Ho:YLF is an attractive laser material to use since it has a very longer upper laser level lifetime (~14 ms) and higher emission cross section than Ho:YAG, which makes it ideal to produce high energy pulses. In addition, the very weak thermal lens on the σ polarization helps to deliver diffraction limited beams even under intense end pumping. However, the Ho:YLF has a somewhat stronger quasi-three-level nature. In order to reach transparency at the 2065 nm line, 22% of the Ho ions need to be pumped into the upper laser level (at room temperature). On the other hand, it already reaches transparency at the 1940 nm pump wavelength with only 56% of the Ho ions in the upper laser level. In addition, the pump absorption cross section at 1940 nm is relatively low and strongly polarized. Due to these constraints, a careful design is required with a trade of between efficient pump absorption and low threshold.

The traditional approach for a fiber-laser pumped Ho-laser system with amplifier is to split the unpolarized pump beam with a polarizing beam splitter and to use the two polarized beams to pump the oscillator and amplifier. In our approach, we use the full unpolarized pump beam to pump a relatively short oscillator crystal, which absorbs roughly half the pump power under lasing conditions. The transmitted pump power is then used to pump the amplifier crystal. The c-axis of the two crystals are orientated perpendicular to each other, in order to optimally utilize the unpolarized pump light and to facilitate lasing on the σ-polarization in the oscillator while amplifying on the stronger π-polarization. The distances between the pump fiber collimator and the crystals were kept short to minimize water absorption at 1940nm.
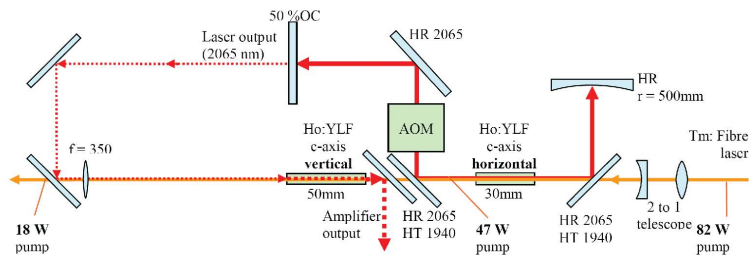
2. Experimental set-up and results

Fig. 1: Schematic diagram of the oscillator/amplifier Ho:YLF system.

A schematic diagram of our experimental setup is illustrated in Figure 1. We used an 80W 1940 nm Tm:fiber laser from IPG Photonics to pump both oscillator and amplifier crystals. The pump beam radius entering the 30 mm 0.5% doped Ho:YLF oscillator crystal was 0.56 mm. The cavity had a length of 340 mm and consisted of a 500 mm CV back-reflector and a flat 50% output-coupler. Two 45° mirrors, which had a high transmission coating for the pump light, were used to couple the pump light in and out of the resonator. The resonator mode had a ~0.6mm radius in the crystal, which was relatively independent of the thermal lens strength.

The oscillator crystal was oriented such that the c-axis (π polarization) is horizontal. The 45° mirrors were coated to reflect vertical polarized light at 2065 nm and therefore selected the σ polarization ($\perp$c-axis). The σ polarization has a lower gain cross section (~0.8×10^{-20} cm^2) but also a much lower thermal lens, which reduces thermal aberrations in the resonator and so maintains beam quality. The oscillator had a threshold of 31 W (17 W absorbed), an overall slope efficiency of 25% and a maximum average output power of 12.4 W.

The oscillator was then pulsed with a fused-silica AOM operating at 100 W RF power. A minimum repetition rate of 1 kHz was used, which resulted in a maximum pulse energy of 10.9 mJ, as indicated in Figure 2. The calculated 33 mJ intra-cavity energy was below the damage threshold of the two 45° mirrors, which was ~35 mJ as previously observed in a similar setup.

The pulsed output of the oscillator was then coupled back into a 50 mm 0.5% doped Ho:YLF amplifier crystal. The pump beam radius entering the amplifier crystal was 21% smaller than in the oscillator crystal due to pump bleaching. The oscillator output beam (the seed) therefore had to be reduced using a f = 350 mm focusing lens. The amplifier crystal was orientated with its c-axis vertical, so that the amplification would take place on the π-polarization with its stronger emission cross section of ~1.3×10^{-20} cm^2. The much stronger (negative) thermal lens of the π-polarization is not critical in the single-pass amplifier. This was confirmed by a beam quality of the amplified beam of M^2 better than 1.1. In addition, this orientation maximizes the absorption of the remaining pump light.

After passing through the amplifier crystal, the slope efficiency of the system almost doubled from 25 to 47%. The maximum pulse energy at 1 kHz was 23.7 mJ and had a pulse length of 74 ns. This gain factor of 2 was confirmed by small signal gain measurements. Measurements below 1 kHz were not attempted in order to prevent optical damage to the oscillator.
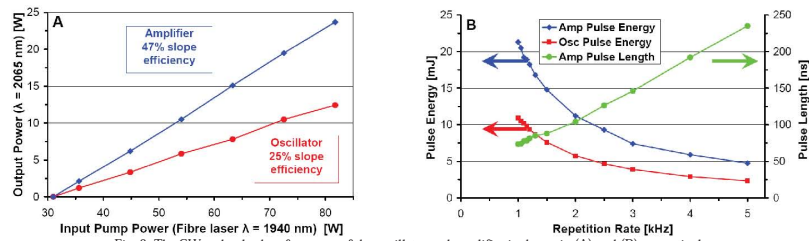

Fig. 2: The CW and pulsed performance of the oscillator and amplifier is shown in (A) and (B) respectively

3. Conclusion

We have demonstrated that a Ho:YLF oscillator and amplifier system can be designed in a compact setup where the pump power from an unpolarized fibre laser utilized efficiently. The system produced more than 20 mJ energy per pulse at 1 kHz, while maintaining a M^2 better than 1.1. This system only utilized single pass pumping of the oscillator and amplifier crystals, with 18 W of pump power which was not absorbed. This excess pump power can be carefully back aligned into the amplifier and oscillator, but we opted not to do this for fear of damaging the fiber pump laser. The seed can also be passed multiple times through the amplifier crystal. Our initial calculations show that by implementing both these measures it is possible to extract even higher energy pulses from this system. This proof of concept architecture therefore shows great promise of delivering highly efficient 2 µm pulsed output with excellent beam quality.

Exploiting the natural doping gradient of Nd:YLF crystals for high-power end-pumped lasers

C. Bollig[1], W. Koen[1, 2], H. Strauss[1, 3], E. Bernhardi[1, 2], R. Botha[3], D. Esser[1], D. Preussler[1]

1. Council for Scientific and Industrial Research: National Laser Centre, PO Box 395, Pretoria, 0001, South Africa
2. University of KwaZulu-Natal, Durban, 4041, South Africa
3. University of Stellenbosch, Private Bag X1, Matieland, 7602, South Africa

Of the various Neodymium-doped materials, Nd:YLF is particularly attractive for use in high-power diode end-pumped solid-state lasers due to its weak thermal lens, especially on the σ-polarisation, and it's long upper laser level lifetime that enables efficient energy storage for Q-switching. However, due to the low thermal fracture limit in Nd:YLF, power scaling has proven to be difficult.

In our previous work, we addressed several issues relating to Nd:YLF in a novel fashion and were subsequently able to demonstrate the highest published power for an end-pumped Nd:YLF laser [1]. The laser delivered a total output power of 60.3 W CW and an average power of 52 W when Q-switched between 5 and 30 kHz, with good beam quality and no sign of lifetime quenching. However, we experienced fracture at 5 kHz.

In order to address the fracture problem we decided to use crystals of a doping concentration below the 0.5% previously used. In addition, we decided to exploit the natural doping gradient along the length of the boule, which is especially pronounced at low concentrations but commonly ignored. In a collaboration, VLOC estimated the doping gradient of a specially manufactured boule (Fig. 2) and maintained the crystal orientation information during the manufacturing process of the 45 mm long, 6 mm diameter crystals. Initial thermal calculations indicate that for these crystals, the lower-doping end can be pumped 58% harder than the higher-doping end before the thermal fracture limit is reached.

To be able to pump each crystal rod from its low-doping end, we implemented a folded resonator (Fig. 1). In addition to using relatively low doping concentrations, we pumped at a wavelength of 805 nm, where the absorption of Nd:YLF is ~5 times lower than the conventionally used 792 or 797 nm. The combination of these techniques resulted in a more even distribution of the heat load along the length of the crystals. As in our previous work, we compensated for the strong astigmatism of the crystals by using two crystals with the c-axis vertical and two with the c-axis horizontal with a λ/2-plate in-between [1].
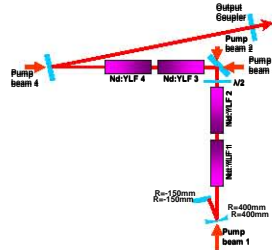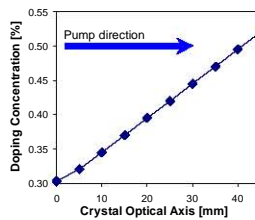

Fig. 1 Laser resonator

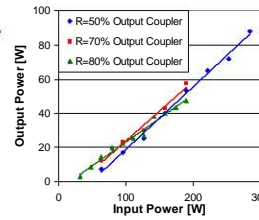**Fig. 2** Crystal doping gradient as estimated by VLOC

Fig. 3 Power under CW operation

With this configuration, no crystal damage occurred, even with all four fibre-coupled 75 W diode laser modules at full power. A total output power of up to 87 W CW was achieved, which is the highest reported so far but still less than expected (Fig**.** 3). Using Findlay-Clay and Caird analysis, the resonator loss was estimated to be 10% and 15% respectively. The crystals' total scatter loss was subsequently measured but was found to be only 1.64% round-trip loss at the laser wavelength.

We observed significant fluctuations in the output power and beam pointing. These could be because the laser operates in Zone II of the thermal stability diagram [2], which makes the laser very sensitive to misalignment and to small fluctuations in the pump overlap and variations in diffraction in the air. We believe that the lower than expected output power is due to this as well, rather than to actual resonator losses.

By redesigning the laser to operate in zone I, efficient and stable operation in excess of 100 W should be achievable. In the next step, Q-switched operation will be investigated, which has the potential to yield high average powers even at repetition rates below 5 kHz.

References

[1] C**.** Bollig, C. Jacobs, H. M. von Bergmann, and M. J. Esser, "High-power end-pumped Nd:YLF laser without lifetime quenching" CLEO/Europe 2005
[2] V. Magni, "Resonators for solid-state lasers with large-volume fundamental mode and high alignment stability," Appl. Opt. **25**, 107 (1986)

High-power diode-end-pumped Tm:GdVO$_4$ laser operating at 1818 nm and 1915 nm

M. J. Daniel Esser*, C. Bollig, D. R. Preussler, C. Jacobs, W. S. Koen, and E. H. Bernhardi
National Laser Centre, CSIR, Pretoria, South Africa

e-mail: desser@csir.co.za
Web page: http://www.csir.co.za/nlc

ABSTRACT

High-power solid-state lasers operating in the 2 μm wavelength region are of interest for a wide variety of applications, including remote gas detection and laser spectroscopy, as drive lasers for high harmonic generation and attosecond applications and for free-space optical communication. One approach to achieve high output power is to optically pump Tm doped lasers that can lase at 1.9 μm, with high-power laser diodes at 0.8 μm. The Tm laser output can then be used to pump Ho doped lasers that can produce output at 2.1 μm.

Tm:GdVO$_4$ is a relatively new laser material that has attracted attention due to its broad absorption spectrum centred around 799 nm which makes it particularly suitable to be pumped with commercially available high-power laser diodes. In addition, it has a broad emission spectra which makes it feasible to operate such a Tm:GdVO4 laser over a wide wavelength range. Despite these advantages, there are a limited number of publications relating to the power scaling of this laser material. The highest output power previously demonstrated from a continuous wave Tm:GdVO$_4$ laser was 2.6 W with its wavelength at 1910 nm [1].

In this paper we report on our initial experiments with a diode-end-pumped Tm:GdVO$_4$ laser. The atomic doping concentration was 3 % and the dimensions of the crystal 2.5 x 2.5 x 3 mm^3. The crystal was placed in a plano-concave resonator of approximate length 26 mm. Two output coupler mirrors were used during the experiments. The first output coupler had 95 % reflectivity at 1.9 μm with 300 mm radius of curvature. The second output coupler had 28 % reflectivity at 1.8 μm and 250 mm radius of curvature. The laser was pumped with a fibre-coupled laser diode from one end only, the fibre of which had a core diameter of 400 μm and N.A. of 0.22. The laser diode was operated in a quasi-continuous wave (QCW) mode with 60 W maximum peak power incident on the crystal at 800 nm. The duty cycle of the pump pulses was kept low in an attempt to prevent crystal fracture. The output at 1.9 μm was measured with a PbS photo diode and a power meter.

The output wavelength of the laser with the 95 % reflectivity output coupler was measured to be 1915 nm ($\pm$ 2.5 nm measuring uncertainty). The pump pulse had an on-time of 20 ms at 5 Hz repetition rate. The measured maximum peak power was 8.7 W for 37.3 W of incident power on the laser crystal. This corresponded to ~175 mJ per pulse of output energy. Increasing the pump power beyond this point resulted in thermal fracture of the laser crystal.

Next the 28 % reflectivity output coupler was used and the pump pulse on-time was reduced to 10 ms. The damaged crystal was replaced with a crystal of similar doping concentration and dimensions. The output wavelength of the Tm:GdVO$_4$ laser was measured to be 1818 nm ($\pm$ 2.5 nm). This reduction in wavelength was expected from the quasi-three level laser with an output coupler with high transmission loss. The maximum peak output power of this laser was measured to be 8.4 W at full pump power from the laser diode, corresponding to ~84 mJ per pulse.

It was shown here for the first time to our knowledge that a Tm:GdVO$_4$ laser can be used in QCW mode with a pulse width of 10 – 20 ms with multi watt output power. It was concluded that this laser is suitable to be used as a pump source for Ho doped lasers which have upper state lifetimes in the 7 - 15 ms range. In addition we have shown that the Tm:GdVO$_4$ laser wavelength can be operated over ~100 nm by adjusting the laser resonator losses. This makes the Tm:GdVO$_4$ a suitable laser source for pumping different types of crystals doped with Ho. Our future work will include further power scaling and continuous wave operation of the Tm:GdVO$_4$ laser.

REFERENCES
[1] Lisiecki, R., *et al*, Comparative optical study of thulium-doped YVO$_4$, GdVO$_4$, and LuVO$_4$ single crystals, Physical Review B, Volume 74, Issue 3, July 2006, Article 035103.